Alaska Department of Transportation & Public Facilities

Research & Technology Transfer

Use of Steel Fiber-Reinforced Rubberized Concrete in Cold Regions – Phase II: Monitoring

Prepared for

Alaska Department of Transportation & Public Facilities
Statewide Research Office
3132 Channel Drive
Juneau, AK 99801-7898

Prepared by

Prof. Osama Abaza, PhD., C. Eng.
University of Alaska Anchorage
College of Engineering
2900 Spirit Drive, EIB 301 L
Anchorage, Alaska 99508
907.786.6117

HFHWY00049 and FHWA-AK-RD-4000(165)
December 2020

REPORT DOCUMENTATION PAGE	Form approved OMB No.

1. AGENCY USE ONLY (LEAVE BLANK)	2. REPORT DATE	3. REPORT TYPE AND DATES COVERED
	October 2020	

4. TITLE AND SUBTITLE	5. FUNDING NUMBERS
Use of Steel Fiber-Reinforced Rubberized Concrete in Cold Regions – Phase II: Monitoring	
6. AUTHOR(S) Prof. Osama Abaza, PhD., C. Eng.	
7. PERFORMING ORGANIZATION NAME(S) AND ADDRESS(ES) University of Alaska Anchorage College of Engineering 2900 Spirit Drive Anchorage, AK 99508	8. PERFORMING ORGANIZATION REPORT NUMBER N/A
9. SPONSORING/MONITORING AGENCY NAME(S) AND ADDRESS(ES) State of Alaska, Alaska Dept. of Transportation and Public Facilities Research and Technology Transfer 3132 Channel Drive Juneau, AK 99801-7898	10. SPONSORING/MONITORING AGENCY REPORT NUMBER HFHWY00049 and FHWA-AK-RD-4000(165)

11. SUPPLENMENTARY NOTES

Performed in cooperation with Department of Civil Engineering at the College of Engineering, University of Alaska Anchorage, under a contract with the Alaska Department of Transportation and Public Facilities (DOT&PF). Osama Abaza, Professor of Civil Engineering, University of Alaska Anchorage, was the Principal Investigator.

12a. DISTRIBUTION / AVAILABILITY STATEMENT	12b. DISTRIBUTION CODE
No restrictions	

13. ABSTRACT (Maximum 200 words)

This report documents the real-world performance of a new pavement product for use in cold regions—steel fiber-reinforced rubberized concrete (SFRRC). During the previous phase of this research project, Phase I: Use of Steel Fiber-Reinforced Concrete in Cold Regions, SFRRC underwent laboratory testing and then pre-cast panels were designed and installed on Abbott Road in the Municipality of Anchorage in the summer of 2017. During the current phase, Phase II, SFRRC was monitored in the field using visual inspection, continuous collection of strain gauge data, deflection measurements, rut depth, skid resistance, and other measures. SFRRC was also investigated on high-traffic urban arterials/intersections to analyze rutting, freeze-thaw resistance and other possible rigid pavement properties, falling weight deflection, skid resistance, and life-cycle cost. A comparative analysis was conducted using the same measuring techniques on hot mix asphalt (HMA) on an adjacent road section. The results show that the SFRRC road sections have significant rutting resistance compared to the adjacent HMA road section, and the results of freeze-thaw resistance and deflection field testing validate the results of the Phase I laboratory testing. Furthermore, comparative life-cycle cost analyses of SFRRC and HMA justifies the use of SFRRC in roadway construction in cold regions in terms of cost effectiveness, enhanced performance, and extended life. This report recommends the use of SFRRC for highway intersections and/or test sections on major arterials as the next phase of introducing this material for roadway construction in Alaska.

14- KEYWORDS:	15. NUMBER OF PAGES
Concrete, steel fiber, crumb rubber, rutting, strain gauge sensors, deflection, skid resistance, deflections, life-cycle cost.	108 (including introductory pages and Appendices)
	16. PRICE CODE N/A

17. SECURITY CLASSIFICATION OF REPORT	18. SECURITY CLASSIFICATION OF THIS PAGE	19. SECURITY CLASSIFICATION OF ABSTRACT	20. LIMITATION OF ABSTRACT
Unclassified	Unclassified	Unclassified	N/A

Notice

This document is disseminated under the sponsorship of the U.S. Department of Transportation in the interest of information exchange. The U.S. Government assumes no liability for the use of the information contained in this document. The U.S. Government does not endorse products or manufacturers. Trademarks or manufacturers' names appear in this report only because they are considered essential to the objective of the document.

Quality Assurance Statement

The Federal Highway Administration (FHWA) provides high-quality information to serve government, industry, and the public in a manner that promotes public understanding. Standards and policies are used to ensure and maximize the quality, objectivity, utility, and integrity of its information. FHWA periodically reviews quality issues and adjusts its programs and processes to ensure continuous quality improvement.

Author's Disclaimer

Opinions and conclusions expressed or implied in the report are those of the author. They are not necessarily those of the Alaska DOT&PF or funding agencies.

METRIC (SI*) CONVERSION FACTORS

APPROXIMATE CONVERSIONS TO SI UNITS

Symbol	When You Know	Multiply By	To Find	Symbol
		LENGTH		
In	inches	25.4		mm
Ft	feet	0.3048		m
Yd	yards	0.914		m
mi	Miles (statute)	1.61		km
		AREA		
in^2	square inches	645.2	millimeters squared	cm^2
ft^2	square feet	0.0929	meters squared	m^2
yd^2	square yards	0.836	meters squared	m^2
mi^2	square miles	2.59	kilometers squared	km^2
Ac	acres	0.4046	hectares	ha
		MASS (weight)		
Oz	Ounces (avdp)	28.35	grams	g
Lb	Pounds (avdp)	0.454	kilograms	kg
T	Short tons (2000 lb)	0.907	megagrams	mg
		VOLUME		
fl oz	fluid ounces (US)	29.57	milliliters	mL
gal	Gallons (liq)	3.785	liters	liters
ft^3	cubic feet	0.0283	meters cubed	m^3
yd^3	cubic yards	0.765	meters cubed	m^3

Note: Volumes greater than 1000 L shall be shown in m^3

		TEMPERATURE (exact)		
ºF	Fahrenheit temperature	5/9 (ºF-32)	Celsius temperature	ºC
		ILLUMINATION		
Fc	Foot-candles	10.76	lux	lx
Fl	foot-lamberts	3.426	candela/m^2	cd/cm^2
		FORCE and PRESSURE or STRESS		
lbf	pound-force	4.45	newtons	N
psi	pound-force per square inch	6.89	kilopascals	kPa

These factors conform to the requirement of FHWA Order 5190.1A *SI is the symbol for the International System of Measurements

APPROXIMATE CONVERSIONS FROM SI UNITS

Symbol	When You Know	Multiply By	To Find	Symbol
		LENGTH		
mm	millimeters	0.039	inches	in
m	Meters	3.28	feet	ft
m	Meters	1.09	yards	yd
km	kilometers	0.621	Miles (statute)	mi
		AREA		
mm^2	millimeters squared	0.0016	square inches	in^2
m^2	meters squared	10.764	square feet	ft^2
km^2	kilometers squared	0.39	square miles	mi^2
ha	hectares (10,000 m^2)	2.471	acres	ac
		MASS (weight)		
g	Grams	0.0353	Ounces (avdp)	oz
kg	kilograms	2.205	Pounds (avdp)	lb
mg	megagrams (1000 kg)	1.103	short tons	T
		VOLUME		
mL	milliliters	0.034	fluid ounces (US)	fl oz
liters	Liters	0.264	Gallons (liq)	gal
m^3	meters cubed	35.315	cubic feet	ft^3
m^3	meters cubed	1.308	cubic yards	yd^3

		TEMPERATURE (exact)		
ºC	Celsius temperature	9/5 ºC+32	Fahrenheit temperature	ºF
		ILLUMINATION		
lx	Lux	0.0929	foot-candles	fc
cd/cm 2	candela/m^2	0.2919	foot-lamberts	fl
		FORCE and PRESSURE or STRESS		
N	newtons	0.225	pound-force	lbf
kPa	kilopascals	0.145	pound-force per square inch	psi

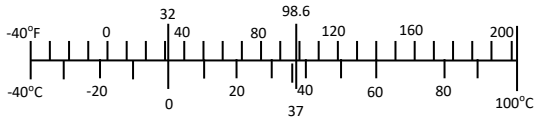

List of Abbreviations

American Concrete Institute	ACI
American Association of State Highway and Transportation Officials	AASHTO
American Society for Testing and Materials	ASTM
Analysis of the Long Term Pavement Performance	LTPP
Annual average daily traffic	AADT
Asphalt concrete	AC
British pendulum numbers	BPNs
Coefficient of thermal expansion	CTE
Department of Transportation and Public Facilities	DOT&PF
Falling weight deflectometer	FWD
Federal Highway Administration	FHWA
Fiber reinforced polymer	FRP
Hot mix asphalt	HMA
Jointed plain concrete pavements	JPCPs
Life cycle cost	LCC
Life cycle cost analysis	LCCA
Load transfer efficiency	LTE
Pavement management system	PMS
Pervious concrete pavement	PrCP
Portland Cement Association	PCA
Portland cement concrete	PCC
Pounds per square inch	psi
Precast concrete pavement	PCP
Skid number	SN
Steel fiber-reinforced rubberized concrete	SFRRC
University of Alaska Anchorage	UAA

Table of Contents

List of Figures

List of Tables

Acknowledgments

The research reported herein was performed by the College of Engineering at the University of Alaska Anchorage in collaboration with the Alaska Department of Transportation & Public Facilities (DOT&PF).

Osama A. Abaza, Professor of Civil Engineering, University of Alaska Anchorage, was the principal investigator. Mahear A. Abou Eid was the temporary employee through the University of Alaska Anchorage for the period 2017–2019. The work was done by and under the supervision of Professor Abaza.

The research team is grateful to the Federal Highway Administration (FHWA) and the Alaska DOT&PF for their sponsorship of this research. The information, findings, and opinions of the research reflected in this report do not represent the views of the sponsoring agencies.

We would like to acknowledge the contributions of the following individuals:

- Anna Bosin, P.E., Program Manager, Research, Development & Technology Transfer DOT&PF;
- James Amundsen, P.E., Chief of Highway Design DOT&PF;
- Mahear A. Abou Eid, Transportation & Public Facilities CRD-Construction, DOT&PF;
- Jason Baxley, P.E., Project manager, DOT&PF;
- Matt Murphy, Transportation Planner I, Transportation Data Programs, DOT&PF;
- Ashley DeVore, P.E., CR Materials, DOT&PF;
- Mahmoud Arafat, Muhammad Saif Uddin and Tanay Datta Chowdhury, graduate students, UAA, College of Engineering;

Abstract

This report documents the real-world performance of a new pavement product for use in cold regions—steel fiber-reinforced rubberized concrete (SFRRC). During the previous phase of this research project, Phase I: Use of Steel Fiber-Reinforced Concrete in Cold Regions, SFRRC underwent laboratory testing and then pre-cast panels were designed and installed on Abbott Road in the Municipality of Anchorage in the summer of 2017. During the current phase, Phase II, SFRRC was monitored in the field using visual inspection, continuous collection of strain gauge data, deflection measurements, rut depth, skid resistance, and other measures. SFRRC was also investigated on high-traffic urban arterials/intersections to analyze rutting, freeze-thaw resistance and other possible rigid pavement properties, falling weight deflection, skid resistance, and life-cycle cost. A comparative analysis was conducted using the same measuring techniques on hot mix asphalt (HMA) on an adjacent road section. The results show that the SFRRC road sections have significant rutting resistance compared to the adjacent HMA road section, and the results of freeze-thaw resistance and deflection field testing validate the results of the Phase I laboratory testing. Furthermore, comparative life-cycle cost analyses of SFRRC and HMA justifies the use of SFRRC in roadway construction in cold regions in terms of cost effectiveness, enhanced performance, and extended life. This report recommends the use of SFRRC for highway intersections and/or test sections on major arterials as the next phase of introducing this material for roadway construction in Alaska.

Summary of Findings

The research team successfully completed the monitoring plan to determine the use of steel fiber-reinforced rubberized concrete (SFRRC) on high-traffic urban arterials/intersections. During the previous phase of the project, Phase I: Use of Steel Fiber-Reinforced Concrete in Cold Regions, the basic parameters were outlined for the installation of pre-cast panels on Abbott Road and full experimental testing, including laboratory testing, mix design, trial slabs and precast slabs testing, design of the roadway section, and installation of the precast slabs. Phase I was an approved Experimental Feature by FHWA which requires monitoring the use of this new SFRRC material in an actual roadway setting. Phase II represents the next step in introducing SFRRC into construction of highway intersections and other experimental pavement sections.

The monitoring plan, represented by Phase II, was conducted on the SFRRC test section, which consists of fifteen precast slabs and adjacent roadway sections composed of hot mix asphalt (HMA), for 2½ years to collect data on the following:

- Pavement deflection (falling weight deflectometer [FWD] testing) to determine joint transfer efficiency and load-bearing capacity.
- Freeze-thaw assessment based on strain gauge data.
- Visual inspection for any cracking or heaving due to freeze-thaw stresses and other possible defects for both the SFRRC and the adjacent HMA, both installed in the same capital project.
- Rut measurements to determine the impact of studded tires on SFRRC versus HMA.
- Skid resistance assessment.

Data from FWD testing was collected twice a year when available using the Alaska Department of Transportation and Public Facilities (DOT&PF) Dynatest RSP 5051 Mark II. Deflection measurements were taken at center, edge, corner, and panel joints. Analysis of the data indicates that the SFRRC slabs follow normal trends in rigid pavements, with seasonal deflection behaviors based on the conditions of the base/subgrade (basin). Furthermore, dowel bars incorporated in the SFRRC slab joints are working as expected to transfer loads across the joints. The SFRRC slabs reported deflections well below the HMA road section under the applied wheel load, suggesting better performance in overcoming Spring Thaw-Weakening in the pavement basin, and this finding might affect axle-truck weight limits enforced during the spring season.

As part of Phase I, strain gauges were embedded in three of the fifteen precast slabs to provide measurements in three locations within each slab: at the edge, corner and center. In addition, temperature data were collected from each of the sensors to determine if there is a correlation with strain measurements. Analysis of the data indicates the normal trend in rigid pavements, with superior performance in limiting expansion and contraction indicated by the lower coefficient of thermal expansion (CTE), which eventually affects the design of the joint opening and dowel bars.

Visual inspections were conducted twice a year to monitor freeze-thaw deterioration, abrasion/erosion, plastic shrinkage cracking, drying shrinkage cracking, thermal cracking, overload damage, loss of support, corrosion of embedded steel fiber, frost heave, surface defects, joint openings, grout condition, and finished surfaces. Observations indicated no signs of such damage. Exposed crumbs of rubber on the road surface resulted from wearing of the thin layer of

paste on the surface and pose no structural or functional issues. In addition, no pop-out steel fibers were noticed on the SFRRC surface, and no loose steel fibers were noticed on the side of the road during the monitoring period.

Rut measurements were conducted twice a year to monitor the depth of the rut on three of the fifteen SFRRC precast slabs and two of the HMA road sections before and after the test section. A trend in rut development was established for both materials. Traffic data were retrieved from the traffic sensors embedded on the road as part of this study through the Abbott Road capital project. Rut development indicates superior performance of SFRRC in resisting the impact of studded tires over the current HMA section as well as the historic data of HMA on the same road section. Comparative analysis of the rut resistance performance of SFRRC and HMA shows that SFRRC can have a maintenance cycle that is about three times (3.28) longer than HMA under the same traffic conditions.

Skid resistance was measured, and the assessment showed an overall average difference of about 5% for SFRRC over HMA. Further monitoring of skid resistance over time is highly recommended. Studies show that Portland cement concrete (PCC) pavements experience very little change in skid resistance over the life of the pavement compared with HMA.

Life-cycle cost (LCC) was determined based on HMA resurfacing/rehabilitation projects implemented by Alaska DOT&PF in the state. The LCC for SFRRC was based on three scenarios, as full real-life data do not exist for the comparative analysis with HMA projects. A worst-case scenario for SFRRC was adopted for comparative analysis using an analysis period of 43 years. The LCC analysis for SFRRC showed $0.64 million per linear lane mile as compared with $1.36 million for HMA for the same analysis period. This finding reflects a cost ratio of HMA to SFRRC of about 2.1 to 1.0.

Based on the findings of this project, further exploration of SFRRC use on highway intersections and in test sections on major arterials is recommended to validate the outcomes of Phase I and II of this research.

CHAPTER 1 – INTRODUCTION AND RESEARCH APPROACH

Background

This project's previous phase, Phase I: Use of Steel Fiber-Reinforced Concrete in Cold Regions, established the need for alternatives in road pavement material to address the long-standing issues in Alaska's South Central Region of short pavement life due to a relatively high rut rate caused by studded tire use during wintertime. The development of a new material—steel fiber-reinforced rubberized concrete (SFRRC)—represents one option for consideration by the Alaska Department of Transportation and Public Facilities (DOT&PF) to prolong pavement life and reduce the frequency of maintenance/rehabilitation over the life of the pavement structure. A research team from the University of Alaska Anchorage (UAA) accomplished the tasks of developing SFRRC (Abaza and Hussein, 2016). In Phase I, the research team validated the use of SFRRC with more laboratory testing, built and monitored the trial slab at the UAA campus, and designed, built, and installed the precast slabs of SFRRC as a test section on Abbott Road in the Municipality of Anchorage for actual monitoring of the material on a high-traffic urban arterial (Abaza and Abou Eid, 2017). Phase II of the project, represented by this report, documents the outcome of monitoring the SFRRC test section for possible use of SFRRC on highway intersections and test sections on major arterials in the state.

Research Objective

The broader acceptance of SFRRC requires real-life monitoring of an active roadway test section under cold region conditions in an area with persistent short pavement life issues. The objective of this investigation is to provide a comparative analysis of SFRRC and HMA to determine if SFRRC can reduce the impact of rutting by studded tires cost-effectively, and if SFRRC can withstand cold weather conditions and increase roadway service life.

Research Approach

Phase I of the project established the basis for the use of SFRRC at highway intersections. A thorough literature review was conducted, and since its completion, more research on several elements of roadway structure has been reported. The additional literature was reviewed and is addressed in Appendix A of this report.

In coordination with the DOT&PF, Abbott Road in the Municipality of Anchorage was selected as an optimal location for implementation of the test section (Abbott Road Rehabilitation – Phase I). The location was chosen, in part, because it consisted of one lane in each direction, along with a shared turn lane that could be utilized during construction and monitoring. One section of the roadway was constructed of SFRRC, and was directly followed by a road section of DOT&PF standard HMA for comparison purposes. The test section was constructed with sensor equipment to calculate temperature changes, displacement (lateral and longitudinal), annual average daily traffic (AADT) volumes, and rutting depths. Criteria were set prior to construction to determine when the lane had reached its service life (Abaza and Abou Eid, 2017). The Experimental Feature approval by FHWA requires post-construction monitoring for possible use of this material in the future.

A 2½ year monitoring plan of the SFRRC test section was completed to document an accurate final assessment of the product. This extended monitoring plan included inspections for center, corner, edge, and joint deflections, surface conditions, cracking of the slabs, grout failure,

joint adhesive failure, and rutting due to studded tire wear. In addition, strain gauge data were monitored continuously and deflection was tested periodically using a falling weight deflectometer (FWD). Pavement Management System data were collected on Abbott Road annually, when available, and compared with adjacent HMA pavement to track rutting, cracking, etc. Surface friction values using a British pendulum unit were taken annually.

The outcome of test section monitoring as well as the life-cycle cost analysis will give feedback for further exploration of the use of the new material by DOT&PF management.

CHAPTER 2 – METHODOLOGY

The methodology used to meet the project's stated objectives can be summarized by describing the setting of the SFRRC test section and the analysis of data from the on-site testing of strain gauge sensors, the FWD, rutting observations, visual inspection, skid resistance data, etc. per the recommendation of Phase I.

Abbott Road Test Section Setting

The DOT&PF chose the project location based on project availability, traffic volumes, and the geometry of the roadway section. The AMATS: Abbott Road Rehabilitation Project was selected, as it was scheduled for the 2017 construction season. In addition, traffic volume on this road is substantial, with an annual average daily traffic (AADT) count of approximately 15,000, which would provide rutting data within several years. The volume of traffic is apparent based on the existing asphalt conditions and recorded traffic counts.

The intended use of SFRRC is at high-volume intersections, but to avoid geometric challenges and traffic-control issues and to eliminate unknown variables, a linear portion of the roadway was chosen as the test section. The test section location has limited turning traffic, acceleration or deceleration, and a shared left-turn lane, simplifying traffic control during construction.

In coordination with the Alaska DOT&PF Highway Data unit, an automated traffic recording station was added to the project for installation immediately succeeding the test section. This recording station would provide data on below-roadway and pavement surface ambient temperature, as well as data on traffic volume and vehicle classification.

The initial plan for placement of the material was to pour it in place. In further discussions about construction sequencing for installation of the material at intersections, it was concluded that it would be impractical to pour in place because the traditional concrete would require a minimum of 7 days to cure before traffic could be allowed, an amount of time that would be difficult at a high-volume intersection In addition, in this location it is impractical for residents and the plans of the parent project construction activities to pour it in place. It was determined that precast panels would be required for the test section.

Research into installation of precast panels was conducted, referring specifically to a report by Minnesota DOT (2005) that used the Super-Slab system. The design and specifications shown in the report provided a template for the design of precast panels to use on Abbott Road. These panels featured slotted and doweled ends, tapered edges, lifting mechanisms, and grouting ports, details that would ensure proper load transfer, ease of placement, and filling of any voids under the panels.

Along with the data provided by the automated traffic recording station, a strain gauge system was designed for embedment in the pre-cast panels. The gauge would provide information on freeze-thaw cycles and any sustained stresses that might occur throughout the life span of the panels (Phase I, 2017).

Data Collection

Data were collected through on-site physical testing, sensors embedded in the SFRRC slabs, and traffic sensors. On-site testing was conducted twice a year, and a traffic plan was developed and approved for that purpose, as shown in Figure 1. Shaman Traffic Control provided the services for lane shifting during the physical testing.

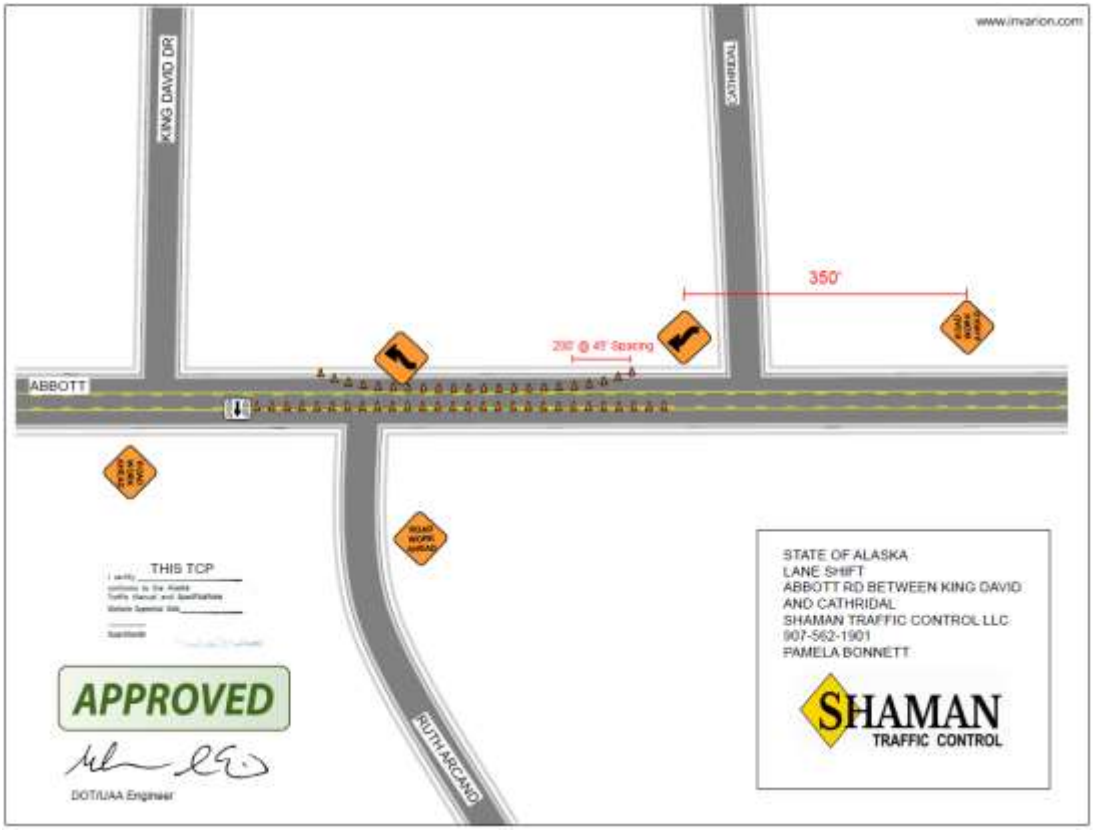

Figure 1: Traffic control plan during physical on-site testing (SHAMAN, Inc., 2018).

A testing location map was developed for on-site physical testing to include the tests needed, the location of tests on the SFRRC slab as well as the adjacent HMA sections, and the number of test points needed for each location. Figure 2 shows the layout of the testing map for this phase of the project.

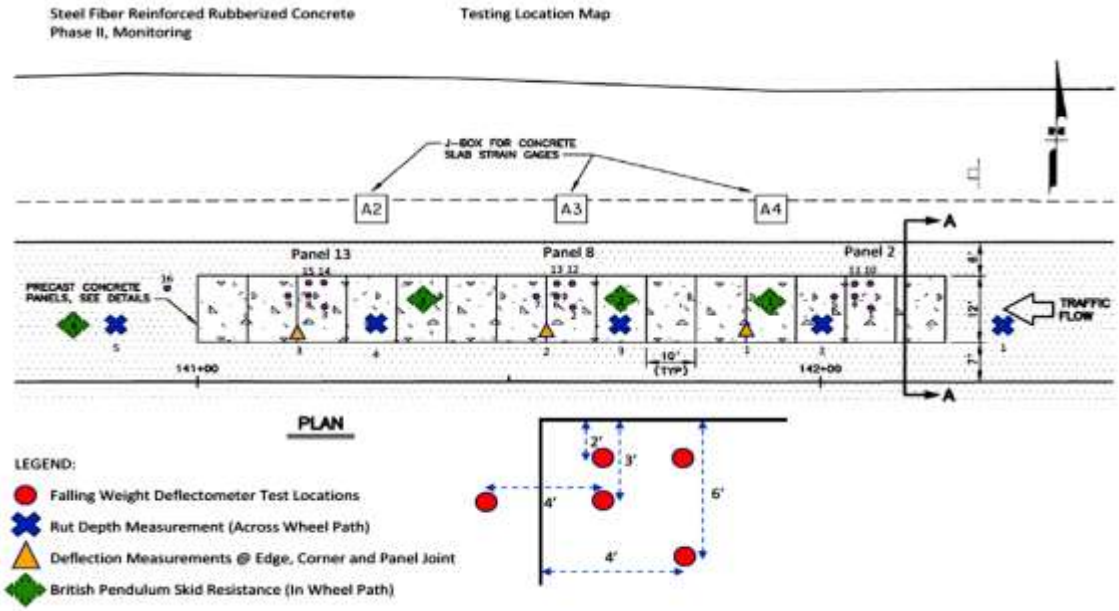

Figure 2: Testing location map for SFRRC, Phase II, Monitoring (Abou Eid, 2018).

Strain data were collected using embedded sensors in the precast slabs as shown in Figure 3 and Figure 4. A Geokon Model 4200 VW Concrete Embedment Strain Gauge was used. This strain gauge sensor type has a 153 mm gauge length and is commonly used for strain measurements in concrete structures; it is extra rugged to resist bending and has large flanges to provide a greater engagement area. Each gauge incorporates a thermistor so that the temperature can be read and displayed by the readout. Sensors were placed in three of the fifteen slabs used to build the SFRRC test section. Three sensors were used in each of the three slabs, placed at the center, corner, and edge of the slab. Engineering services for collection and continuous retrieval of the data were provided by SubTerra, Inc. Two and a half years of data were collected as of June 2017.

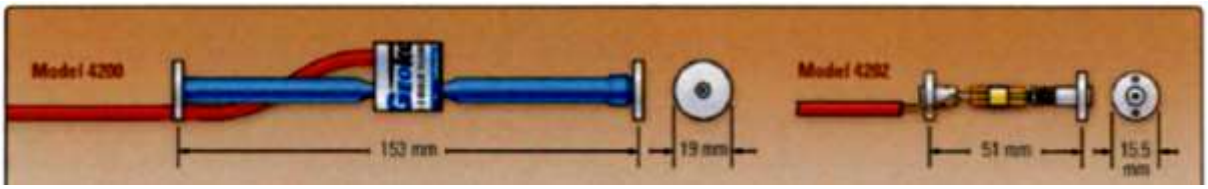

Figure 3: Dimensions of the 4200 Series Strain gauge (Geokon, Geotechnical and Structural Instrumentation).

Figure 4: Strain gauge sensor placed in the precast SFRRC slabs (Abaza, 2016).

The FWD data were collected by the Alaska DOT&PF Pavement Management System (PMS) team. The PMS team depends on the Dynatest (FWD) RSP 5051 Mark II, which applies a dynamic load that simulates the loading of a moving wheel as shown in Figure 5. Data were collected every 6 months when possible and compiled to measure the deflection at specified locations. Figure 6 shows locations of FWD testing for each site visit.

Figure 5: Falling weight deflectometer testing device used (Abaza, 2018).

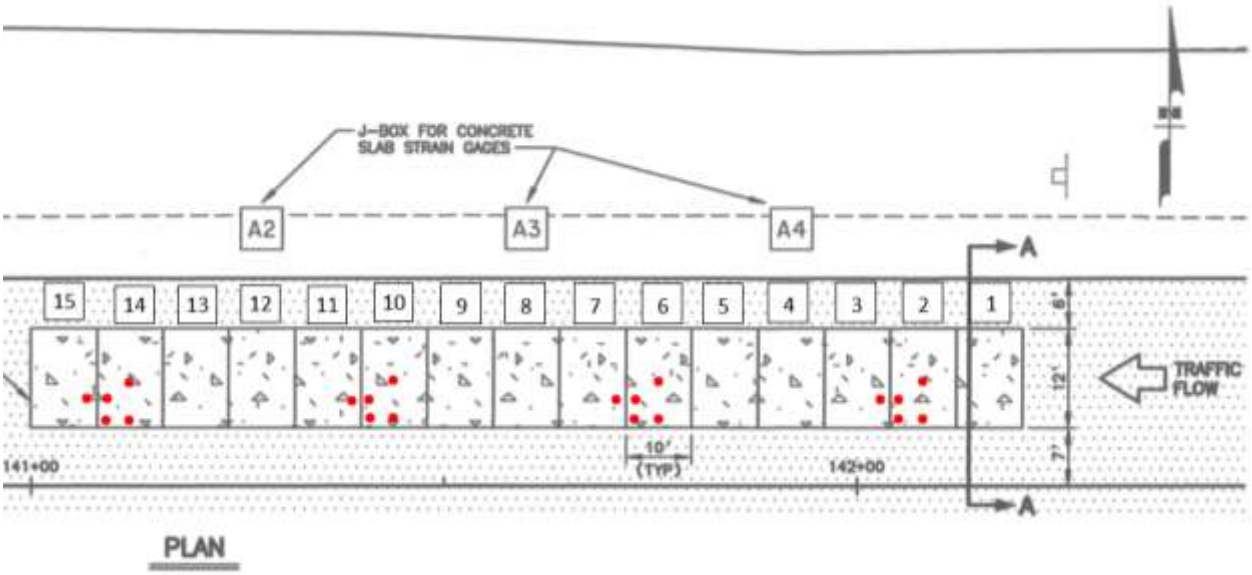

Figure 6: Locations of FWD tests at center, edge, corner and joint on the SFRRC test section (Abou Eid, 2018).

For each testing cycle of the SFRRC section, a visual inspection was conducted to detect cracking or heaving due to freeze-thaw stresses. This visual inspection included any signs of joint filling failure, erosion or scaling of the concrete surface, the presence of steel fibers on the surface (embedment and geometry), striping damage, etc. Figure 7 shows a typical close-up view of the slab. Figure 8 shows a typical view of crack filling, edge striping, and the slab shoulder joint.

Figure 7: Typical close-up view of the SFRRC surface (Abaza, 2018).

Figure 8: Typical view of crack filling, edge striping, and the slab shoulder joint (Abaza, 2018).

Rut measurements to determine abrasion resistance to studded tires were conducted on the test section and adjacent HMA. Figure 2 shows the locations of rut measurements on the SFRRC and HMA sections during the monitoring period. Figure 9 shows a typical rut measurement using a straight edge in accordance with ASTM E1703 / E1703M – 10 (2015). In addition, Alaska DOT&PF PMS database rut data will be used in the analysis utilizing Mandlii LCMS, which was used until the end of 2017 and Fugro LCMS Road Surface Profiling (RSP) equipment, in use since 2018, which consists of distance measuring lasers and accelerometers and the Laser Crack Measurement System (LCMS) that provides high-definition 3D profiles and 2D images of the road surface (PMS, ADOT&PF). Figure 10 shows a typical rut profiler system. A comparative analysis of rut development on the two pavement sections was conducted for use as a criterion for life expectancy of each material, and life-cycle cost analysis was developed based on the outcome.

Figure 9: Rut measurements using a straight edge of adjacent HMA (Abaza, 2018).

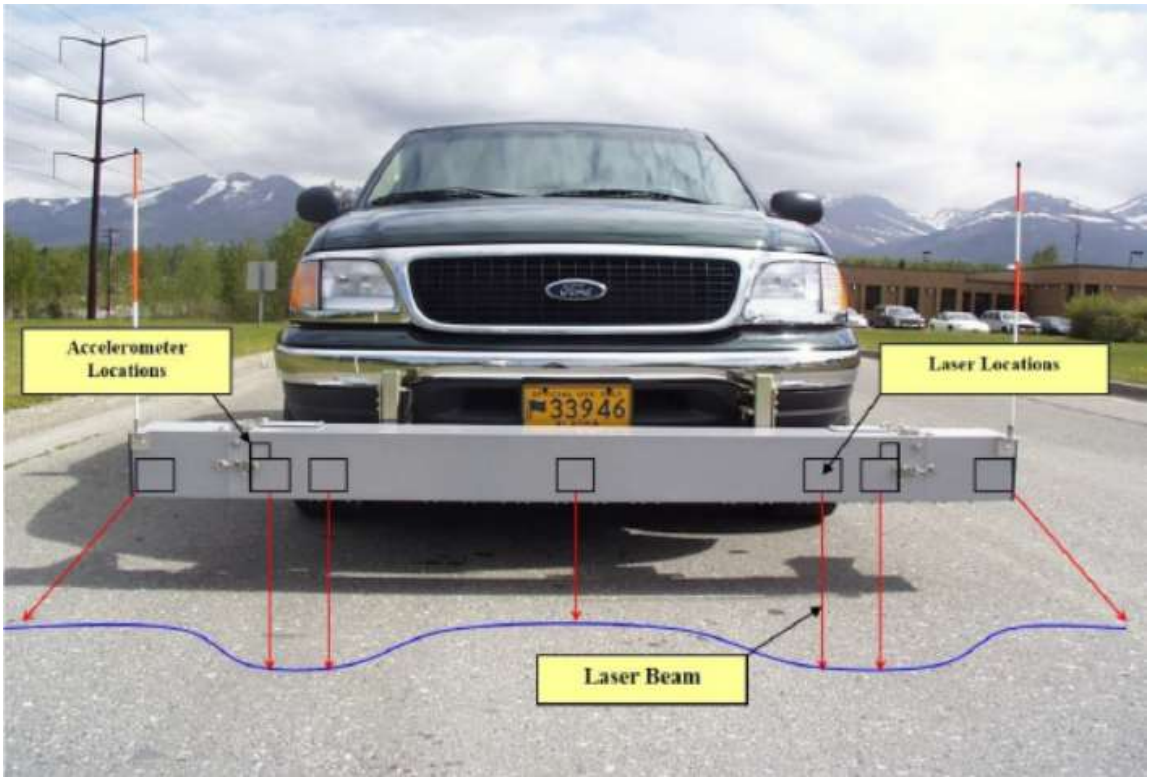

Figure 10: Rut Surface Profiler (Dahms, 2020).

Skid resistance tests were conducted at each of the on-site testing locations following the American Society for Testing and Materials (ASTM) E303 – 93, "Standard Test Method for Measuring Surface Frictional Properties Using the British Pendulum Tester." This step represents the safety aspect of the comparative analysis. The locations of the road section tests are shown in Figure 2. Figure 11 shows typical testing done on SFRRC and HMA at the Abbott Road test section.

Figure 11: Skid resistance testing for SFRRC and HMA (Abaza, 2017).

Life-Cycle Cost

A life-cycle cost analysis was conducted using the following methodology:

1. Determine items necessary for conducting the analysis:
   a. Review literature on life-cycle analysis
      i. Ontario, Asphalt vs. Concrete (Applied Research Associates, Inc., 2011)
      ii. Villacres, J, Pavement Life-Cycle Cost Studies Using Actual Cost Data
   b. AADT and vehicle classification (mainly % of trucks)
   c. HMA type (mainly three types)
   d. Structural section (surface course and subsequent lifts)
   e. Excavation
   f. Striping
   g. Unit prices per pavement type/mix
   h. Routine maintenance
      i. Rout and seal
      ii. Mill HMA
      iii. Traffic control
      iv. Marking/striping per year/cycle and cost
   i. Net present worth analysis
      i. Discount rate in Alaska

2. Research major arterials with highway pavement resurfacing for cost analysis:
   a. ArcGIS
   b. As-builts
   c. EDocs system
   d. Bid tabs
   e. Verify resurfacing conducted due to poor pavement condition
      i. IRI annual data
      ii. Rut profile/radius of curvature if available
      iii. As-built documents

3. Determine cost per square foot for a proposed analysis period based on rehabilitation/maintenance, initial costs, and present worth.
4. Per rut developed from the test section for SFRRC and HMA, a life cycle cost will be developed using the present worth method. A comparative analysis of the rut development for HMA from other arterials in the Central Region with similar road characteristics will be used to further validate the rut development of HMA on-site to take into consideration the full surface life rather than 2½ years of data.

Based on the LCC developed, in addition to other technical outcomes from the SFRRC test section, recommendations will be given on the further use of SFRRC material in Alaska's roadway network, mainly for highway intersections and test sections on major arterials as a next step.

CHAPTER 3 – INTERPRETATION, APPRAISAL, AND APPLICATIONS

The use of steel fiber-reinforced rubberized concrete (SFRRC) as paving material in Alaska, a cold region environment, was tested in a laboratory setting and proved successful at addressing the crucial issues of pavement distress in the state. Field validation of SFRRC was needed, using the same parameters tested in the lab in addition to observing pavement response to traffic loads, the impact of environmental conditions, and surface characteristics. The outcome of the assessment of SFRRC based on the collection of 2½ years of field data is as follows:

Assessment of Strain Gauge Sensor Data

The following are the findings of the strain gauge data analysis (Appendix B):

- Strains in the SFRRC slab on Abbott Road follow the norms of expansion and contraction with change in pavement temperature expected from a rigid pavement structure.
- Strains taken at the corner, center, and edge of the SFRRC slabs showed higher values at the corner followed by the edge and the center, respectively. Some variation exists depending on the moisture conditions underneath the slabs as well as the slab confinement conditions.
- Of the three slabs embedded with strain gauges, sensors in slabs four and eight provided a more reliable outcome than slab thirteen.
- It was determined that each slab has its own characteristics with regard to strain values depending on conditions of basin and placement of the slabs, and can be analyzed separately, but still follows the general trends in rigid pavements.
- The coefficient of thermal expansion (CTE) for SFRRC was reported to be 3.60×10^{-6} /°C (6.48×10^{-6} /°F) reflecting 38% of the mechanistic-empirical pavement design guide (MEPDG) American Association of State Highway and Transportation Officials (AASHTO) recommended value.
- The CTE value for SFRRC can significantly reduce the design of the joint opening for jointed concrete pavements (JCP), which will result in reducing stresses on the dowel bars. In addition, this will reduce dowel bar diameter and might eliminate the use of temperature reinforcement required in jointed reinforced concrete pavements (JRCP).
- The CTE for SFRRC allows for longer joint spacing, reducing the cost of JCP.

Assessment of Falling Weight Deflectometer Data

The following are the findings of the pavement deflections analysis using the falling weight deflectometer (FWD) data (Appendix C):

- Cases of deflections in SFRRC follow normal trends in rigid pavements, where maximum deflections were reported at the corner of the slab followed by the edge and the center, respectively.
- The FWD testing performed on the SFRRC test section showed seasonal deflection behaviors based on the conditions of the base/subgrade (basin). Deflections reported for the three loading cases were higher at the end of the winter season than at the end of the summer season.

- Load transfer efficiency (LTE) recorded at the joints was 90% and 95% for the end of the winter and summer seasons, respectively. Dowel bars incorporated in the SFRRC joints are working efficiently and are expected to transfer loads across the joints.
- Deflection behavior in SFRRC showed no signs of deficiency in load-carrying capacity for the material or the dowel bars.
- Comparative analysis of deflection showed lower maximum deflections under the applied wheel load for SFRRC than for HMA, suggesting that SFRRC performs better at overcoming frost heave action in the pavement basin. This finding might affect truck weight limits and duration enforced during the spring season.
- Back-calculation based on the field deflection of SFRRC showed overdesign of about 20% in thickness compared with the ACI rigid pavement design method.

Assessment of Rut Data

Rut depth readings were collected over the project's duration to provide a comparative analysis of rut development in SFRRC and HMA paving materials on Abbott Road. Locations of rut measurement are shown in Figure 2. Figure 12 gives the actual readings over the study period. Locations 1 and 5 are on the HMA surface located before and after the SFRRC test section, and Locations 2, 3, and 4 are on slab numbers four, seven, and eleven of the SFRRC surface test section. HMA rut development follows the normal trend in the area for arterial roads per the findings of the DOT&PF report titled "Survey and Economic Analysis of Pavement Impacts from Studded Tire Use in Alaska" (Abaza, 2019). SFRRC showed very mild rut development compared to HMA before and after the test section. Concrete does not rut under wheel loads (Halsted, 2009). The rut readings measured on SFRRC are due to studded tire use during wintertime and normal wear as a result of traction between wheel and surface.

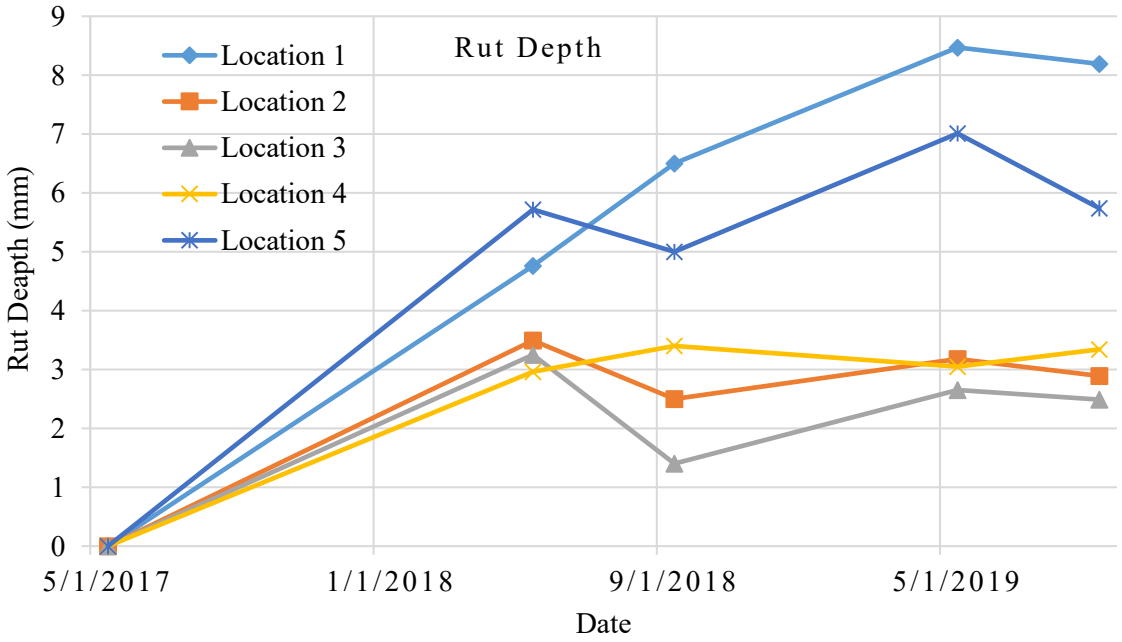

Figure 12: Actual rut readings on Abbott Road over the study period.

Average rutting for SFRRC and HMA based on the values measured are shown in Figure 13 as well as the historic rut data for Abbott Road (DOT&PF-PMS database) between Lake Otis Parkway and Elmore Road, where the test section is located. Figure 13 shows the general trend for rut development over the study period and the three historic maintenance cycles from 2000–2016. The historic reduction in rutting over time for the three cycles reflects the improvement in mix designs using improved aggregates and polymer modifiers. In addition, the maintenance/reconstruction in 2017 showed further improvement in this regard. The rutting trend for the new SFRRC material indicates superior performance over the HMA.

Based on the three historic cycles, the actual average overall rut depth at the time of maintenance was 0.97 in., which suggests that the next maintenance for HMA should occur in about the year 2030, with an overall service life of about 13 years. Comparative performance analysis of HMA and SFRRC shows that SFRRC can have a maintenance cycle that is about three times (3.28) longer than HMA. Appendix D gives a more detailed analysis on the rut development and rut rates of HMA and SFRRC on Abbott Road.

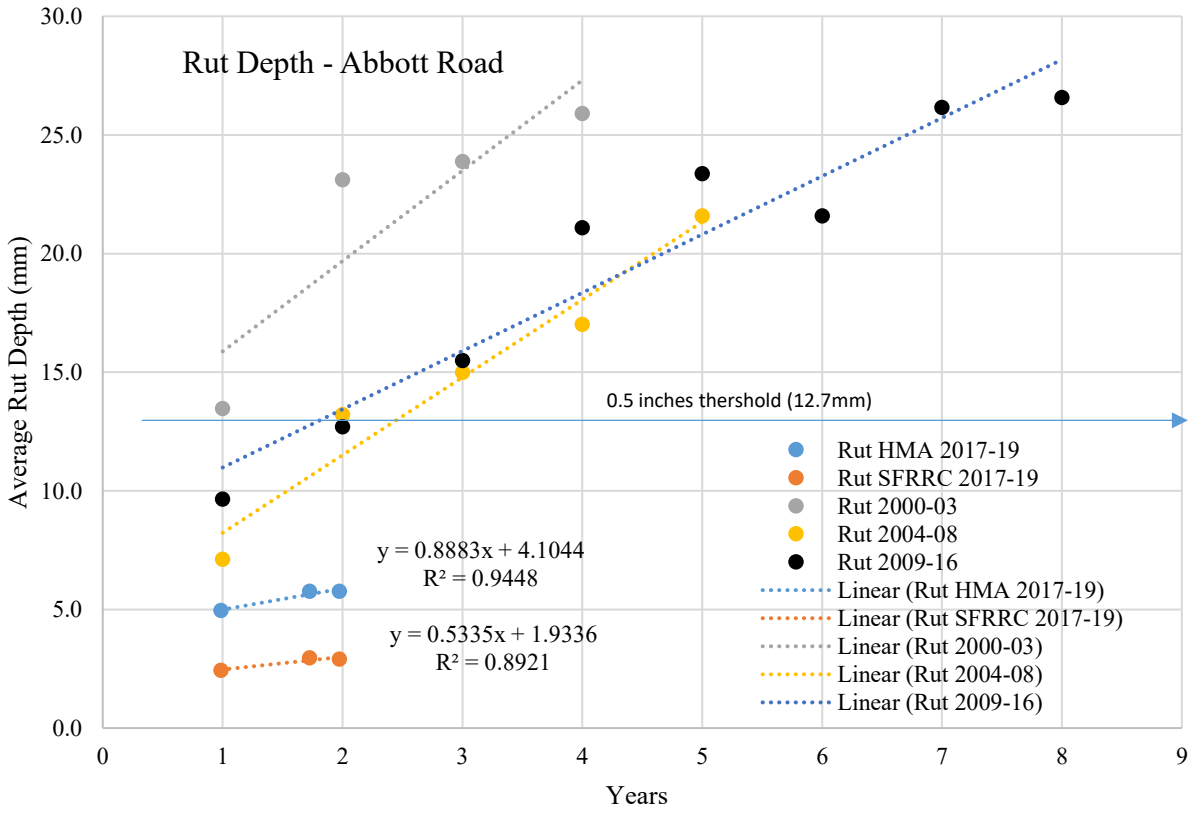

Figure 13: Average rut depth for HMA, SFRRC, and historic HMA rut on Abbott Road between Lake Otis and Elmore Road.

The following are the findings of the pavement rut data analysis:

- The SFRRC test section showed superior performance at resisting the impact of studded tires in comparison to the current HMA section as well as the historic data of HMA on the same road section.
- Rut data validate the lab results conducted in Phase I of the project.

- Comparative analysis of HMA and SFRRC rut resistance performance shows that SFRRC can have a maintenance cycle that is about three time (3.28) longer than HMA under the same traffic conditions.
- The rut rate of SFRRC is about 44% that of HMA based on the current mix design used on Abbott Road, and the rut rate is expected to decrease with time, as SFRRC does not rut under wheel loads.
- Historic data on the same road section showed an improvement in HMA mix design as reflected in rut development over several cycles of rehabilitation/maintenance on Abbott Road.
- Rut performance measurement of the SFRRC test section over the coming years is highly recommended, as the latest readings showed mild change and flattening of the curve, indicating very slow rut development compared with HMA. The overall future rut rate might be significantly lower than the measured value to date.

Assessment of Visual Inspection

Several parameters were used to evaluate the integrity of SFRRC using visual inspection including freeze-thaw deterioration, abrasion/erosion, plastic shrinkage cracking, drying shrinkage cracking, thermal cracking, overload damage, loss of support, corrosion of embedded steel fiber, frost heave, surface defects, joint openings, grout condition, and finished surfaces.

One of the distinguishing features in the new SFRRC material is the use of flat end steel fiber, which acts as distributed reinforcement throughout the volume of the material. Distributed reinforcement usually prevents any development of cracks/micro-cracks in the material in all directions rather than around the typical reinforcements used to control expansion and contraction. Traditional reinforcement provides localized control of stresses, creating inconsistencies in the way stresses are distributed throughout the concrete mass. In addition, random distribution of steel fiber provides better control of material expansion and contraction. Most of the surface defects in concrete discussed in this section can be prevented/controlled by using steel fiber. Furthermore, the use of crumbed rubber in the mix will give the material more flexibility under severe cold climate conditions.

The main key parameters related to the new SFRRC observed over the monitoring period are presented in this section. More details are provided in Appendix E.

Freeze-thaw deterioration

When water/moisture freezes in concrete, it produces pressure in the capillaries and pores of the concrete. If the pressure exceeds the tensile strength of the concrete, the cavity will dilate and rupture. The cumulative effect of successive freeze-thaw cycles and disruption of paste and aggregate can eventually cause significant expansion and cracking, scaling, and crumbling of the concrete (PCA). Alaska is categorized as having greater frequency of exposure to freeze-thaw cycles than most regions in the United States. Freeze-thaw testing in Phase I showed no signs of damage in the SFRRC in the lab environment as well as in the UAA trial slab. The field observations added crucial data for future use of this material. Typical signs of freeze-thaw can be noticed in the form of scaling of the concrete surface as shown in Figure 14a. No signs of scaling were noticed on the SFRRC test section over the project period as shown in Figure 14b. In addition to steel fiber and crumbed rubber in the SFRRC, air entrainment helped prevent freeze-thaw deterioration.

a. PCA, IS536 b. Abaza, July, 2020

Figure 14: (a) Freeze-thaw scaling of concrete slabs, (b) SFRRC surface on Abbott Road.

Abrasion/erosion

Abrasion damage in PCC occurs when the surface of concrete is unable to resist wear caused by rubbing and friction. As the outer paste of concrete wears, fine aggregate and coarse aggregate are exposed, and abrasion and impact will cause additional degradation related to aggregate-to-paste bond strength and hardness of the aggregate. Tire chains and studded snow tires cause considerable wear to concrete surfaces. In the case of tire chains, wear is caused by flailing and scuffing as the rotating tire brings the metal in contact with the concrete surface (PCA). One of the main objectives in developing SFRRC is its use as a pavement material in cold region environments. In Alaska, the use of studded tires to improve traction is common, but this practice creates a challenge for building an abrasion-resistant surface that will withstand such aggressive action. Roadway rutting is a visible sign of studded tire use. Abrasion of floors and pavements may result from production operations or vehicular traffic. Many industrial floors as well are subjected to abrasion by steel or hard rubber wheeled traffic, which can cause significant rutting. Figure 15 shows an example of visible signs of rutting on typical rigid pavement. Figure 16 shows the developed rut on HMA adjacent to the test slabs 1 year after construction. Figure 17 shows a snapshot of SFRRC on Abbott Road. No notable signs of rut are visible on the SFRRC test section. Appendix E provides further details on measured rut depth of HMA and SFRRC.

Figure 15: Typical rigid pavement rut (PCA [70156]).

Figure 16: HMA rut on Abbott Road (Abaza, 2018).

Figure 17: SFRRC Abbott Road (Abaza, 2018).

Thermal cracking

Concrete expands when heated and contracts when cooled. An average value for the thermal expansion of concrete is about 10 millionths per degree Celsius (5.5 millionths per degree Fahrenheit) (PCA). This amounts to a length change of 5 mm for 10 m of concrete (2⁄3 in. for 100 ft of concrete) subjected to a rise or fall of 50°C (90°F). Thermal expansion and contraction of concrete varies with factors such as aggregate type, cement content, water-cement ratio, temperature range, concrete age, and relative humidity. Allowing for movement by using properly designed expansion or isolation joints will help minimize the effects of temperature variations. In the case of SFRRC, the inclusion of steel fiber significantly reduces expansion and contraction, eventually reducing the effect of thermal cracking (see Appendix D for field strain gauge measurements). In addition, expansion joints were considered in the design of the SFRRC test section. No signs of thermal cracking are visible in the SFRRC test section, as shown in Figure 18.

a. (ACI) b. Abaza (July, 2020)

Figure 18: (a) Typical thermal cracking in concrete slabs, (b) SFRCC.

Corrosion of embedded steel fiber

Corrosion of reinforcing steel and other embedded metals is the leading cause of deterioration in concrete. When steel corrodes, the resulting rust occupies a greater volume than steel. This expansion creates tensile stresses in the concrete, which can eventually cause cracking, delamination, and spalling. In the case of the test section on Abbott Road, steel fibers were used to enhance the material characteristics for cold region environments. The steel fibers showed no signs of corrosion, and no signs of damage to the concrete material were noted. Figure 19 shows an example of visible steel fiber on-site.

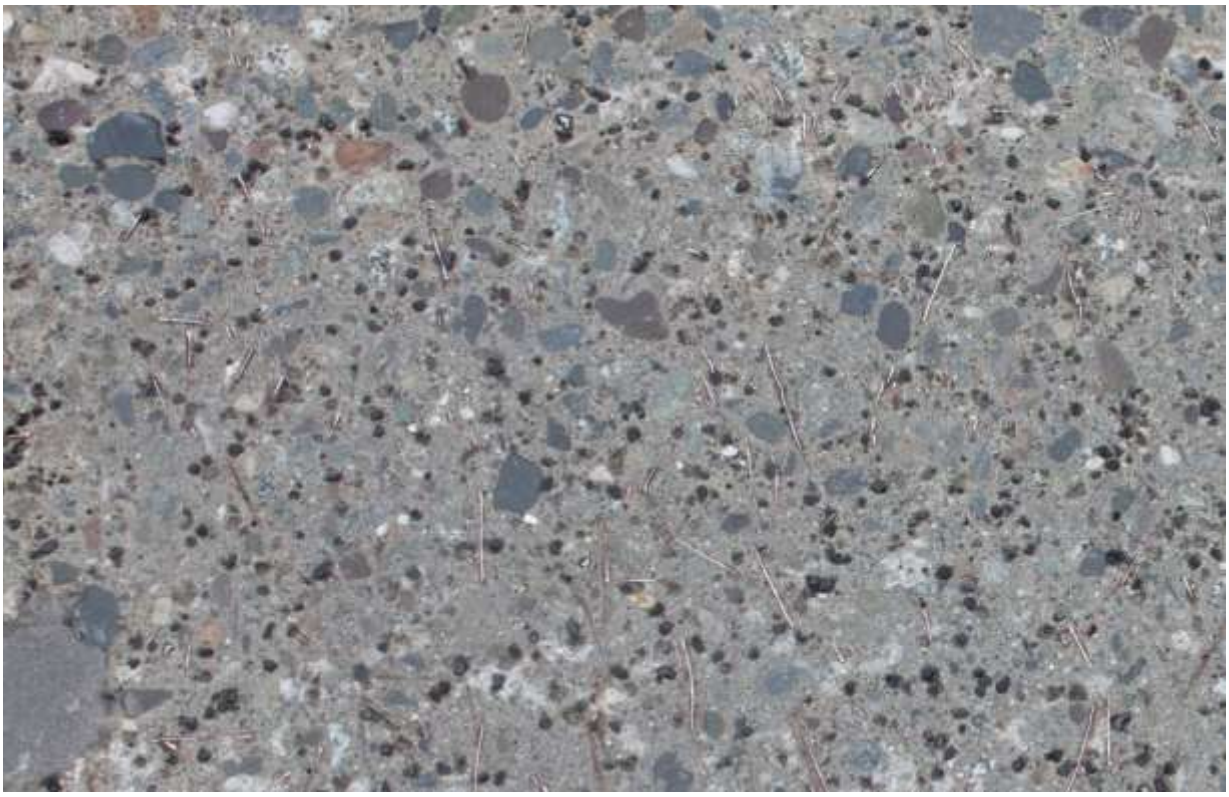

Figure 19: Steel fiber in the test section (Abaza, July 2020).

Frost heave

Frost heaves are upward swelling of soil/base during freezing conditions caused by an increasing presence of ice as it grows towards the surface, upwards from the soil depth where freezing temperatures have penetrated the soil or base. In the design of the SFRRC test section, special precautions were taken to reduce the impact of frost heave by building a non-frost susceptible base layer to a depth proportional to frost penetration in the locality. Concrete is less dependent upon subgrade soils and is better able to "bridge" soft spots (Thomas, 2020). No signs of frost heave or upheaval were noted during the monitoring period.

The following are the findings of the visual inspection analysis:

- All possible defects that might occur in normal PCC were monitored on the SFRRC test section, and no defects were reported based on visual inspection. This includes freeze-thaw deterioration, abrasion/erosion, plastic shrinkage cracking, drying shrinkage cracking, thermal cracking, overload damage, loss of support, corrosion of embedded steel fiber, frost heave, surface defects, joint openings, grout condition, and finished surfaces.
- Exposed crumbed rubber on the surface resulted from wearing of the thin layer of paste on the surface and poses no structural or functional issues.
- No pop-out steel fiber was noticed on the SFRRC surface during the monitoring period, and no loose steel fiber was noticed on the side of the road.
- Some exposed lateral steel fiber was noticed on limited spots as a result of wearing of the thin paste layer on the surface, and poses no structural or functional issues.

Assessment of Skid Resistance Data

Skid resistance testing was done to investigate surface microtexture differences between the two paving materials, SFRRC and HMA, used on Abbott Road. Skid resistance readings were collected over the project duration to provide this comparative analysis. Locations of skid resistance measurements are addressed in Figure 2. Table 1 and Figure 20 show the actual readings over the project period. Readings one, two, and three were taken on the SFRRC test section, and reading four on the HMA surface after the test section. Figure 21 shows the average readings of skid resistance over the study period. The overall average difference between the two materials indicates that SFRRC skid resistance is higher by about 5%.

Table 1: Skid resistance readings on Abbott Road.

Skid Resistance Readings (British Pendulum Numbers [BPNs])				
Date	**5/9/2017**	**5/15/2018**	**9/1/2018**	**5/1/2019**
Location 1	50.9	62.8	57	64
Location 2	49.6	62.7	56	69.33
Location 3	54.9	58.8	56	64
Location 4		57.8	51	58.33

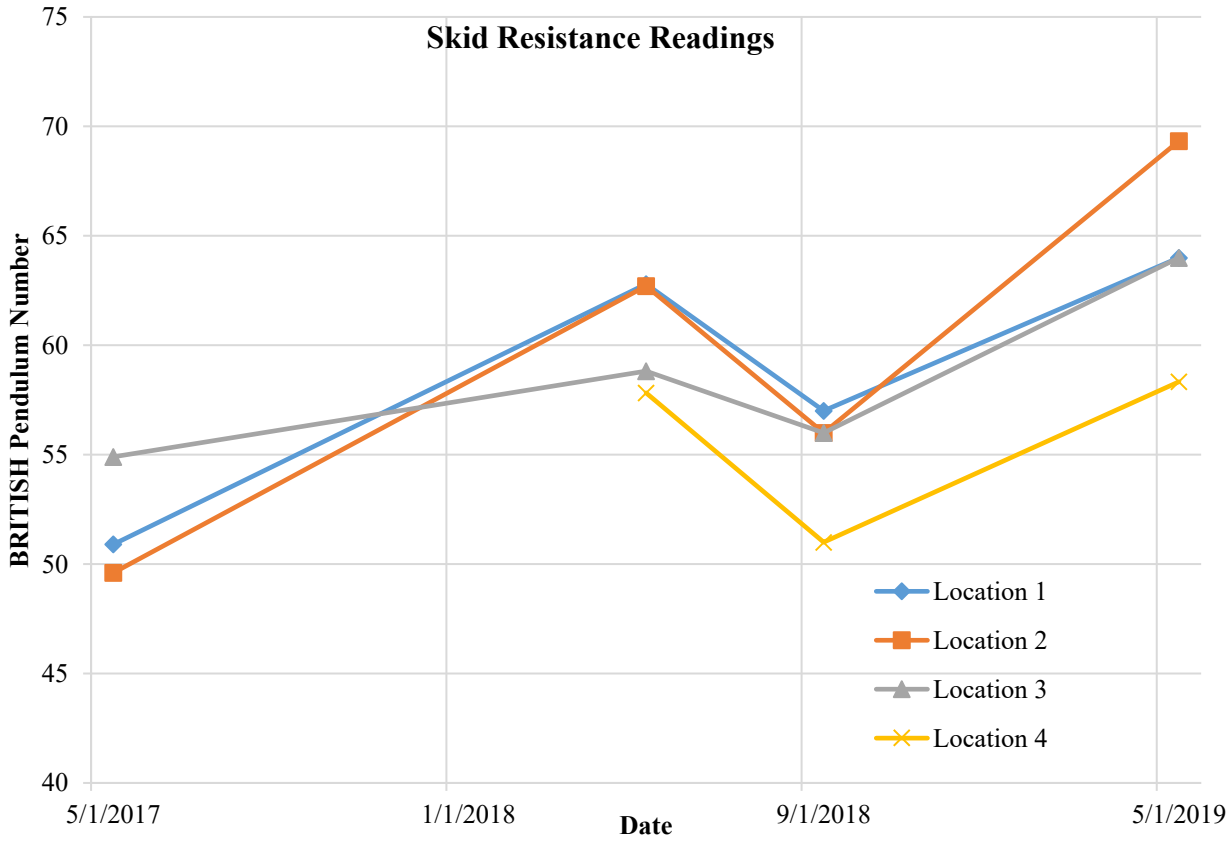

Figure 20: Skid resistance reading on Abbott Road.

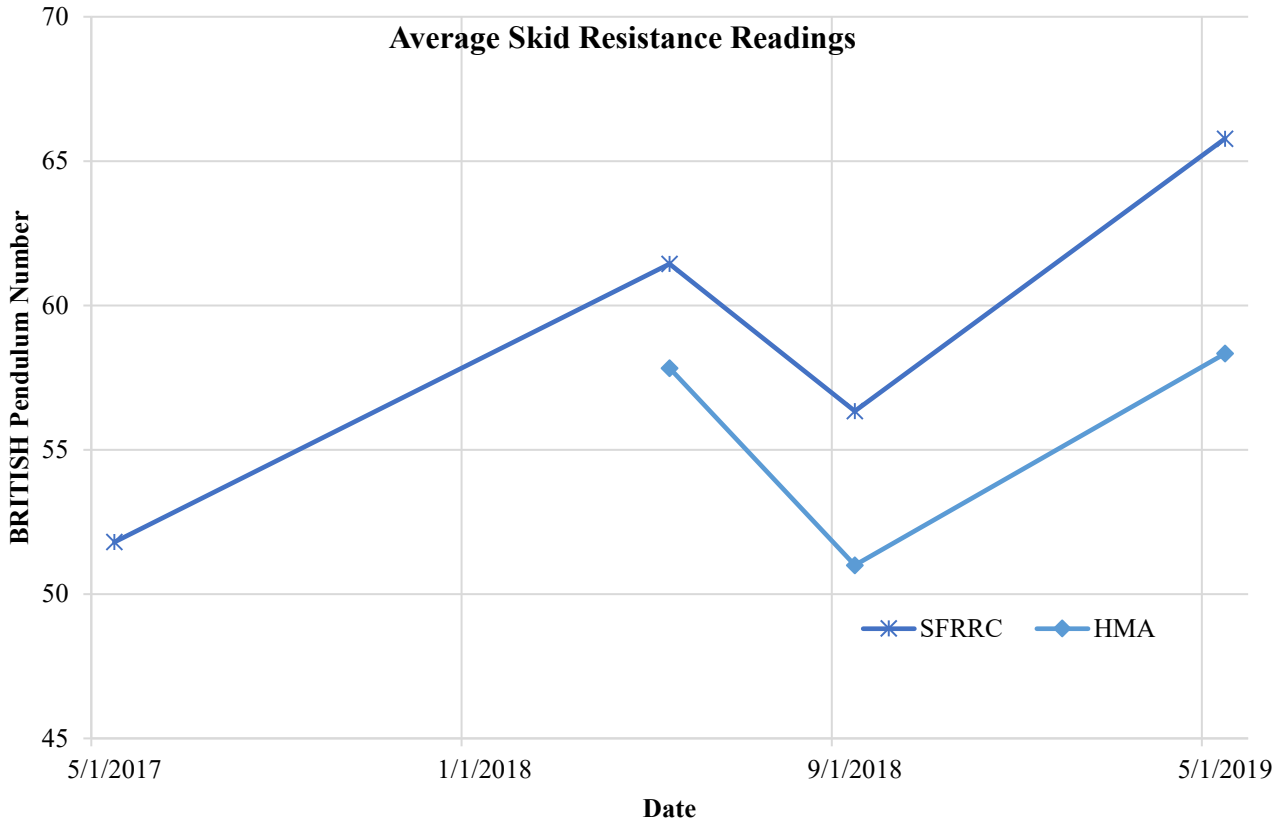

Figure 21: Average skid resistance readings on Abbott Road.

The following are the findings of the analysis of skid resistance data (Appendix F):

- British pendulum numbers (BPNs) reported for HMA are typical for this material, with those of Abbott Road being higher compared with those reported by Masad et al. (2008).
- BPNs for PCC are usually higher than HMA depending on the kind of concrete and aggregate used. The general trend of SFRRC skid resistance readings is consistent with the trend in the rigid pavement studies cited (Ahammed and Tighe, 1997).
- The overall average difference between HMA and SFRRC BPNs is 5% with SFRRC being higher.
- Analysis of the Long Term Pavement Performance (LTPP) program data has shown that surface friction reduces at 0.7 skid number (SN) and 1.2 SN per year for PCC and asphalt concrete (AC) pavements, respectively (Ahammed, 2009).
- Measurement of the skid resistance of HMA and SFRRC on the Abbott Road section over time is highly recommended for validation of skid resistance performance.

Assessment of Life-cycle Cost

The following are the findings of the life-cycle cost (LCC) analysis (Appendix H):

- Evaluation of the LCC of HMA was based on actual resurfacing/rehabilitation projects using HMA implemented in the state by Alaska DOT&PF.

- The LCC for SFRRC was based on the cost of the precast slabs installed on Abbott Road as well as real-life projects implemented in the Lower 48 for PCC, adjusted for the cost of steel fiber and rubber content additives to account for the limited scale of the SFRRC job on Abbott Road and the lack of a bidding process for full-scale application of this material.
- The SFRRC LCC worst-case scenario was adopted for comparative analysis of the potential trial use of this material for highway intersections.
- An analysis period of 43 years was considered for comparative analysis of HMA and SFRRC.
- The LCC of SFRRC over the analysis period showed $0.64 million per linear lane mile compared with $1.36 million for HMA for the same period.
- The cost ratio of HMA to SFRRC is about 2.1 to 1.0 over the analysis period.
- Several cost items were not considered in the LCC, such as routine maintenance during the analysis period; the thickness adjustment for SFRRC based on back-calculation of field deflections; the FHWY-DOT&PF adopted rut threshold of 0.5 inch; crash cost as a result of ruts; and highway user cost as a result of traffic interruptions during resurfacings/rehabilitations.
- Based on the comparative LCC of the materials considered for future paving, SFRRC can be explored further for use on an experimental basis for highway intersections and for test sections on major arterials.

CHAPTER 4 – CONCLUSIONS AND RECOMMENDATIONS

Monitoring of the SFRRC experimental precast slabs over a period of 2½ years, analysis of the sensor, and on-site data suggest that performance of the newly developed SFRRC material has advantages over traditional HMA pavement for cold regions paving applications, especially in regions where winter studded tire use is common. The results of Phase II further validate the laboratory results and performance of the trial slab at the UAA campus, which were part of Phase I of this study. The LCC analysis of the two paving materials shows that SFRRC is cost-effective over the life of the structure and demonstrates superior performance. Based on the findings of this project, SFRRC can be explored further for use on an experimental basis at highway intersections as well as for test sections on major arterials.

Modifications in construction practices when using the newly developed material as well as implementation of a long-term monitoring scheme are recommended. The process for placement of the pre-cast panels required approximately 4–5 days of work and was considerably more expensive than pouring in place. Pouring in place provides a smoother and better final product if the standard measures of placing and curing of the material are adopted. Note that pouring in place requires less equipment. Based on the total time needed to prepare the bedding layer, place the pre-cast panels, grout, and place the joint sealant, it is recommend that pouring in place be considered as a viable option in future work. Furthermore, continuous monitoring of the SFRRC slabs on Abbott Road by DOT&PF is highly recommended, as rut development in SFRRC, for example, showed a flattening trend contrary to HMA in its current mix design or the historical rut data on that road. The local cost of SFRRC should be reviewed, as the current cost per cubic yard for the Abbott Road project had a value of about 2.5 that of similar PCC having the same compressive strength, while the cost of material and labor for pouring in place of SFRRC are about 1.6.

REFERENCES

A Synthesis on Studded Tires. Washington State Department of Transportation Research Report WA-RD 471.1. Washington State Department of Transportation. Olympia, WA.

AASHTO. (1976). Task Force for Pavement Design of the AASHTO Operating Subcommittee on Design. Guidelines for Skid Resistant Pavement Design. American Association of State Highway and Transportation Officials. Washington, DC.

AASHTO. (1993). Guide for Design of Pavement Structures. American Association of State Highway and Transportation Officials; Washington, DC, USA.

AASHTO. (2008). Mechanistic-empirical pavement design guide – A manual of practice, Interim Ed., Washington, DC.

Abaza, O. (2019). Survey and Economic Analysis of Pavement Impacts from Studded Tire Use in Alaska. Report No. FHWA-AK-RD-4000(175), (pp. 1–95). Anchorage, Alaska.

Abaza, O., and Abou Eid, M. (2017). Use of Steel Fiber-Reinforced Rubberized Concrete in Cold Regions. Alaska DOT&PF, FHWA-AK-RD-76319, HFHWY00001 report.

Abaza, O., and Hussein, Z.S. (2016). Flexural Behavior of Steel Fiber-Reinforced Rubberized Concrete. Journal of Materials in Civil Engineering, 163–170.

Abaza, O., Chowdhury, T., and Arafat, M. (2019). "Evaluating Laboratory Rutting Performance of HMA Under A New Studded Tire Protocol for Cold Climates." Transportation Research Board 2019 Annual Meeting, Washington, DC, January.

ACI Committee 201. (1992). Guide to Durable Concrete, ACI 201.2R-92, American Concrete Institute, Farmington Hills, Michigan.

ACI Committee 222. (2001). Protection of Metals in Concrete Against Corrosion, ACI 222R-01, American Concrete Institute, Farmington Hills, Michigan.

ACI Committee 224. (1993). Causes, Prevention, and Repair of Cracks in Concrete, ACI 224.1R-93, American Concrete Institute, Farmington Hills, Michigan.

Ahammed and Tighe (2007), Evaluating skid resistance of different asphalt concrete mixes, Building and Environment, 42(1`): 325-329.

Ahammed, M.A., (2009). Safe, "Quiet and Durable Pavement Surfaces", Doctoral Dissertation, Department of Civil and Environmental Engineering, University of Waterloo, Ontario, Canada.

Alland, K., Bech, N, and Vandenbossche, J (2017), Interrupting Falling Weight Deflectometer (FWD) Data for Asphalt and Concrete Pavements, University of Pittsburgh for Commonwealth of Pennsylvania Department of Transportation.

American Concrete Pavement Association (ACPA). (1991). Design and construction of joints for concrete highways. Illinois.

Annual Book of ASTM Standards, Section four: Construction. Vol. 4.03. American Society for Testing and Materials. West Conshohocken, PA.

Applied Research Associates, Inc. (2011). Methodology for the development of Equivalent Pavement Structural Design Matrix for Municipal Roadways Including Maintenance and Rehabilitation Schedules and Life Cycle Cost Analysis. Toronto: Applied Research Associates, Inc.

ARA, Inc. (2013), Evaluating Pavement Markings on Portland Cement Concrete (PCC) and Various Asphalt Surfaces: Results of Year 1, 2, 3, and 4 Data Collection, Illinois Department of Transportation Bureau of Materials and Physical Research.

ASTM 1703 Standard (2015), Standard Test Method for Measuring Rut-Depth of Pavement Surfaces Using a Straightedge.

ASTM E303 – 93. (2013). "Standard Test Method for Measuring Surface Frictional Properties Using the British Pendulum Tester." (Reapproved 2013).

ASTM E1703 / E1703M – 10. (2015). "Standard Test Method for Measuring Rut-Depth of Pavement Surfaces Using a Straightedge."

Avanaki, Mohammad Jamshidi. (2019). "Response Modification Factors for Seismic Design of Steel Fiber Reinforced Concrete Segmental Tunnels." Construction and Building Materials, Vol. 211, Elsevier.

Avishreshth, Bansal, Prem Pal, and Chopra, Tanuj. (2017). "Characterization of Steel Fiber Reinforced Pervious Concrete for Applications in Low Volume Traffic Roads." ASCE Conference, New Delhi, India.

Bishnoi, Shashank. (2004). "Strain variations in concrete subjected to cyclic freezing and thawing." Thesis, Department of Civil Engineering, University of Tokyo, Tokyo, Japan.

Bouteillier, C., and Gustafson, W. (2017). "Life Cycle Cost Analysis Considerations in Pavement Type Selection in Red Deer and Construction Challenges." Transportation Association of Canada, Ottawa, Ontario.

Brunette, B., and Lundy, J. (1996). "Use and Effects of Studded Tires on Oregon Pavements." Transportation Research Record, Issue Number 1536, ISSN: 0361-1981.

Concrete in Practice. (1998). National Ready Mix Concrete Association (NRMCA).

Corley-Lay, 1998, Friction and Surface Texture Characterization of 14 Pavement Test Sections in Greenville, North Carolina. Transportation Research Record 1639. Transportation Research Board, National Research Council. Washington, D.C. pp. 155-161.

Correction of Field Skid Measurements for Seasonal Variations in Texas. Transportation Research Record 1639. Transportation Research Board, National Research Council, Washington, DC, pp. 147–154.

Dahms, D. (2020). "Studded Tire Wear Performance Evaluation of the Asphalt Mix Designs of the State of Alaska." Thesis, University of Alaska Anchorage, June.

Damon Thomas. (2006). "Choosing between asphalt and concrete pavement." Concrete construction, https://www.concreteconstruction.net/business/management/choosing-between-asphalt-and-concrete-pavement_o, as of July 2020.

Dwyer, Carmine E., Vavrik, William R., and Becker, Rachel L. (2013). "Evaluating Pavement Markings on Portland Cement Concrete (PCC) and Various Asphalt Surfaces: Results of Year 1, 2, 3, and 4 Data Collection." Applied Research Associates, Incorporated, Champaign, IL.

Embacher, R., and Snyder, M. (2001). "Life-Cycle Cost Comparison of Asphalt and Concrete Pavements on Low-Volume Roads: Case Study Comparisons." Transportation Research Record No. 1749, Maintenance of Transportation Pavements and Structures, Washington, DC.

Freeze Thaw Resistance of Pervious Concrete. (2004). National Ready Mix Concrete Association (NRMCA), May.

Friction and Surface Texture Characterization of 14 Pavement Test Sections in Greenville, North Carolina. Transportation Research Record 1639. Transportation Research Board, National Research Council. Washington, DC, pp. 155–161.

Gschösser, F., and Wallbaum, H. (2013). Life Cycle Assessment of Representative Swiss Road Pavements for National Roads with an Accompanying Life Cycle Cost Analysis. Vol. 47, No. 15, pp. 8453–8461.

Gula, S., and Naseerb, S. (2019). "Concrete Containing Recycled Rubber Steel Fiber." Procedia Structural Integrity, Vol. 18, pp. 101–107.

Halsted, G. (2009). Roller-Compacted Concrete Pavements for Highways and Streets, Advances in Pavement Design and Construction, 2009 Annual Conference of the Transportation Association of Canada Vancouver, British Columbia.

Liu, H, Luo, G., Gong, Y., and Wei, H., (2018). "Mechanical Properties, Permeability, and Freeze-Thaw Resistance of Pervious Concrete Modified by Waste Crumb Rubbers." Applied Sciences, Materials, 8(10), 1843.

Havel, S., Archilla, A., and Shen, L. (2015). “Coefficient of Thermal Expansion of Concrete Mixes in Hawaii: Determination and Implications for Concrete Pavement Design.” ASCE Journal of Materials, 27(5): 04014164.

National Cooperative Highway Research Program Synthesis of Highway Practice 14: Skid Resistance. Highway Research Board, National Academy of Sciences, Washington, D.C.
Huang, Y.H. (2004). Pavement Analysis and Design. Upper Saddle River: Pearson Education, Inc.

Hoffman, M and Thompson, M (1981), Comparative Study of Selected Non destructive Testing Devices, Transportation Research Record 852.

Ingrassia, L, Virgili, A and Canestrari, F (2020), Effect of geocomposite reinforcement on the performance of thin asphalt pavements: accelerated pavement testing and laboratory analysis, Case Studies in Construction Materials, Volume 12, June 2020, e00342.

Jahangirnejad, S., Buch, N., and Kravchenko, A. (2009). “Evaluation of coefficient of thermal expansion test protocol and its impact on jointed concrete pavement performance.” ACI Mater. J., 106(1): 64–71.

Jayawickrama, P., and Thomas, B., (1998). “Correction of Field Skid Measurements for Seasonal Variations in Texas.” Transportation Research Record 1639. Transportation Research Board, National Research Council, Washington, DC. pp. 147–154.

Kay, R.K., Mahoney, J.P., and Jackson, N.C. (1993). The WSDOT Pavement Management System – A 1993 Update. Washington State Transportation Center (TRAC). Washington State Department of Transportation, Olympia, WA.

Khayat, Kamal H. (2020). “Performance-Based Specifications of Fiber-Reinforced Concrete with Adapted Rheology to Enhance Performance and Reduce Steel-Reinforcement in Structural Members.” MoDOT Research Report No. cmr 20-006, Missouri University of Science and Technology.

Masad, E., Rezaei, A., Chowdhury, A., and Harris, P. (2008).“Predicting Asphalt Mixture Skid Resistance Based on Aggregate Characteristics.” Texas A&M University for Texas Department of Transportation, FHWA/TX-09/0-5627-1.

McQueen, J., and Timm, D. (2005). “Statistical Analysis of Automated Versus Manual Pavement Condition Surveys.” Journal of Transportation Research Records, TRB, Washington, DC.

Minnesota DOT. (2005). Installation of Precast Concrete Pavement Panels on TH 62. Richfield: Minnesota DOT Office of Construction and Innovative Contracting.

National Academies of Sciences, Engineering, and Medicine 2008. Falling Weight Deflectometer Usage. Washington, DC: The National Academies Press. https://doi.org/10.17226/13675.

Robbins, M., and Tran, N., (2018), Review of Initial Service Life Determination in Life Cycle Cost Analysis (LCCA) Procedures and in Practice, National Center for Asphalt Technology.

National Ready Mixed Concrete Association, (2020), PI, https://pavementinteractive.org/reference-desk/pavement-management/pavement-evaluation/deflection/

National Cooperative Highway Research Program Synthesis of Highway Practice 14: Skid Resistance. Highway Research Board, National Academy of Sciences, Washington, DC.

NCHRP Synthesis 494. (2016). "Life-Cycle Cost Analysis for Management of Highway Assets." Project 20-05 (Topic 46-15) ISSN 0547-5570, Transportation Research Board Washington, DC.

New-Generation Skid Testers for the 1990s. Surface Characteristics of Roadways: International Research and Technologies, ASTM STP 1031, Meyer, W.E. and Reichert, J., eds. American Society for Testing and Materials. Philadelphia, PA. pp. 138–153.

Nondestructive Testing of Flexible Pavements Field Testing Program Summary. Report No. UILU-ENG-81-2003. Illinois Department of Transportation. Springfield, IL.

Rao, C. (2014), Guidelines for PCC Inputs to AASHTOWare Pavement ME, Mississippi Department of Transportation for, Federal Highway Administration, FHWA/MS-DOT-RD-14-260.

Robbins, M. and Tran, N (2018), Review of Initial Service Life Determination in Life Cycle Cost Analysis (LCCA) Procedures and in Practice, NRMCA.

Pavement Interactive. (2020). https://pavementinteractive.org/reference-desk/pavement-management/pavement-evaluation/deflection/, June.

PCA. (2001). Concrete Slab Surface Defects: Causes, Prevention, Repair, IS177, Portland Cement Association.

Pierce, L., Uhlmeyer, J., Weston, J., Lovejoy, J., and Mahoney, J.P. (2003). "Ten-Year Performance of Dowel Bar Retrofit—Application, Performance, and Lessons Learned." Transportation Research Record 1853, Transportation Research Board, National Research Council, Washington, DC, pp. 83–91.

Qi, Y., A. El Gendy, and F. Wang. (2012). Evaluation of MDOT's Distress Thresholds for Maintained Pavement Projects, State Study No. 221, Mississippi Department of Transportation, Jackson, MS, 2012. Available: https://rosap.ntl.bts.gov/view/dot/24969.

Raj, Anand, M.Tech; Praveen Nagarajan and Shashikala A P. (2020). "Application of Fiber Reinforced Rubcrete for Crash Barriers." *ASCE Materials Journal*.

Robbins, Mary, and Tran, Nam, (2018). "Review of Initial Service Life Determination in Life Cycle Cost Analysis (LCCA) Procedures and in Practice." National Center for Asphalt Technology, Auburn, AL.

Shoukry, S. (2005). "Evaluation of Load Transfer Efficiency Measurement." Report by West Virginia University, Mid-Atlantic Universities Transportation Center for West Virginia Department of Transportation, No. WVU-2002-04.

Smith, Tim. (2006), "Helping Build a Sustainable Future by Constructing Roadways with Portland Cement Concrete Pavement." Annual Conference & Exhibition of the Transportation Association of Canada, 2006. Charlottetown, Prince Edward Island, Canada.

Studded Tire Pavement Wear Reduction and Repair. (1973). Washington State Highway Department Research Program, Phase 1, Report No. 9.1.

Thomas, D. (2006), Choosing Between Asphalt and Concrete Pavement. Concrete construction, https://www.concreteconstruction.net/business/management/choosing-between-asphalt-and-concrete-pavement_o

Treleaven, L. (2010). *Use of PCC Pavement to Reduce Maintenance Costs and Address Urban Intersection Rutting.* Edmonton: EBA Engineering Consultants Ltd.

Trisch, Holly P. (2019). "Developing Performance Prediction Models for Flexible Pavements Using Rutting Criteria in Anchorage, Alaska." Thesis, University of Alaska Anchorage, December.

Uhlmeyer, J., and Pierce, L.M. (2001). "Reconstruction of Urban Intersections Using Portland Cement Concrete Pavement." Seventh International Conference on Concrete Pavements. The Use of Concrete in Developing Long-Lasting Pavement Solutions for the 21st Century, Orlando, Florida.

Villacres, Jorge N. (2005), "Pavement Life-Cycle Cost Studies Using Actual Cost Data – A Synthesis," Asphalt Pavement Alliance, Lexington, KY.

Vijay, P.V., Li, Hui, GangaRao, and Hota, V.S. (2020). "Laboratory testing, field construction, and decade long performance evaluation of jointed plain concrete pavement with FRP dowels." International Journal of Pavement Engineering, 21(6), Taylor & Francis.

2019 Report on the Life-Cycle Cost Analysis (2019), Minnesota Department of Transportation, St Paul, MN.

WSDOT – State Materials Laboratory. (2008). Pavements and Studded Tire Damage. Spokane: WSDOT.

LIST OF APPENDIXES

Appendix A – Literature Review

Introduction

The literature review in Appendix B of the project's previous phase, Phase I: Use of Steel Fiber-Reinforced Concrete in Cold Regions, stressed the development of materials to address design, maintenance, and environmental issues. More focus was placed on the use of steel fiber and crumb rubber in PCC. The purpose of this section in Phase II is to focus on the assessment of performance of PCC and HMA, the additional studies utilizing additives in highway pavements and other elements, and finally the life-cycle cost (LCC) of HMA and PCC pavements and their application.

Freeze-thaw assessment

A study conducted by Hanbing et al. (2018), titled "Mechanical Properties, Permeability, and Freeze-Thaw Resistance of Pervious Concrete Modified by Waste Crumb Rubbers," investigated the effect of rubber particle size (fine and coarse) and dosage (2%, 4%, 6%, and 8%) on the properties of pervious concrete. Permeability, compressive strength, flexural strength, flexural strain, and freeze-thaw resistance tests were carried out on rubber-modified pervious concrete. The study mainly addressed laboratory testing with an outcome that agrees with Phase I results; many other studies regarding compressive and flexural strengths arrived at the same conclusions. In addition, rubber-modified pervious concrete has better freeze-thaw resistance than that of control pervious concrete when subjected to the same freeze-thaw cycles. A high rubber incorporation level generates high freeze-thaw resistance. Fine crumb rubber is superior to coarse crumb rubber in improving the freeze-thaw resistance of pervious concrete. This is in agreement, too, with the freeze-thaw testing done in Phase I.

Another study by Terje Finnerup Rønning (2001) attempted to establish a correlation between the laboratory and field results for freeze-thaw performance. After two winter seasons of test section use at a highway with frequent usage of de-icing salt, all the mixes investigated had very small to no visible surface damages and no visible cracking. The study also indicated that 2 years of field exposure is too little time to draw conclusions of field performance and thus on the relation to laboratory testing.

Many field test sections for freeze-thaw evaluations used visual inspection as the only means of performance evaluation. A report by National Ready Mix Concrete Association (NRMCA, 2004) documented the freeze-thaw performance of pervious concrete for ten projects in many parts of the United States. The only means used in these projects was visual inspection, and the NRMCA's conclusion as to successful performance was based on field observation, noting that freeze-thaw damage in PCC might take several years before it is noticeable in the field. Without more sophisticated means of measuring expansion and contraction of the material, such as the use of strain gauge, it becomes difficult to predict freeze-thaw performance in the early stages of construction.

Many agencies developed a visual scheme for freeze-thaw inspection. The methods used by the NRMCA, American Concrete Institute (ACI), and Portland Cement Association (PCA) are among several examples of visual inspection used to identify signs of freeze-thaw damage. Scaling is the main sign of freeze-thaw damage, described as local flaking or peeling of the finished surface of hardened concrete. Generally, this damage starts with localized small patches which later may merge and extend to expose larger areas. Moderate scaling exposes the

aggregate and may involve loss of up to one-eighth to three-eighths of an inch of the surface. In severe scaling, more surface has been lost and aggregate is clearly exposed and noticeable.

Very little research utilizing strain readings in the assessment of freeze-thaw damage has been done. In one notable study, strain gauge embedded in PCC showed that an increase in the number of freeze-thaw cycles generates higher strains (Bishnoi, 2004). The results showed that the approximate shape of the strain-temperature curves remained the same with an increase in freeze-thaw cycles, but a shift occurred in the curves such that the strain increases with the progress of freeze-thaw cycles. This change in strain, when measured at the same temperature, with the progress of cyclic freezing and thawing is referred to as "Residual Strain." Though the strain-temperature behavior is not perfectly linear, a comparison of average slopes in the positive and negative temperature regions shows a higher strain-temperature rate below 0°C. This strain-temperature rate can be referred to as the apparent thermal expansion coefficient (α_{app}) since it represents the fractional change in length of the specimen upon inducing a 1°C temperature change in the specimen. Figure A1 shows a sample from this study, where the difference in the average apparent thermal expansion coefficients for the 7 cm specimen was used. A similar variation can be observed in the strain-temperature behavior of the larger specimens. The author stated that the quantification of damage in concrete in terms of residual strains would be advantageous for monitoring structural health and other parameters related to the strain-temperature behavior of concrete and can be used to evaluate and even predict the performance of concrete.

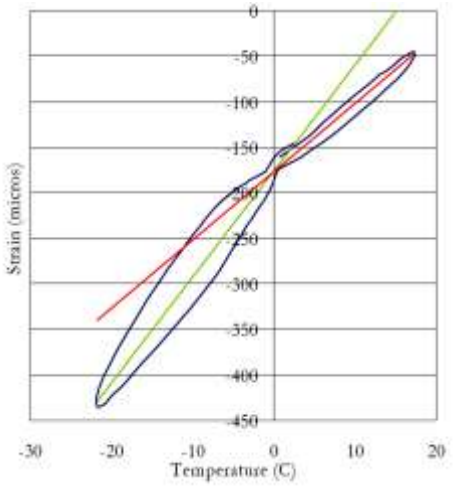

Figure A1: Higher apparent thermal expansion coefficient below 0°C (Bishnoi, 2004).

Bishnoi (2004) concluded that the strain-temperature trend of "healthy" concrete would display no discontinuous behavior and dilatations upon freezing. In addition, residual strains can be used as a quantitative measure of freeze-thaw deterioration.

Applications of steel fiber rubberized concrete

Since the development of SFRRC by Abaza and Hussein and the validation of their results in Phase I by Abaza and Abou Eid, several studies and applications of the use of crumbed rubber and steel fiber in PCC have been developed.

Khayat (2020) used steel fiber to retrofit bridges. The project seeks to optimize the coupled effect of fiber characteristics, an expansive agent (EA), saturated lightweight sand

(LWS), and external moisture curing on mechanical properties, shrinkage, and corrosion resistance of such classes of high-performance concrete. This project also aims to replace steel reinforcement in flexural members with steel fibers partially. Another study (Avishreshth et al., 2017) utilized steel fiber in pervious concrete for applications in low-volume traffic roads. The test results confirm that PCC with 1.5% hooked end (4-D) steel fibers showed the maximum increase in compressive and flexural strengths by 7.5% and 21.5%, respectively, over the control mix while maintaining adequate permeability. The improved flexural strength was later used for structural and hydrological design of pervious concrete pavement (PrCP). The inclusion of hooked end (4-D) steel fibers in PrCP reduced the slab thickness by 25 mm when compared with conventional PrCP.

Avanaki (2019) used steel fiber in fiber reinforced concrete (FRC) as the primary constitutive material of segmental tunnels in active seismic zones. Another application of steel fiber was used in the development of crash barriers for highways (Raj, 2020). One additional study that examined the recycled rubber steel fiber (RRSF) from waste tires concluded that the replacement rate up to 1% of RRSF by volume of concrete did influence the compressive and split tensile strength of concrete, but the samples with RRSF somehow showed ductile behavior rather than brittle. Such behavior can prove beneficial for structures that require good impact resistance properties. The author recommended the use of this kind of concrete for the construction of light-weight concrete structures (Gula and Naseerb, 2019).

The use of steel fiber in PCC is widespread for different structural and highway elements due to its impact resistance, higher toughness, and enhanced expansion and contraction characteristics. The use of crumbed rubber will further enhance these characteristics especially in cold region environments.

Assessment of deflections of SFRRC slab test section

Pavement surface deflection measurements are the primary means of evaluating a flexible pavement structure and rigid pavement load transfer. Although other measurements can be made that reflect (to some degree) a pavement's structural condition, surface deflection is an important pavement evaluation method because the magnitude and shape of pavement deflection is a function of traffic (type and volume), pavement structural section, temperature affecting the pavement structure, and moisture affecting the pavement structure. Deflection measurements can be used in back-calculation methods to determine pavement structural layer stiffness and the subgrade resilient modulus. Thus, many characteristics of a flexible pavement can be determined by measuring its deflection in response to load. Furthermore, pavement deflection measurements are non-destructive (NRMCA, 2020).

Surface deflection is measured as a pavement surface's vertical deflected distance as a result of an applied (either static or dynamic) load. More advanced measurement devices record this vertical deflection in multiple locations, which provides a more complete characterization of pavement deflection. The area of pavement deflection under and near the load application is collectively known as the "deflection basin." Deflections can be static using a Benkelman Beam, which is considered low-cost but is slow and labor intensive and does not provide a deflection basin. Deflection also can be steady-state, using equipment that measures the dynamic deflection of pavement produced by an oscillating load or impact load. The main advantage of steady-state deflection equipment over static deflection equipment is that it can measure a deflection basin. Dynaflect and Road Rater are the most common types of steady-state deflection equipment. The equipment is most suitable for use on thinner pavements, including low-volume rural highways,

county roads, municipal streets, and parking lots. Finally, deflection can be measured using impact (impulse) load response; all impact load devices deliver a transient impulse load to the pavement surface. The subsequent pavement response (deflection basin) is measured by a series of sensors. The most common type of impact load response equipment is the FWD. Figure A2 shows the FWD machine used in measuring deflections by Alaska DOT&PF at the SFRRC test section on Abbott Road.

Figure A2: FWD testing on Abbott Road (Abaza, 2018)

Correlations were built over the years between the different methods of measuring deflections, as addressed by WSDOT (1993), ASTM, Vol. 4.03, and Hoffman and Thompson (1981).

Ingrassia et al. (2020) assessed the effect of geocomposite reinforcement on fatigue cracking, reflective cracking, and permanent deformation accumulation of thin asphalt pavements. A full-scale trial section was constructed with different interfaces: unreinforced (reference) and reinforced with three types of geocomposites, formed by the combination of a bituminous membrane with a fabric or grid. The experimental program included accelerated pavement testing (APT) carried out by means of a fast-falling weight deflectometer (FastFWD) and laboratory tests (three point bending tests) on samples taken from the trial section. Figure A3 shows a comparative analysis from this study of the pavement surface deflection recorded at the end of APT sessions for all test fields for fatigue cracking (FC) sections and reflective cracking (RC) sections. The findings indicate that geocomposites can extend the service life of thin asphalt pavements in terms of both cracking and permanent deformation accumulation.

Another study evaluated the performance of jointed plain concrete pavement with fiber reinforced polymer (FRP) dowels and compared it with jointed plain concrete pavements (JPCPs) (Vijay et al., 2020). Some of the field evaluations consisted of static, dynamic, and FWD tests. After 5 and 13 years of field service, FWD tests showed that the LTE of joints with FRP dowels was around 90% and met the applicable performance requirements.

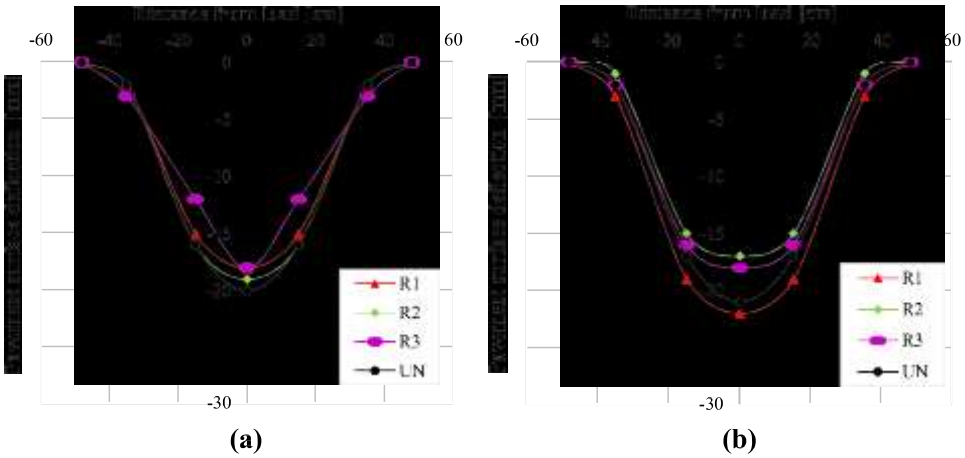

(a) (b)

Figure A3: Pavement surface deflection at the end of APT for (a) FC sections and (b) RC sections (Ingrassia et al., 2020).

Alland et al. (2017) attempted to interpret FWD data of HMA and PCC pavements for the Pennsylvania Department of Transportation (PennDOT). For JPCPs, FWD testing was used to detect voids, monitor joints and crack performance, and back-calculate the modulus of elasticity of the existing PCC and the k-value of all supporting layers. For asphalt concrete (AC) pavements, FWD testing was used to back-calculate the stiffness of each layer and to estimate the amount of damage in the existing asphalt. This report summarizes the recommended testing protocols and data analysis procedures in three primary sections. The first section describes the testing protocols recommended for FWD data collection. The second section defines the changes proposed to current PennDOT documents (including Publication 242, Publication 408, and the PennDOT Pavement ME Design Preliminary User Input Guide) based on the findings of this study. The third section is four separate appendices: A – Scheduling and performing FWD testing; B – Data analysis guidelines; C – Research findings; and D – Laboratory and field testing.

Much research has been conducted to evaluate pavement deflections using the FWD testing technique. The PennDOT report, in addition to other published research, is considered a basis for interpretation of the data from this project.

Assessment of rutting of SFRRC slab test section and HMA

A crucial part of this project is rutting assessment of the new SFRRC material being studied for possible future use at highway intersections. Rutting data collected in the field for the SFRRC slabs and the adjacent HMA followed the roadmap in Figure 2. Rutting in pavement evaluation is widely used in research and by agencies on local and state levels. This section will address the latest techniques and analysis in rut data collection and analysis.

Rutting is surface depression in the wheel path. Pavement uplift (shearing) may occur along the sides of the rut. Ruts are particularly evident after rainfall, when they are filled with water. There are two basic types of rutting: mix rutting and subgrade rutting. Mix rutting occurs when the subgrade does not rut, yet the pavement surface exhibits wheel path depressions as a result of compaction/mix design problems. Subgrade rutting occurs when the subgrade exhibits wheel path depressions due to loading. In this case, the pavement settles into the subgrade ruts, causing surface depressions in the wheel path. Rutting in Alaska's South Central Region is

mostly caused by studded tires. Details of rut wear rate and extent can be found in the latest DOT&PF report (Abaza, 2019).

Studded tires have been shown to cause significant damage to both flexible and rigid pavements. Specifically, studded tires create ruts which fill with ice and water, causing spray and hydroplaning; they may polish some aggregates, which reduces skid resistance, creates a more slippery driving surface, and removes pavement markings (NRMCA, 2020). A typical passenger car without studded tires produces negligible pavement damage (typically < 0.0001 ESALs per car) and can thus be ignored in pavement structural design. However, the same typical passenger car equipped with studded tires becomes a significant pavement damage concern (in the form of studded tire ruts) and must be accounted for through use restrictions, maintenance costs, and mix design (WADOT, WA-RD 471.1). To prevent rutting, the pavement structure needs to provide sufficient support for the roadway surface, while the design and construction of the asphalt mix must produce a pavement that resists deformation (NRMCA, 2020) and provides a hard surface to reduce the impact of studded tires.

The stability of the asphalt mix is an important element in its ability to resist rutting and is thus a key factor to evaluate. At the same time, however, the performance of a particular mix design depends on environmental conditions including traffic (weight and studded tires), temperature, and humidity. These factors are often seasonal, and mix designs can be exposed to a variety of environments across different projects, making it a challenge to reliably predict the rut resistance of a given HMA. Alaska DOT&PF took several measures to produce new mix designs that can withstand or reduce the impact of weather and studded tires, but met with limited success in prolonging the life cycle of HMA.

The Superpave mix design method does not require a specific performance test for wheel rut resistance. Earlier approaches like the Hveem method and the Marshall method do incorporate simple mechanical tests, such as the Hveem stabilometer or the Marshall stability and flow test, in which a load is applied and the resistance of the mix is measured, along with its displacement or deformation. Many agencies still use these established older methods to evaluate rut resistance during the mix design process. However, these evaluations are often done on a pass-fail basis without an attempt to predict performance or to factor in changes in loads or environmental conditions. To date, no performance tests incorporate studded tire rutting in mix design.

Newer sophisticated test methods use accelerated loading to test mix performance by simulating the cumulative effect of traffic loading within a short period of time. They may also be able to test at different load levels or specific temperature and humidity conditions, thus providing a more realistic evaluation. Some of the most common devices include:

- The Asphalt Mixture Performance Tester (AMPT), formerly known as the Simple Performance Tester (SPT).
- The Hamburg Wheel Tracking Device (HWTD).
- The Asphalt Pavement Analyzer (APA), formerly known as the Georgia Loaded-Wheel Tester.

The wheel tracking device was used in Phase I of this project to evaluate laboratory rutting performance of SFRRC and HMA. However, laboratory testing may not reflect actual rutting in the field. A study by Abaza et al. (2019) showed discrepancies in the laboratory reading using the wheel tracking device versus actual field rutting; laboratory test conditions had a significant influence on the rut reading for each locality. Field evaluation was incorporated in this phase of

the study to reflect real-life performance of the new material compared with HMA and to further validate the differences reported in the lab.

To obtain accurate and repeatable network-level pavement rutting measurements, practitioners and researchers have developed manual and automated rutting measurement technologies. Due to the limited SFRRC section length (150 ft) for this project, more focus was directed at the manual measurements. The traditional method for measuring rut depth is the straightedge method, suggested in ASTM 1703 Standard (2010). Other manual methods are static profiling technologies, such as the rod and level method (ASTM E-1364 2005) and the Dipstick profiler, which were mostly used in research studies to measure rutting. The Alaska DOT&PF rut measurement database utilizes Mandlii LCMS (used until the end of 2017) and the Fugro LCMS Road Surface Profiling (RSP) equipment (used as of 2018), consisting of distance measuring lasers and accelerometers and the Laser Crack Measurement System (LCMS), providing high-definition 3D profiles and 2D images of the road surface (PMS, DOT&PF).

The discrepancies between the manual and automated data led the Alabama Department of Transportation (ALDOT) to question the continuity between its manual and automated pavement condition survey programs. A regression analysis was completed to look for any systematic error or general trends in the error between automated and manual data (McQueen and Timm, 2005). Among other outcomes, the regression analysis showed that the automated data over-reported outside wheel path rut depth. The manual method is considered the reference in rut measurement for actual reading and calibration of automated readings.

Assessment of skid resistance of SFRRC slab test section and HMA

Skid resistance is the force developed when a tire that is prevented from rotating slides along the pavement surface (Highway Research Board, 1972). Skid resistance is an important pavement evaluation parameter because:

- Inadequate skid resistance will lead to higher incidences of skid-related accidents.
- Most DOT agencies have an obligation to provide users with a roadway that is "reasonably" safe.
- Skid resistance measurements can be used to evaluate various types of materials and construction practices.

Skid resistance depends on a pavement surface's microtexture and macrotexture (Corley-Lay, 1998). Microtexture refers to the small-scale texture of the pavement aggregate component (which controls contact between the tire rubber and the pavement surface), while macrotexture refers to the large-scale texture of the pavement as a whole due to the aggregate particle arrangement (which controls the escape of water from under the tire and hence the loss of skid resistance with increased speed) (AASHTO, 1976). Skid resistance changes over time. Typically, it increases in the first 2 years following construction as the roadway is worn away by traffic and rough aggregate surfaces become exposed, and then decreases over the remaining pavement life as aggregates become more polished. Skid resistance is also typically higher in the fall and winter and lower in the spring and summer. This seasonal variation is quite significant and can severely skew skid resistance data if not compensated for (Jayawickrama and Thomas, 1998).

Skid resistance is generally quantified using some form of friction measurement such as a friction factor or skid number given in Equation A1:

Friction factor (f) = Frictional resistance (F) / Load perpendicular to interface (L) (A1)

In general, the friction resistance of most dry pavements is relatively high; wet pavements are the problem. The number of accidents on wet pavements is twice as high as the number of accidents on dry pavements (but other factors such as visibility are involved in addition to skid resistance). Table A1 shows some typical skid numbers (SNs); the higher the SN, the safer the pavement (NRMCA, 2020).

Table A1: Typical skid numbers (from Jayawickrama et al., 1996)

Skid Number	Comment-Action
Less than 30	Take measures to correct
Larger or equal to 30	Acceptable for low volume roads
31-34	Monitor pavement frequently
Larger or equal to 34	Acceptable for heavily traveled roads

Several techniques were developed to measure skid resistance, including the locked wheel tester, the spin up tester, and the surface texture measurement. Automated skid resistance testers are beyond the scope of this project, as the length of the test section is limited. A surface texture measurement was utilized—the ASTM E303 – 93, "Standard Test Method for Measuring Surface Frictional Properties Using the British Pendulum Tester"; this measurement represents the skid resistance safety aspect of the comparative analysis.

Asphalt versus concrete pavements

Public agencies have the challenge of making a strategic decision, i.e., choosing between HMA and PCC pavements. Over time, agencies have made the decision based on road class, maintenance requirements, or life-cycle cost. This section provides some perspective on the advantages and disadvantages of each with respect to several parameters.

Hard-surfaced pavements, which make up about 60% of U.S. roads, typically are constructed with either HMA or PCC. Of those roads, more than 90% are asphalt. Both asphalt and concrete pavements can be designed for long life with routine maintenance and can be constructed as quality products. However, there are many practical, economical, and even political reasons for choosing one type of pavement material over the other (Thomas, 2006).

Table A2 addresses the comparative analysis between flexible pavements (HMA) and rigid pavements (PCC). While there are some recognized benefits to selecting one material over the other, many political factors come into play. Many issues, such as life expectancy, ease and cost of maintenance, and long-term smoothness are hotly debated in the industry. In the end, personal/agency preference and construction costs are often the deciding factors in whether to select asphalt or concrete (Thomas, 2006).

This section of the report presents another perspective on the use of a new paving material (SFRRC), addressing possible additional advantages over HMA and PCC and possibly raising more issues. In Alaska's Central Region, issues of pavement damage and rehabilitation schemes are different than in other areas in the states/world. Such issues add more complexity to the choice of using typical highway paving materials.

Table A2: Comparative analysis of flexible pavements (HMA) versus rigid pavements (PCC).

Flexible pavements	Rigid pavements
Asphalt pavements have a lower initial construction cost, allowing agencies to pave more with less funding.	Concrete pavements are typically more expensive initially; however, the life-cycle cost of concrete can be comparable to that of asphalt.
Traffic noise is generally lower with asphalt pavements.	The increased stiffness of concrete makes it able to withstand heavier wheel loads without risk of rutting. This is the main reason concrete pavement is used for bus stops, areas of heavy truck traffic, and even loading docks and warehouse slabs.
Newly constructed asphalt pavements can have a very smooth ride.	Since concrete does not rut, there is less risk of water accumulation on the pavement, which reduces the chance of vehicles hydroplaning.
The flexibility of asphalt pavement can help it perform well in areas of expansive soils, especially when coupled with proper subgrade stabilization.	During construction, concrete is less dependent upon the subgrade soils and is better able to "bridge" soft spots.
Routine maintenance can be performed quickly, reducing service interruptions.	Routine maintenance can be reduced for some concrete pavements. When maintenance is required, it can be smaller in scope when having to replace select concrete areas.
	Concrete can be colored and/or stamped into a pattern that can be aesthetically appealing.

Life-cycle cost

A crucial decision of public DOT agencies, selecting the type of highway pavement—HMA versus PCC—is based on life-cycle cost of the material and proposed projects. This section offers examples of such choices and perspectives on decisions as well as highway elements related to the subject matter. Sometimes, opinions presented depend on the agency/sectors conducting the study. All perspectives are addressed here.

Per State of Minnesota Statute 174.185, a life-cycle cost analysis (LCCA) is required for every project in the reconditioning, resurfacing, and road repair funding categories constructed after July 1, 2011. The LCCA is a comparison of life-cycle costs among competing paving materials, using equal design lives and equal comparison periods. Documentation required by the statute includes lowest life-cycle cost; alternatives considered; chosen strategy; and documented justification if the chosen strategy is not the low-cost option. In 2019, 35 construction projects were in the reconditioning, resurfacing, and road repair funding categories and required a LCCA according to the Minnesota Department of Transportation (MnDOT) Pavement Design Manual. Four projects required two LCCAs for a total of 39 LCCAs. Hot mix asphalt was the low-cost option for 37 LCCAs. Of these, the low-cost option was selected for 35 projects, one project selected a different hot mix asphalt option and one selected a PCC option. Documented justification for selecting an option that was not the low-cost option is provided. Portland cement

concrete was the low-cost option for two LCCAs, and both projects were selected for construction. A table of LCCA results and copies of the LCCAs submitted by MnDOT districts is included in their report (MnDOT, 2019). Other annual reports of life-cycle costs are documented by MnDOT.

The Illinois Department of Transportation (IDOT), Bureau of Materials and Physical Research, through Applied Research Associates, Incorporated (ARA), developed a guide for evaluating life-cycle cost for marking based on pavement type. The IDOT uses a variety of pavement marking systems and has experienced a wide range of pavement marking performance. To maximize marking performance and to optimize marking selection, IDOT initiated a research project to evaluate the performance of all currently approved marking types to develop a pavement marking selection guide based on performance results. The purpose of that project is to evaluate the performance of pavement markings on both PCC and HMA pavements over a period of 4 years. Field investigations were conducted to gather data on the durability and visibility of markings and the compatibility between markings and pavement materials. From the results of the study and a life-cycle cost analysis, ARA developed a pavement marking selection guide. Because the successful performance of marking depends largely on controlling many variables during the installation of the marking, this guide includes pavement marking installation inspection methods for use by IDOT inspectors (ARA, 2013).

Asphalt Pavement Alliance conducted a study addressing life-cycle cost using actual cost data (Villacres, 2005). This publication describes how the performance and economy of highway pavements is a matter of critical importance to governmental agencies, highway engineers, paving contractors, and others who are involved in the highway industry. The results of studies of interstate highways in three states were presented in this publication to show the comparison of LCC between HMA pavements and PCC pavements. Historically, there has been a difference of opinion as to whether HMA (or flexible) pavements are more economical or less economical over time than PCC (or rigid) pavements. Each industry claims that its product is more economical or longer lasting, or both. Even experienced state highway agencies and highway engineers disagree on the subject. While the study does not settle the argument, it does show that careful, detailed studies in three states indicate that HMA pavements are more economical over time; that is, they have lower life-cycle costs. The three studies use actual costs from agency records and the times at which the costs were incurred to determine the total cost of the pavements over a period of time. This information is typically difficult to assemble, requiring diligent searching of agency construction and rehabilitation records. This difficulty makes these three studies unique and valuable. In all cases, comparisons were made to the greatest extent possible of HMA and PCC pavements with similar traffic and age.

A report was developed by the National Center for Asphalt Technology (Robbins and Tran, 2018) addressing life-cycle cost. This report analyzes LCCA and the methodology to determine initial service life. A survey of state departments of transportation and a literature review were used to examine the determination of initial service life; performance measures for the determination of actual service life; the first major rehabilitation activity; and pavement roughness at time of rehabilitation. Asphalt concrete and PCC pavement sections in the U.S. and Canada in the LTPP program were investigated for initial service life values; actual pavement age at time of first rehabilitation; type of rehabilitation; and climate zone. The initial service life values in the LCCA do not represent the actual pavement age at first rehabilitation for asphalt concrete pavements. The report concludes with recommendations for calculating LCCA initial service life in AC and PCC pavements.

In 2016, the City of Red Deer, Canada, issued a Request for Proposals (RFP) to complete intersection/roadway improvements and upgrading of the 67 Street and Johnstone Drive intersection and the 66 Street and Orr Drive intersection. The RFP contained alternative bid options for AC and PCC. Pavement type selection is one of the most challenging decisions for municipalities. The use of LCCA as part of the alternative bid process allows for a better understanding of the true costs of a roadway as opposed to considering only an initial cost of the pavement. The equivalent pavement structures were compared in terms of their net present value. This LCCA approach provided the initial construction costs for each pavement structure and the costs of future maintenance and rehabilitation. Based on the LCCA, the concrete option was selected; the initial construction costs were comparable for both options but the preservation costs over the life cycle were substantially lower for PCC. A report by the Transportation Association of Canada (2017) discusses the selection process and the challenges of traffic accommodation and construction.

Tim (2006) from the Transportation Association of Canada (TAC) addressed a paper on sustainability of constructing roadways with OPCC pavement. The purpose of this paper was to analyze the sustainable performance characteristics of concrete pavement by examining and documenting some of its social, economic, and environmental advantages. Sustainability issues are generally not considered part of such an analysis, but including them provides government agencies with a better understanding of the true cost of roadway structures. This paper examines not only the social benefits, including reduced potential for hydroplaning, good nighttime visibility, improved stopping distance, and enhanced ride and comfort, but also the benefits of PCC pavement. The paper includes the findings of the Athena Sustainable Materials Institute on the Life Cycle embodied Energy for concrete and asphalt roadways; findings of several studies on truck fuel savings from traveling on PCC compared to asphalt concrete pavement (ACP) and the resulting reduction in greenhouse gas (GHG), and research on concrete pavement as a potential CO_2 sink. Portland cement concrete pavement (PCCP) can also be recycled as a base material for new pavement or as aggregate for new pavement. The paper presents typical PCC structures to demonstrate the aggregate savings realized when utilizing PCCP systems. In addition, economic benefits such as life-cycle cost, two pavement systems, and the potential for reduced lighting requirements for PCC are provided.

Uhlmeyer and Pierce (2001) described the transformation of an intersection to PCC pavement. In 1994, the Washington State Department of Transportation (WSDOT) began replacing selected AC intersections with full depth PCC pavement. This decision was made because of the high visibility of urban intersections and the high rate of rutting that occurred in a short period of time (8 years or less). Though costs to remove and replace just the rutted asphalt layer always has a lower initial cost than removing and replacing with full depth PCC, the life-cycle cost and the disruption to the traveling public indicates that reconstruction with PCC is an appropriate and vital option. With continued experience of WSDOT and the contracting community, in PCC intersection construction, and the use of partial and full road closures. Lengthy construction periods are longer warranted or necessary.

Embacher and Snyder (2001) published a paper on the life-cycle cost of HMA and PCC pavements. The costs of pavement construction, maintenance, and rehabilitation are primary factors considered by most local agencies in the selection of pavement type (HMA or PCC) for new construction. The optimal use of agency funds for any given project can be determined only through an economic analysis of all associated agency costs and the performance of the pavement. Life-cycle cost analyses were performed on HMA and PCC highway pavements in

Olmsted and Waseca Counties, Minnesota. The Means Heavy Construction Historical Cost Index and the Minnesota Department of Transportation Surfacing Indices were used to convert all expenditures over time into equivalent constant-dollar values. Direct comparisons were made on roadway sections with similar traffic volumes, ages, and environmental conditions. For Olmsted County, the favored pavement type depended somewhat on the cost index values that were used in the analysis; however, index selection had no effect on the outcome for the Waseca County comparisons. When the results were normalized for traffic volumes (i.e., cost per lane mile per million vehicles carried), PCC pavements were clearly more cost-effective in all Olmsted County cases and all but one Waseca County case, regardless of the cost index value used. Portland cement concrete pavements generally incurred significantly lower maintenance and rehabilitation costs than HMA roadways in both counties.

A study in Switzerland performed an environmental life-cycle assessment and life-cycle analysis of processes needed to construct and maintain various pavement types applicable for the Swiss roadway network, including concrete, asphalt, and composite road pavements. The study analyzed new construction and maintenance processes over a life span of 75 years, considered to be 1.5 times the average lifetime of a subbase layer. Costs included for new construction were generated from Cost Analysis 2011 available through the Swiss Builders Association. Because concrete and composite pavements have not been built in Switzerland over the past two decades, the costs were determined by comparison with cost values from Germany and Austria, and a ratio of 1:1.53 between costs for asphalt and concrete pavements was used. The cost calculation utilized a discount rate of 2% and a life span of 75 years. The authors concluded that all three pavement types have very similar new construction costs; however, the concrete pavement resulted in overall lower costs over the analysis period. Although the new construction costs for all three types of pavement were comparable, concrete pavements were determined to have high initial environmental impacts and a longer service life. It was also noted that concrete pavement has specific environmental and economic benefits as compared with composite and asphalt pavements (Gschösser and Wallbaum, 2013).

Many other studies analyzed life-cycle cost for different types of HMAs, PCCs, and their components. To date, the only case of the use of SFRRC as a pavement material is the test section on Abbott Road. Further enhanced characteristics of SFRRC over the typical rigid pavements (PCC pavements) by the use of steel fiber and crumbed rubber in rigid pavements might answer the current concerns in roadway paving in cold regions as well as other regions, and reflect on cost savings as well.

Appendix B – Strain Gauge Sensors Analysis

Based on the strain data collected from the embedded sensors in the precast slabs, 2½ years of data were retrieved as of June 2017. Three sensors were placed at the center, edge, and corner in three of the fifteen slabs used to build the SFRRC test section. This gave a total of more than 350,000 data points. In addition, the sensors report temperature readings for each strain reading from a thermistor embedded along with the strain gauge. The temperature taken reflects the pavement temperature corresponding to each strain gauge reading. Table B1 displays the typical raw data reported, showing the reading date and time along with the strain and temperature readings in units of microstrain and degree Celsius, respectively, from the nine sensors. (three for each slab, for three slabs). Note that the table shows a sample of raw data for the first slab with three sensors.

Table B1: Sample raw data from the field sensors.

Time-Stamp	CSG1	CSG1	CSG2	CSG2	CSG3	CSG3
	uE	C°	uE	C°	uE	C°
6/7/2017 16:00	-112.25	18.8	-80.85	18.5	-136.83	18.8
6/7/2017 17:00	-116.64	19.3	-84.67	19.1	-141.08	19.7
6/7/2017 18:00	-117.75	18.9	-86.34	18.9	-144.07	19.8
6/7/2017 19:00	-117.68	18.7	-86.04	18.7	-144.1	19.8
6/7/2017 20:00	-120.56	18.3	-87.55	18.4	-145.79	19.5
6/7/2017 21:00	-119.71	17.6	-87.05	17.8	-145.61	18.9
6/7/2017 22:00	-119.15	17	-86.62	17.2	-145.08	18.3
6/7/2017 23:00	-119.61	16.4	-86.76	16.7	-144.85	17.7
6/8/2017 0:00	-118.73	15.6	-86.83	16	-145.08	17
6/8/2017 1:00	-116.34	14.8	-85.74	15.2	-143.78	16.1
6/8/2017 2:00	-114.89	14.3	-85.09	14.7	-142.6	15.4
6/8/2017 3:00	-113.62	13.8	-84.37	14.2	-141.53	14.8
6/8/2017 4:00	-112.72	13.4	-83.77	13.8	-140.6	14.3
6/8/2017 5:00	-111.98	13	-83.31	13.5	-139.88	13.8
6/8/2017 6:00	-111.09	12.7	-82.86	13.1	-139.27	13.4
6/8/2017 7:00	-110.17	12.4	-82.31	12.9	-138.57	13.1
6/8/2017 8:00	-108.58	12.3	-81.6	12.7	-137.61	12.8
6/8/2017 9:00	-107.91	12.4	-81.25	12.7	-137.04	12.8

In the analysis of typical feedback from the sensor in the center of slab number four, Figure B1 shows the general trend of strain raw data over time as well as the measured temperatures. It is clear that the slab expands and contracts in response to changes in temperature. To have a better sense of the change and due to the amount of data, a 250 data point moving average was applied to the data as shown in Figure B2. The change in strain over this period showed an increase with increases in temperature over time as well as season to season.

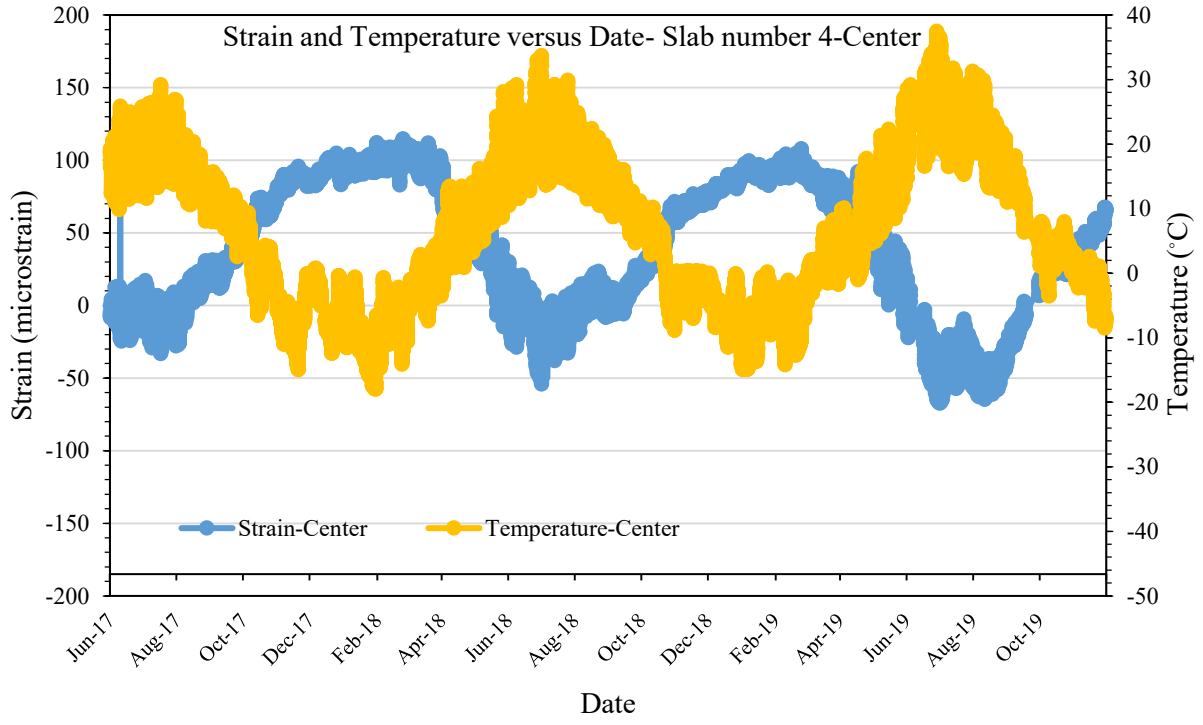

Figure B1: Trend of strain and temperature raw data in the SFRRC on Abbott Road (Center-slab 4).

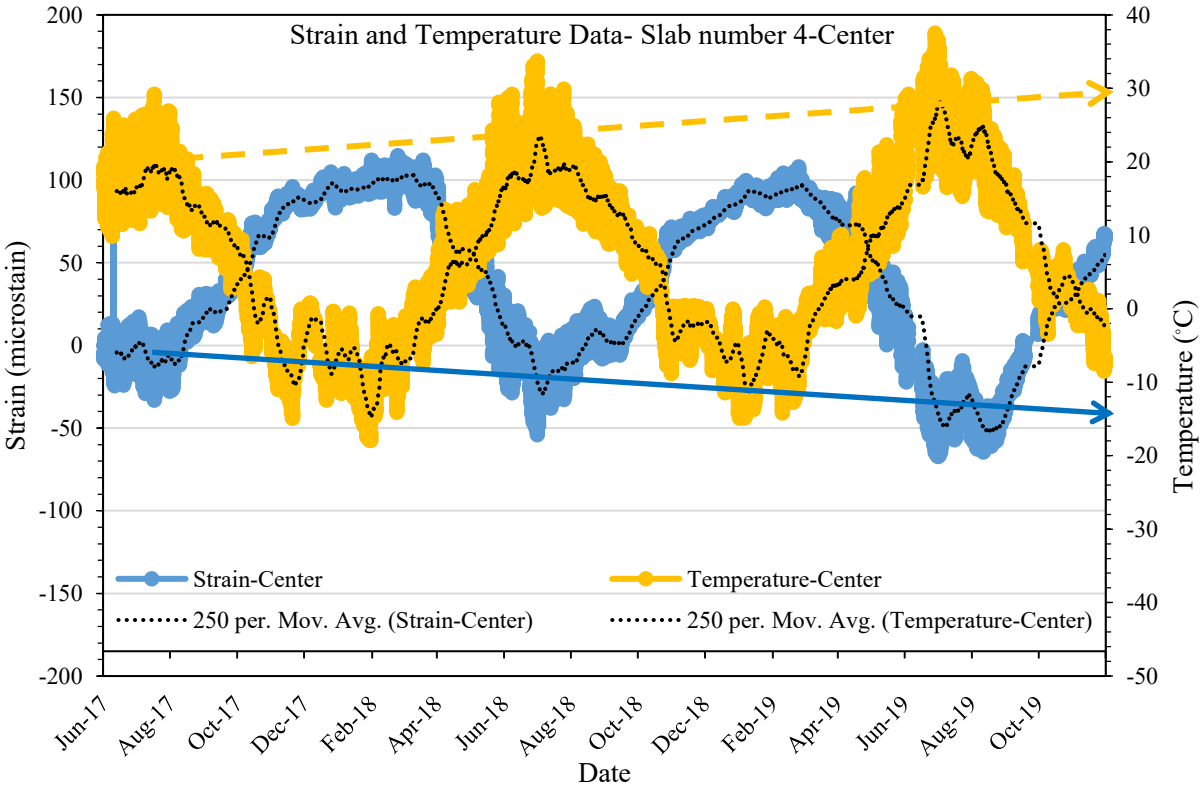

Figure B2: Trend of strain and temperature moving average in the SFRRC on Abbott Road (Center-slab 4).

Note that the temperature readings reflect pavement temperature while not necessarily reflecting ambient temperature. Among other factors, pavement temperature is affected by wind, precipitation, air temperature, weather conditions, and solar radiation as controlled by the thermal properties of the pavement. Data showed some but limited spikes in higher and lower temperatures compared with normal ambient temperature. These instances do not influence much of the overall trend because of the amount of data and the moving average used.

In further analysis of the change in strain versus temperature for the three locations (center, edge, and corner) on slab number 4, Figure B3 shows the seasonal cycles of freezing and thawing over this period. The record of temperatures from the three locations is consistent, with insignificant differences in the readings. On the other hand, significant differences were reported between the strain gauge readings for the center, edge, and corner. A moving average was applied to the data for depicting the change in strain over time and between the three locations. A distinct difference was reported for strain at the corner compared with the center and edge, with higher strain or expansion and contraction with changes in temperature. This is normal behavior, as corners have relatively less restraint from movements compared with the edge and center of a slab. Frictional forces with subbase are least impactful for corners, followed by edges and centers, respectively. The difference between edge and center strain is less apparent than the corner, with a higher difference during the winter season. This difference mainly depends on the slab-base interaction under higher or lower temperatures and moisture conditions as well as moisture variation under the slab. Higher moisture during spring/summer seasons provides less interaction (less frictional forces), while the reverse is true during winter due to frozen ground. The opposite can be said for less moisture during the summer season and moisture at the edge versus center. Typically, more moisture exists under the slab near the edge than at the center. The general trend in slab number four shows that the center has relatively higher strain (expansion and contraction) during the summer season and vice versa during winter season, with corner strain being the highest.

In further exploring this behavior in the other slabs, Figures B4 and B5 give the trends of change in strain versus temperature for slabs eight and thirteen. The trends in slab number four (Figure B3) are repeated in slab number eight with higher strain at the corner compared with the edge and center. The difference between the corner and edge is relatively small in this case, but there is a clearer difference between the corner and edge compared with the center of the slab as of summer 2018. The trend in slab number thirteen is less clear, but generally follows the same trend. There is no explanation of the discrepancies in slab thirteen except the confinement around the slab that restricts the slab from movement. This confinement can be the result of a very tight joint, which restricts movement at the edge, resulting in comparable strains at edge and corner.

For perspective on the average values of strains recorded during this period, Table B2 shows maximum and minimum averages of strains recorded for the slab edge as well as average temperatures for the seasons. Strains and temperatures addressed are extremes of the seasons and do not necessarily correlate. As stated earlier, the temperature readings from the three slabs show consistency in the trends and the overall results. In addition, overall results for strain at the edge showed consistency, except for the reported readings from summer 2019. Combining the results of the three slabs showed inconsistency in the trends for the three locations of center, edge, and corner. This inconsistency in trends indicates that the reading for each slab should be analyzed separately to draw valid conclusions. Furthermore, readings from slab numbers four and eight are more reliable in reflecting the trends compared with readings of slab number thirteen.

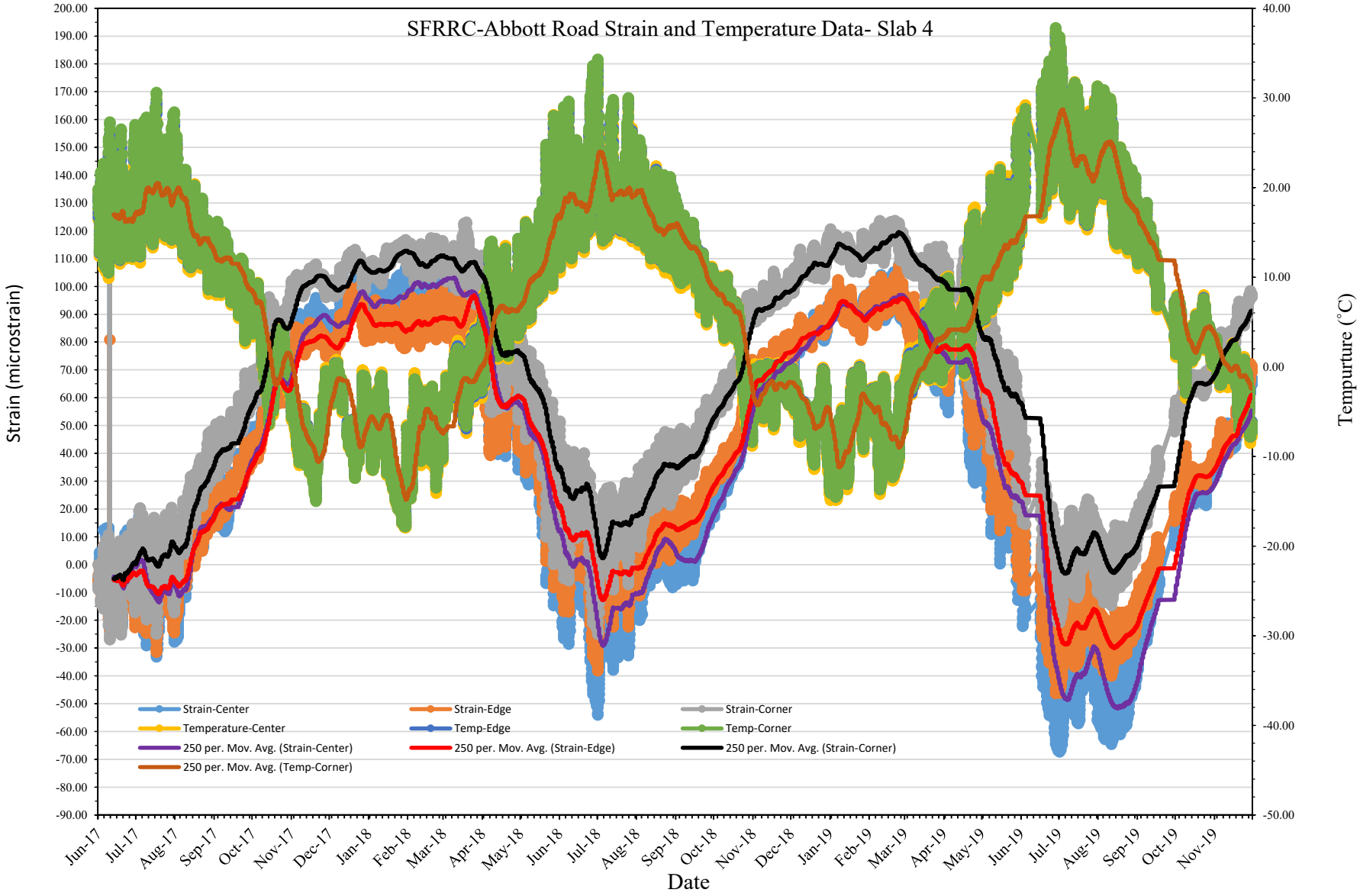

Figure B3: Seasonal changes in strain and temperature for slab number 4 at center, edge, and corner on Abbott Road.

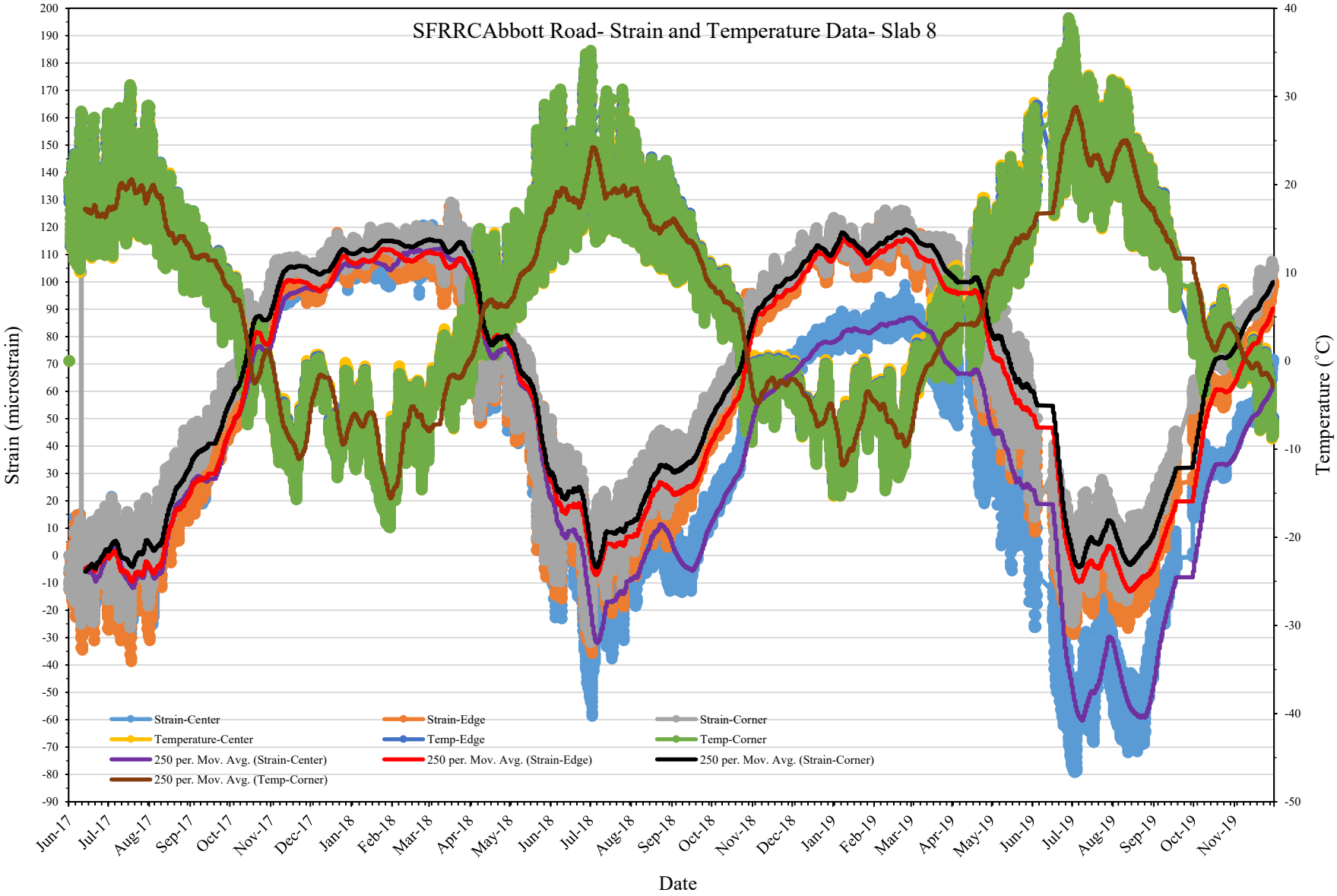

Figure B4: Seasonal changes in strain and temperature for slab number 8 at center, edge, and corner on Abbott Road.

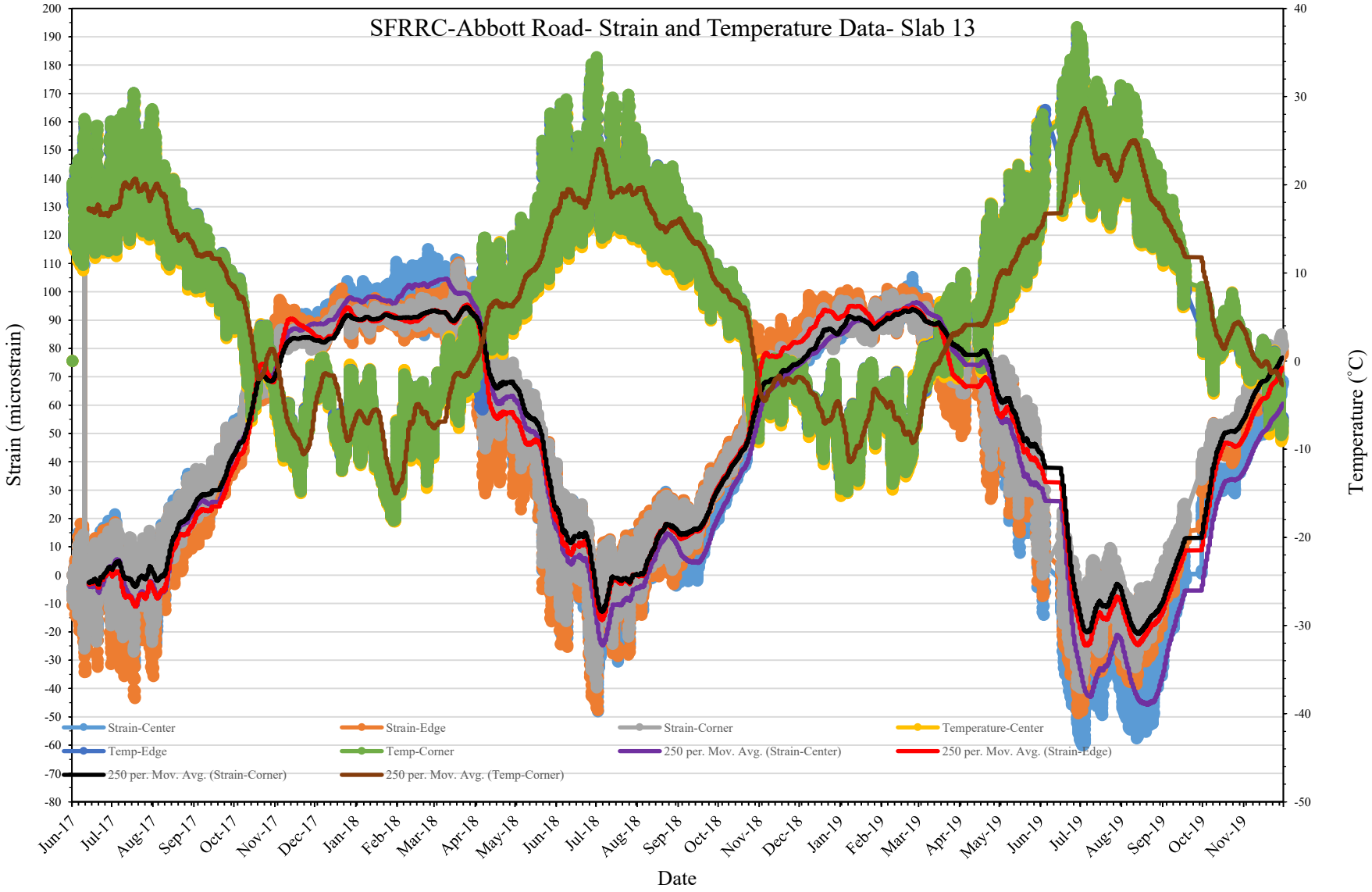

Figure B5: Seasonal changes in strain and temperature for slab number 13 at center, edge, and corner on Abbott Road.

Table B2: Maximum and minimum average strain and temperature at the edge of the slabs.

Season	Summer 2017	Summer 2018	Summer 2019	Winter 2018	Winter 2019
Slab Number Four					
Max. Ave. Temperature	21	24	28	-14	-12
Max. Ave. Strain	-12	-14	-32	94	90
Slab Number Eight					
Max. Ave. Temperature	21	25	28	-15	-15
Max. Ave. Strain	-10	-10	-18	110	114
Slab Number Thirteen					
Max. Ave. Temperature	22	24	28	-15	-12
Max. Ave. Strain	-10	-15	-26	95	90
Overall Ave. Strain	-10.7	-13.0	-25.3	99.7	98.0
Standard Deviation	1.2	2.6	7.0	9.0	13.9
CV	-0.11	-0.20	-0.28	0.09	0.14

The coefficient of thermal expansion (CTE) of PCC, defined as the unrestrained change in unit length per degree of temperature change, has significant influence on the design of joints and temperature-related pavement deformations (expansion/contraction and curling) in jointed concrete pavements (JCPs) (Jahangirnejad et al., 2009). The inclusion of rubber and steel fiber in SFRRC in this project are expected to change the normal CTE for SFRRC/PCC pavements. The available data give a comparative analysis of CTE for the new SFRRC material compared with PCC. Despite its importance, the CTE was not directly used as a design input in the AASHTO Guide for the Design of Pavement Structures (AASHTO, 1993); instead, it was only employed to determine the magnitude of joint movement and sealant reservoir dimensions. However, the MEPDG, developed under National Cooperative Highway Research Program (NCHRP) Project 1-37A (NCHRP 2014), recognized it as an important factor by using it as a direct input design variable to analyze critical slab distresses and joint/crack openings (Havel et al., 2015).

Considering the full 2 years of strain-temperature data form the center of slab number four, Figure B6 gives the general correlation. Data fit well for two seasons, with regression fitting exceeding 84% for each. In addition, there is no significant difference in the correlation between the two seasons leading to the earlier note of consistency in the data for each separate slab/location separately. A similar outcome was achieved in the correlation of strain-temperature for slab number eight, with comparable regression fitting of more than 86%. Tables B3 gives the calculated CTE for both slabs.

Table B3: Coefficient of thermal expansion for SFRRC.

Slab Number	Slab Four		Slab Eight	
Season	First Season	Second Season	First Season	Second Season
CTE (length/°C)	3.64×10^{-6}	3.58×10^{-6}	3.68×10^{-6}	3.52×10^{-6}
Average (length/°C)	3.61×10^{-6}		3.60×10^{-6}	
	3.6×10^{-6}			

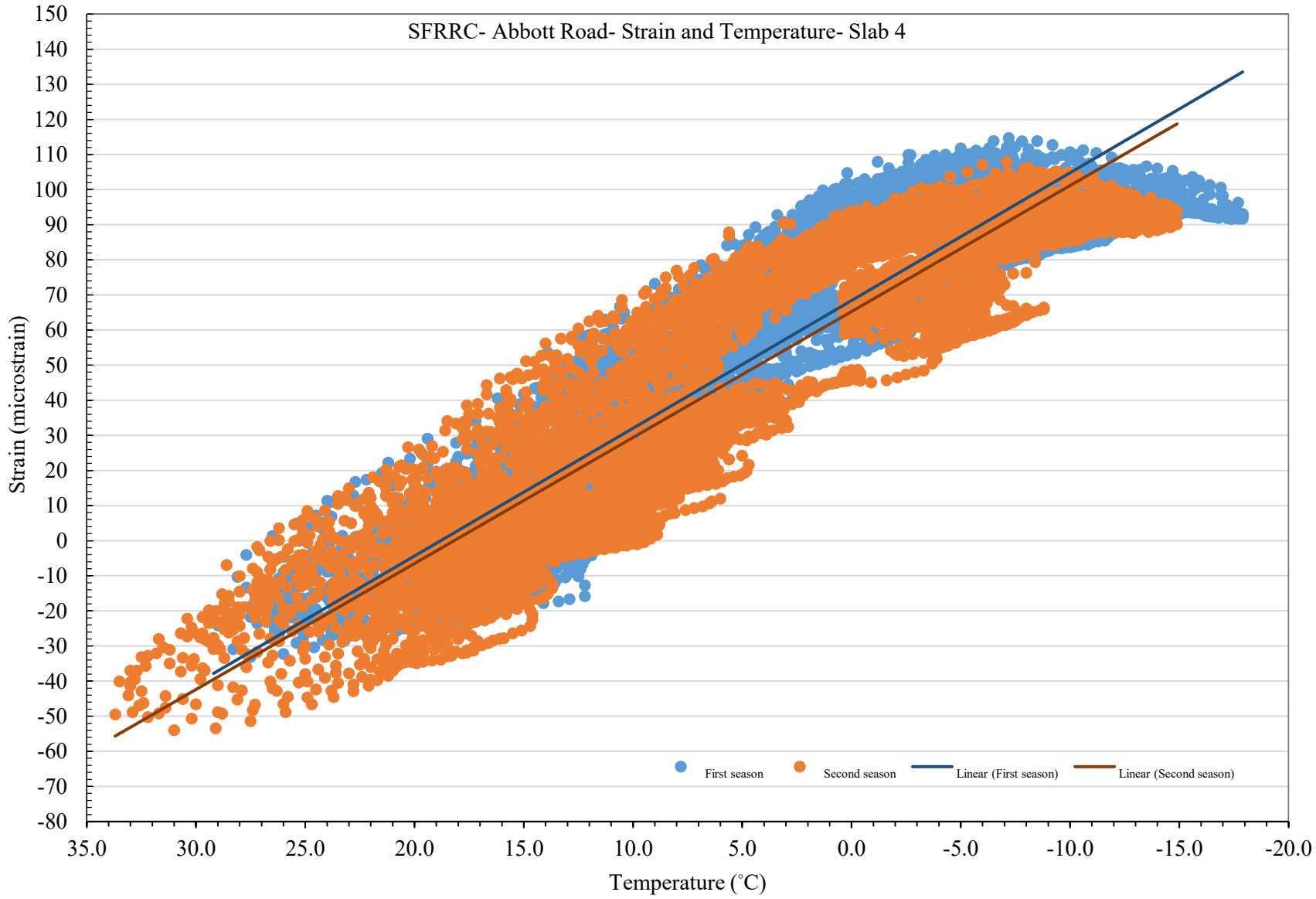

Figure B6: Strain-temperature data for the center of slab number four for SFRRC test section.

A general value for concrete's CTE is about 5.5 millionths/°F (11 millionths/°C) or 5.5 × 10^{-6} /°F (9.9 × 10^{-6} /°C). For example, if an unrestrained, 100-foot-long slab on grade was exposed to a 100°F temperature drop throughout its cross section, it would contract about 0.66 in. (100 ft × 12 in./ft × 100°F × .0000055). In the case of concrete slabs on a base, slabs develop internal stresses and may not expand as much. The values of CTE vary depending on many factors such as the water-cement ratio, concrete age, richness of mix, relative humidity, and the type of aggregate in the mix. The recommended CTE value in the MEPDG manual of practice (AASHTO 2008) is 5.2 × 10^{-6}/°F (9.4 × 10^{-6}/°C). In the case of SFRRC, values reported in Table B3 show that the overall average reflects a CTE value of 3.60 × 10^{-6} /°C with a standard deviation of 0.07. Results from locations other than the center of the slab for slab numbers four and eight showed comparable outcomes. The CTE for SFRRC from this project showed a value of about 38% of the recommended MEPDG AASHTO value. This outcome translates to significant restrainment to the pavement slab, which can be achieved by use of SFRRC. In addition, the SFRRC CTE can limit/control the slab joint opening to the minimum, reducing the overall expansion and contraction as well as stresses on the dowel bars. Furthermore, it will significantly reduce the amount of temperature steel in jointed reinforced concrete pavements (JRCP).

Summary of strain gauge analysis

Per the analysis of the strain gauge data, the following can be concluded:

- Strains in the SFRRC slab on Abbott Road follow the norms of expansion and contraction with change in pavement temperature expected from rigid pavement structures.
- Strains taken at the corner, center, and edge of the SFRRC slabs showed higher values at the corner followed by edge and center, respectively. Some variation exists depending on moisture conditions underneath the slab and the slab confinement conditions.
- Of the three slabs embedded with strain gauges, sensors in slab numbers four and eight provided more reliable outcomes compared with slab number thirteen.
- It has been determined that each slab has its own characteristics with regard to strain values depending on conditions of basin and placement of the slabs, and can be analyzed separately but still follow the general trend.
- The CTE for SFRRC was reported to be 3.60 × 10^{-6} /°C (6.48 × 10^{-6} /°F) reflecting 38% of the recommended MEPDG AASHTO value.
- The observed CTE for SFRRC can significantly reduce the design of the joint opening for jointed concrete pavements (JCP) and as a result reduce stresses on the dowel bars. In addition, the SFRRC CTE will reduce dowel diameter and might eliminate the use of temperature reinforcement required in jointed reinforced concrete pavements (JRCP).
- The CTE for SFRRC allows for longer joint spacing, reducing the cost of JCP.

Appendix C – Deflection Analysis

Falling weight deflectometer (FWD) testing was used to evaluate the structural condition of existing pavements in the SFRRC slabs and the adjacent HMA. For PCC, FWD testing is used to detect voids, monitor joints and crack performance, and back-calculate the modulus of elasticity of PCC and the k-value of all supporting layers. For HMA pavements, FWD testing is used to back-calculate the stiffness of each layer and to estimate the amount of damage in the existing asphalt. In this project analysis, deflections in the slabs and load transfer efficiency (LTE) across the joints were evaluated for SFRRC, and deflections in HMA were evaluated. The data were collected by the Alaska DOT&PF PMS team using Dynatest (FWD) RSP 5051 Mark II, which applies a dynamic load that simulates the loading of a moving wheel. The advantage of FWD testing is that it gives the deflection characteristics of pavement and the deflection basin. Data for this project were collected every 6 months when possible and compiled to measure the deflection at the center, edge, corner, and panel joint. Figure C1 shows the testing locations 1 through 16 (1 through 15 on the SFRRC slabs and location 16 on the HMA), and Figure C2 shows the FWD deflection readings per location away from the center of the impact load of the FWD device. D_1 is at zero distance from the standard impact load (10,000 pounds), and D_9 is the farthest from D_1 at 3000 mm. The rest of the readings are recorded at distances shown in the figure.

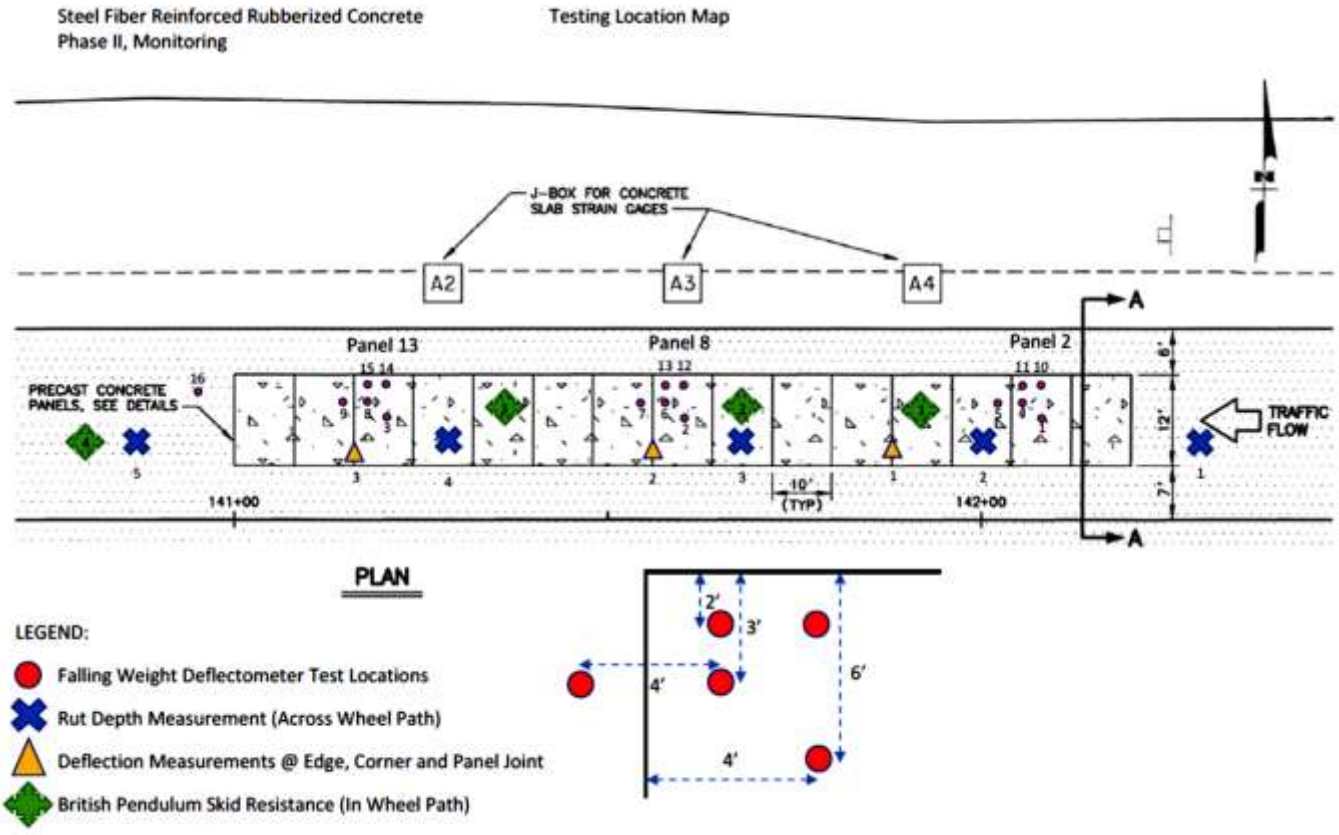

Figure C1: Testing location map for SFRRC, Phase II, Monitoring (Abou Eid, 2018).

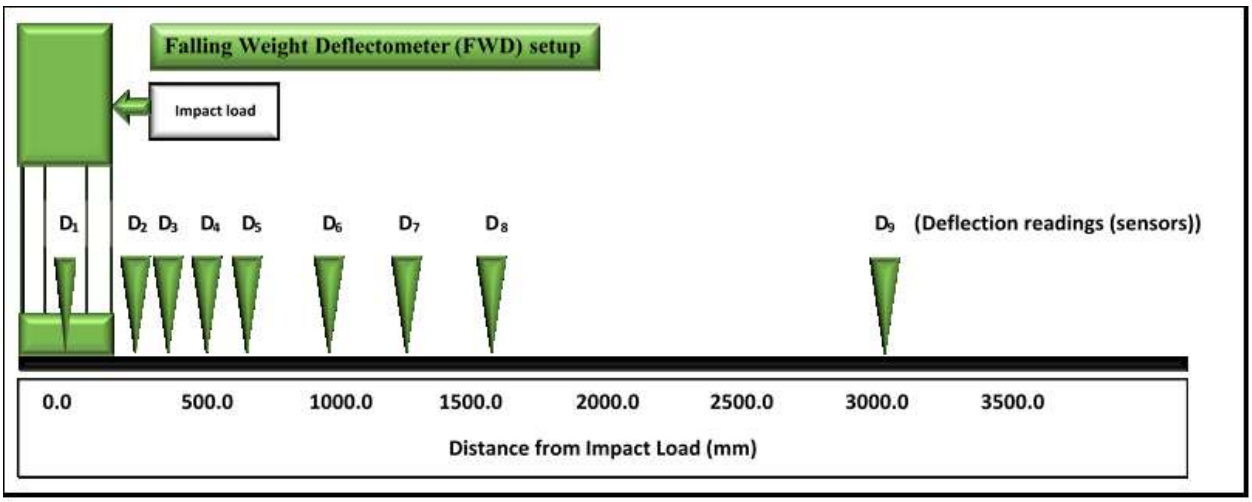

Figure C2: Location of deflection readings from sensors in the FWD device (Abaza, 2020).

Slab center (interior) deflections

Typical readings from station one at the center of SFRRC slab number two during the study period are shown in Table C1, and Figure C3 is a typical graphical representation of this data. The data show that deflection decreases significantly away from the impact load. In addition, with time, the deflection behavior shows two phenomena, depending on the condition of the subgrade/base conditions at the time of testing. Rounds of testing done at the end of the winter season showed generally higher deflection due to the moisture conditions of the subgrade/base, where the soil is still moist compared with relatively dryer soil at the end of the summer. Figures C4 and C5 show similar trends for locations 2 and 3 at the center of SFRRC slabs number eight and thirteen, respectively. Note that a much higher deflection was reported at location 3 compared with locations 1 and 2, which most probably reflects higher moisture conditions under slab number three at the end of the winter season. Comparable values were reported for the three slabs at the end of summer, which further explains the moisture condition under slab three at the end of the winter season. Figure C6 shows the overall average for each of the three locations at the center of the slab at the end of winter and summer, which relatively reflects the same trend except for slab number three at the end of the winter season. Figure C7 gives the overall average center deflections for locations 1, 2, and 3 at the end of the winter and summer seasons.

Table C1: Typical reading from location 1 at the center of SFRRC slab number two.

Location	Date				
	10/17/2017	5/15/2018	9/4/2018	5/31/2019	9/24/2019
D1	3.81	4.765	3.29	4.98	
D2	3.71	4.5	3.16	4.47	3.76
D3	3.5	4.165	2.86	4.05	3.49
D4	3.15	3.695	2.50	3.60	3.04
D5	2.41	2.795	1.94	2.92	2.25
D6	1.72	2.085	1.47	1.14	1.62
D7	0.89	0.97	0.91	0.86	1.00
D8	0.7	0.705	0.68	0.63	0.78
D9	0.52	0.51	0.49	0.44	0.56

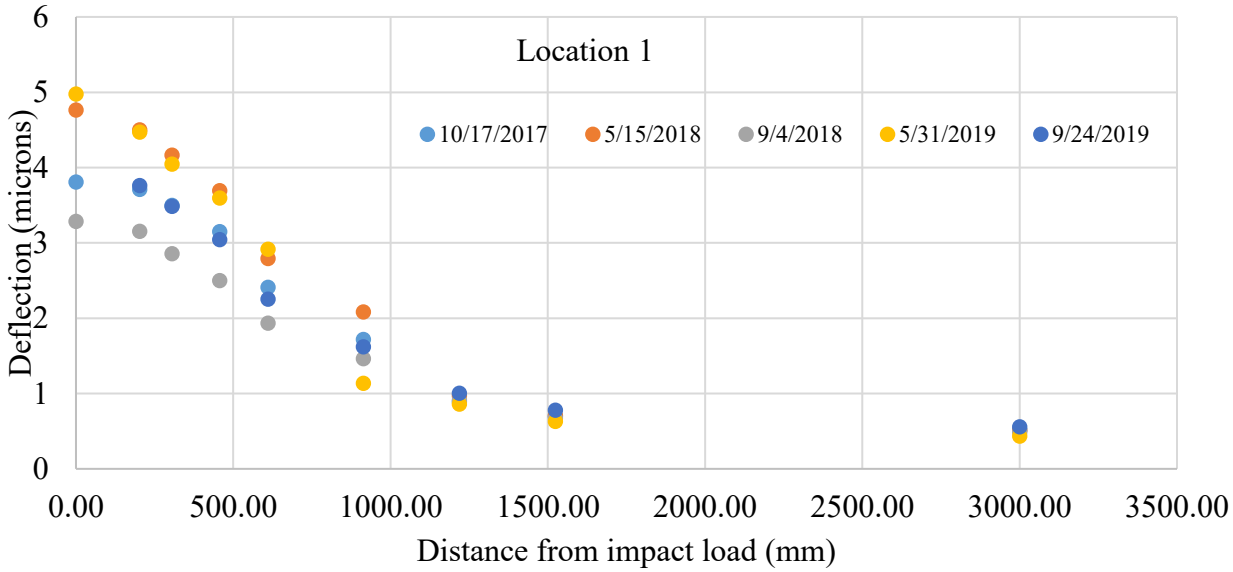

Figure C3: Readings of deflections taken from location 1 at the center of SFRRC slab number two.

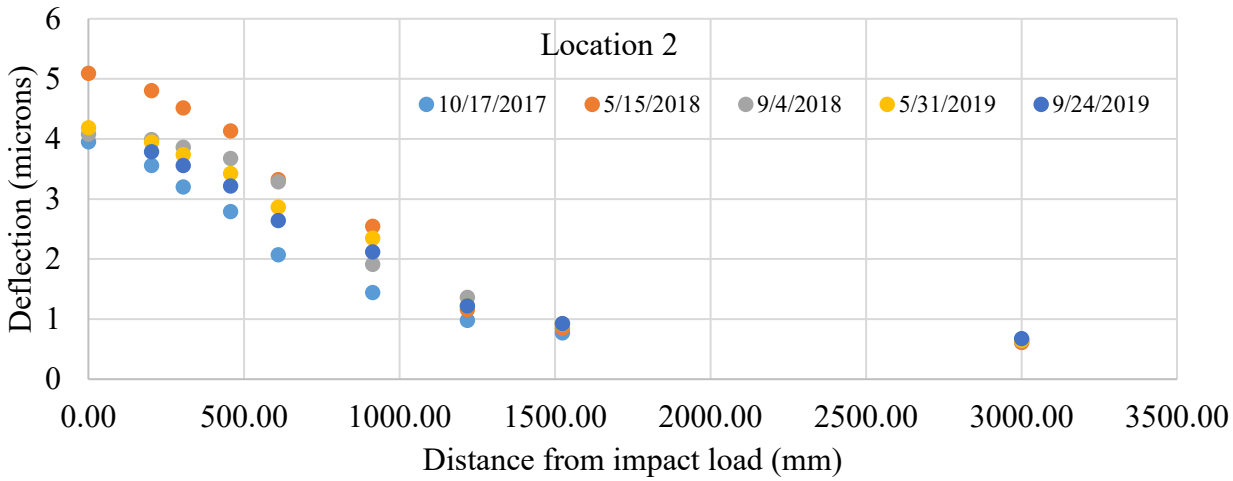

Figure C4: Readings of deflections taken from location 2 at the center of SFRRC slab number eight.

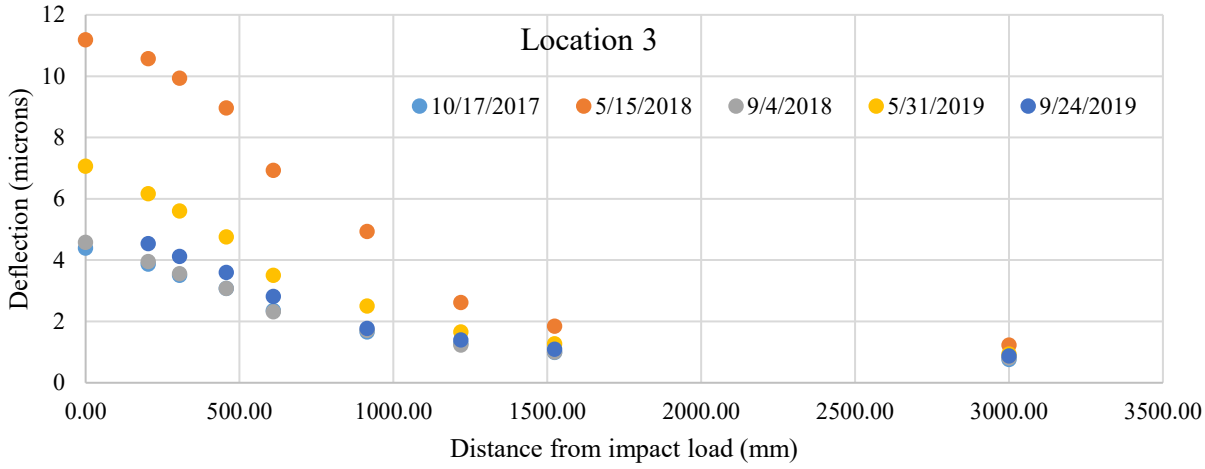

Figure C5: Readings of deflections taken from location 3 at the center of SFRRC slab number thirteen.

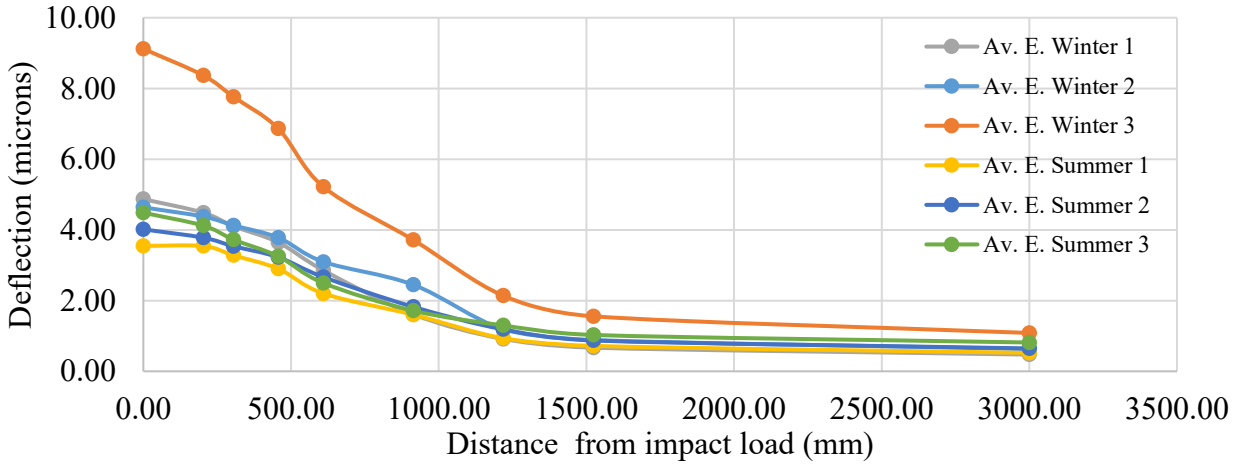

Figure C6: Graphical representation of the three locations at the center deflections of the slab at the end of winter and summer seasons.

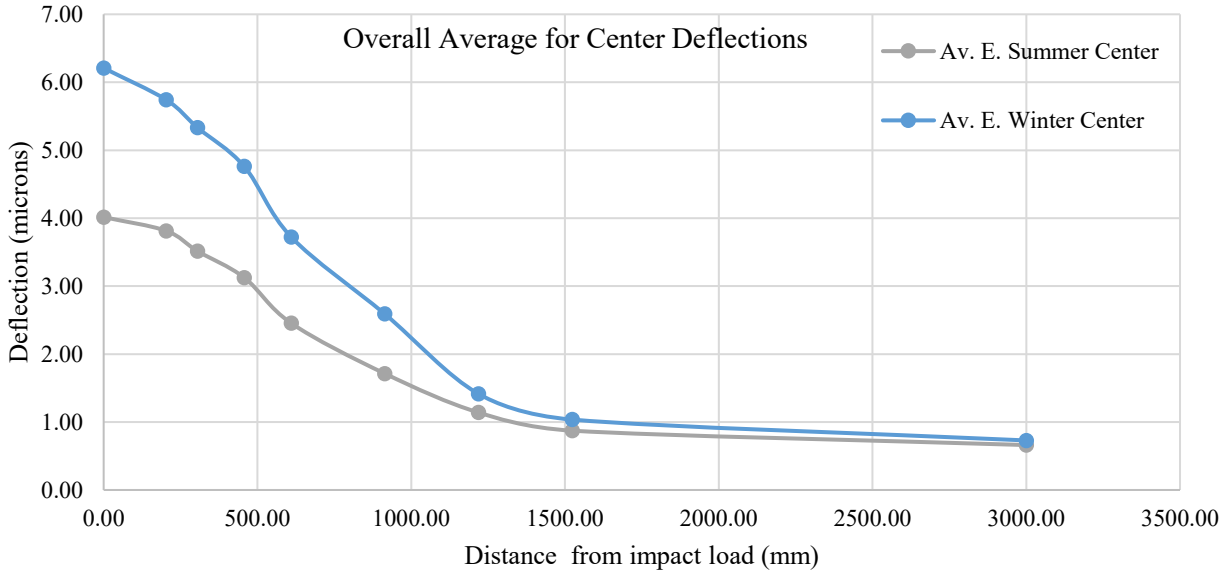

Figure C7: Overall average center deflections for locations 1, 2, and 3 at the end of winter and summer seasons.

Slab edge deflections

Deflection readings at the edge of slab numbers two, eight, and fourteen or locations 10, 12, and 14 are shown in Figure C1. No seasonal trends are observed from individual data per Figure D8, but the overall average in Figure C9 depicted such a trend as observed in the center loading. Figure C10 shows overall average deflection at the edge for locations 10, 12, and 14 at the end of the winter and summer seasons. In addition, a comparison of center and edge loading for the same locations per Figure C11 shows higher deflection at the edges as expected and as documented in the literature (Huang, 2004, and others).

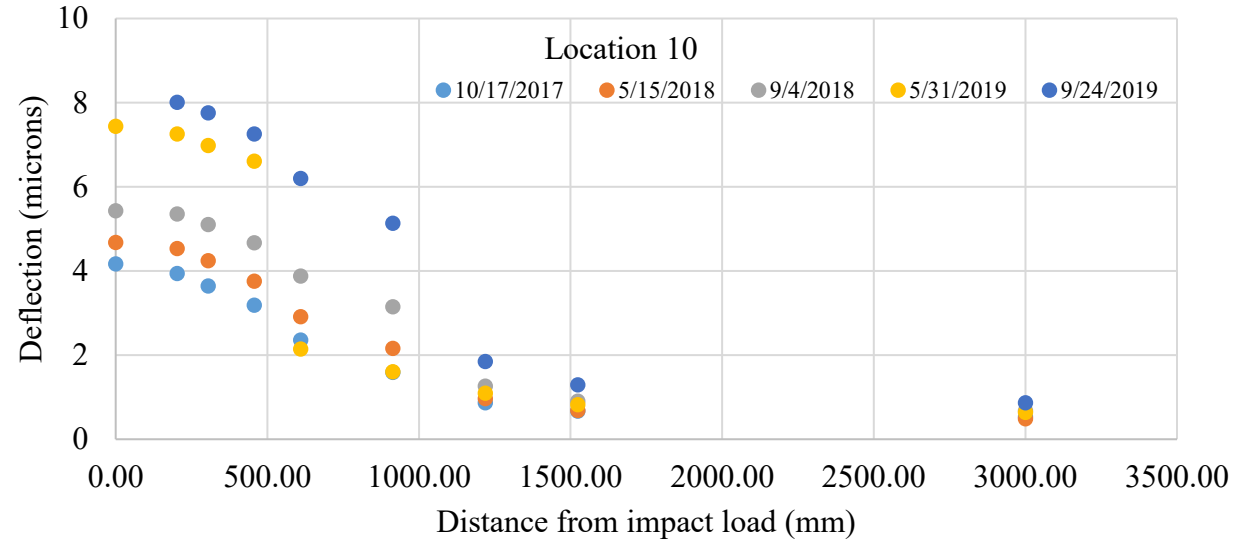

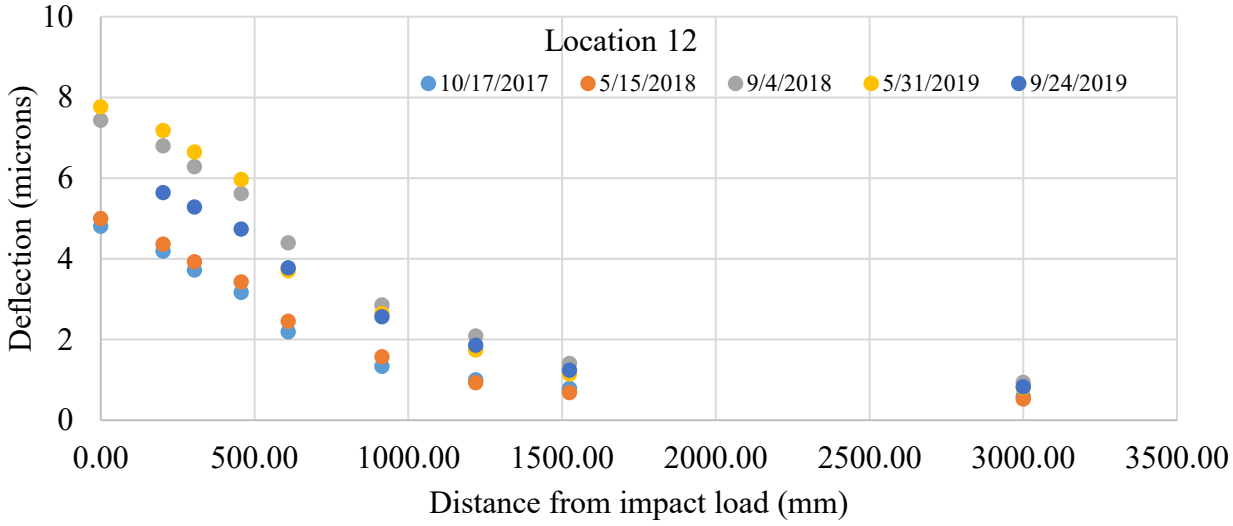

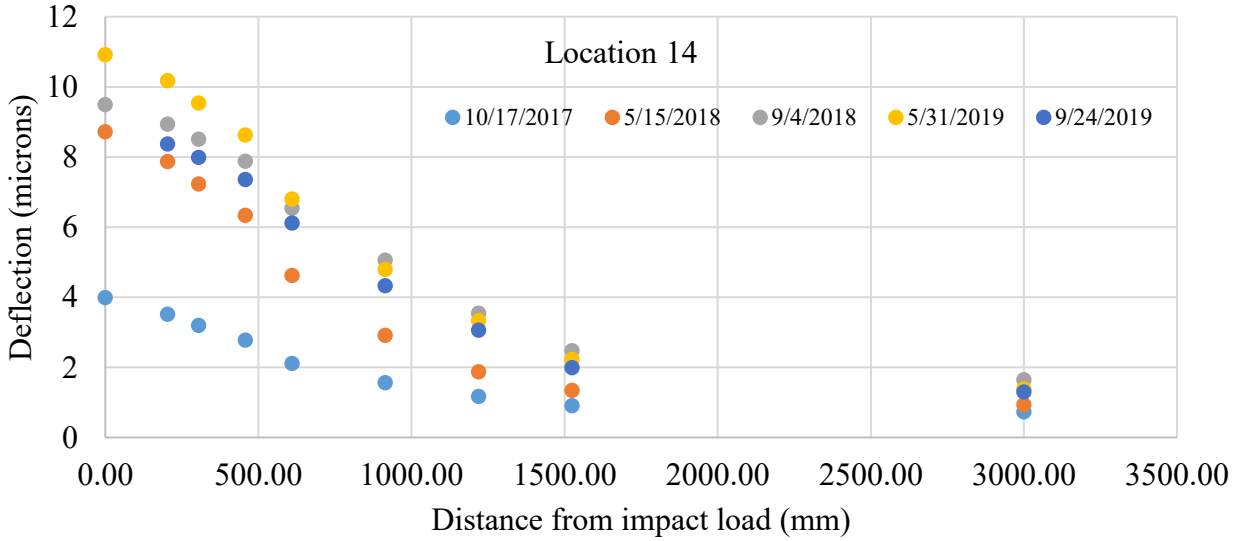

Figure C8: Deflections readings at the edge of slabs two, eight and thirteen, locations 10, 12, and 14.

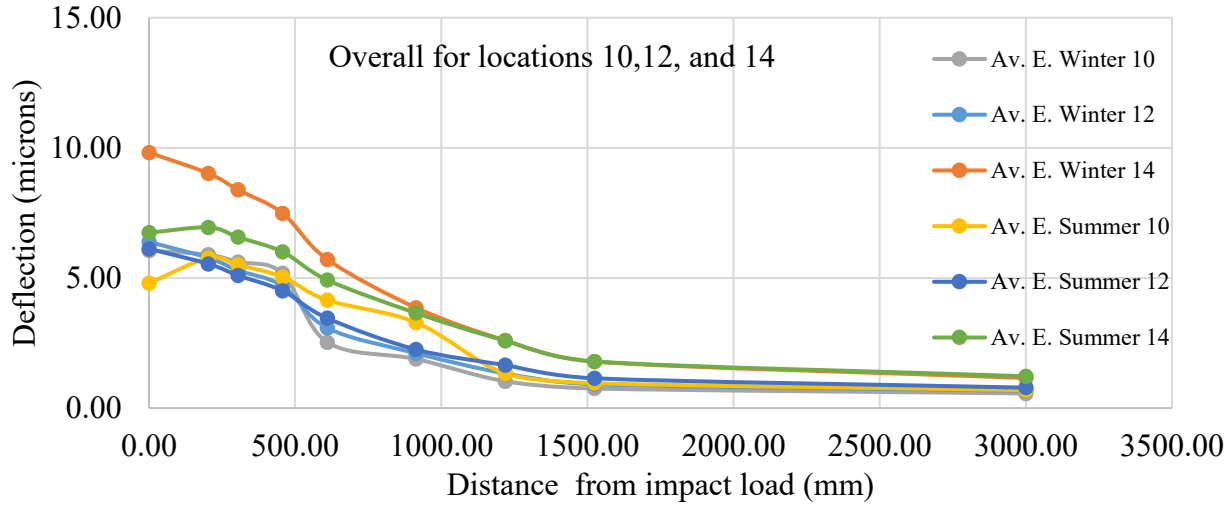

Figure C9: Graphical representation of deflections on the three locations at the edge of the slabs for end of winter and summer seasons

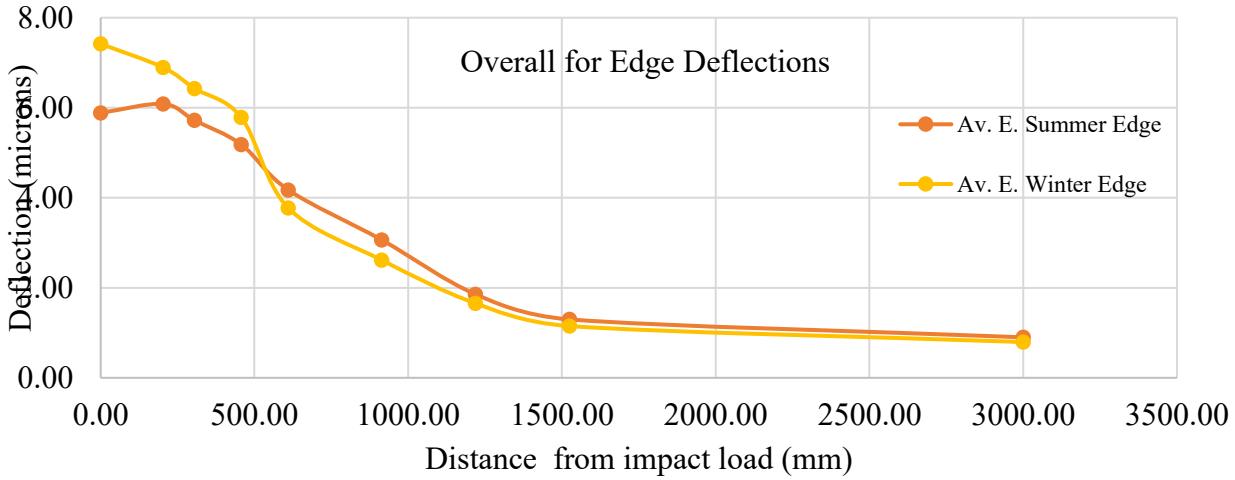

Figure C10: Overall average edge deflection for locations 10, 12, and 14 at the end of winter and summer seasons.

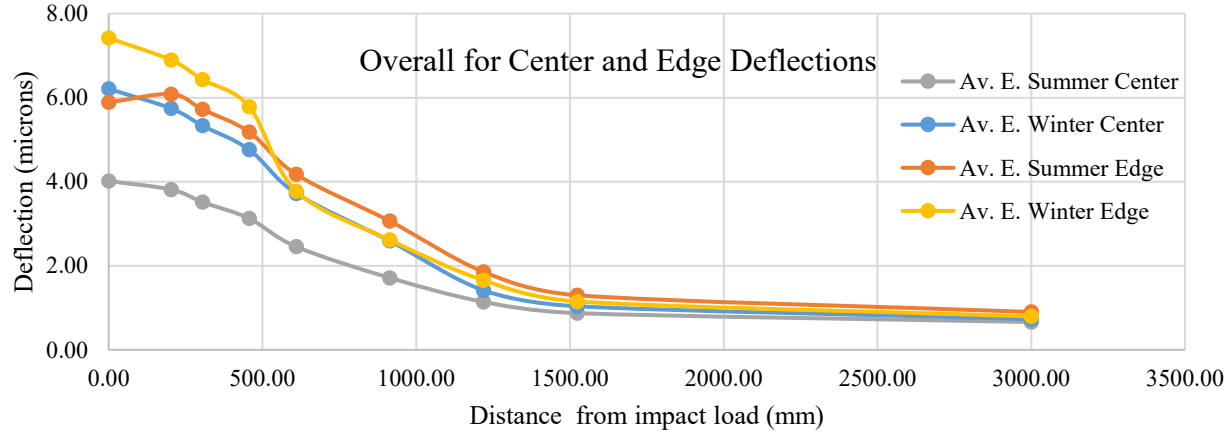

Figure C11: Overall average edge and center deflections for locations 10, 12, and 14 at the end of winter and summer seasons.

Slab corner deflections

For the analysis of deflections at the corner of slabs two, eight, and fourteen or locations 11, 13, and 15, Figure C12 shows a summary of the readings. No seasonal trends are observed from individual data per Figure C13, as the main support of the slab at the corner are dowel bars (Huang, 2004) transferring load to the adjacent slab and not totally dependent on conditions of the basin. Figure C14 shows the overall average corner deflection at the end of the winter and summer seasons, where the end of summer deflection readings are higher near the joint/corner, after which they are about equal to that of the end-of-winter deflection. In other words, at about 400 mm from the joint/corner, the corner deflection resembles that of the edge deflection. Furthermore, the shape of the curve is dependent on the point of loading and the existence of a dowel bar at that location. Figure C15 gives an overall summary of the center, edge, and corner deflections. The highest deflection occurs at the corner, followed by edge and center, respectively. The deflection at these three locations follows the trend reported in the literature (Huang, 2004, and others).

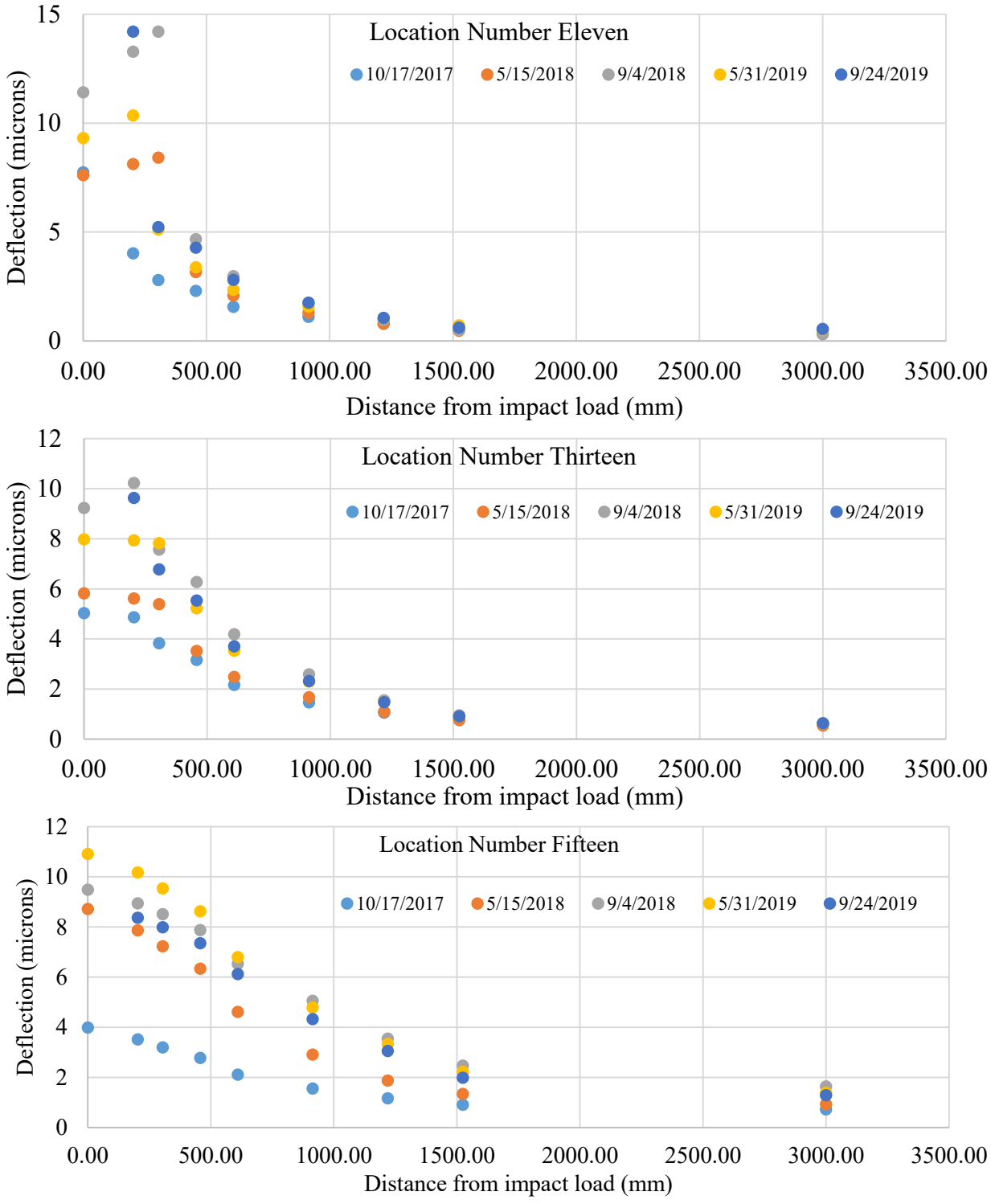

Figure C12: Deflection readings at the edge of slabs two, eight and thirteen, locations 11, 13, and 15.

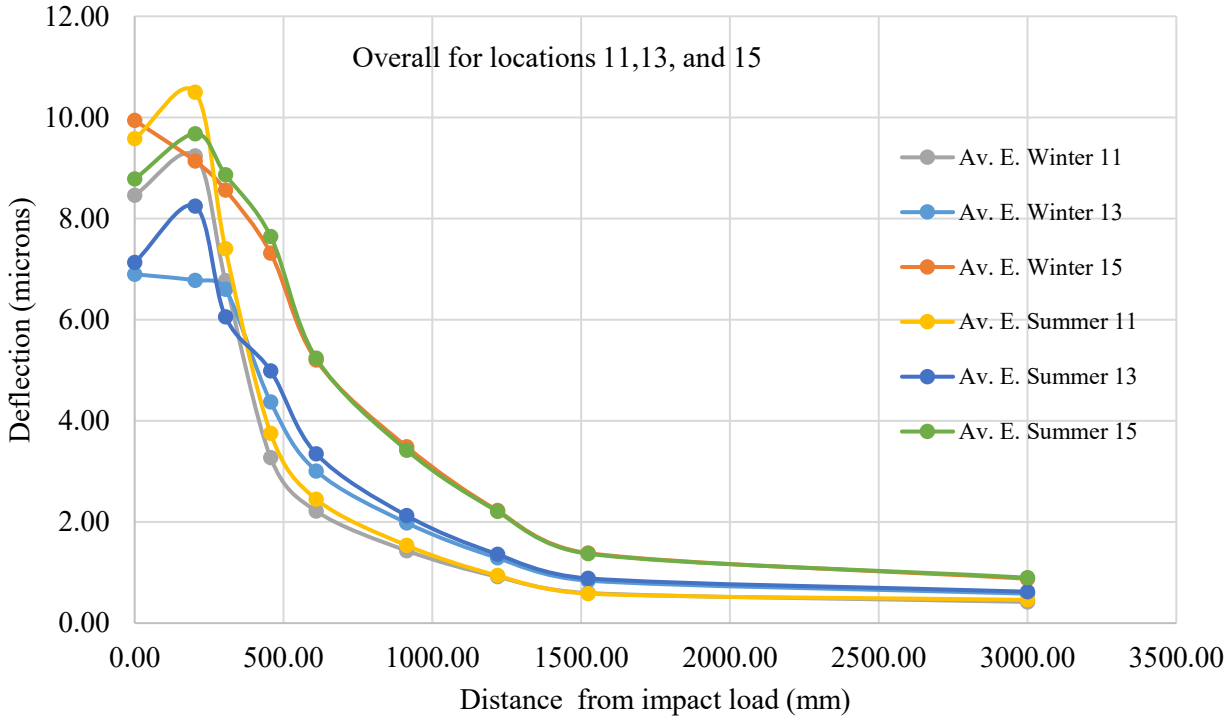

Figure C13: Graphical representation of deflections on the three locations at the corner of the slabs for end of winter and summer seasons.

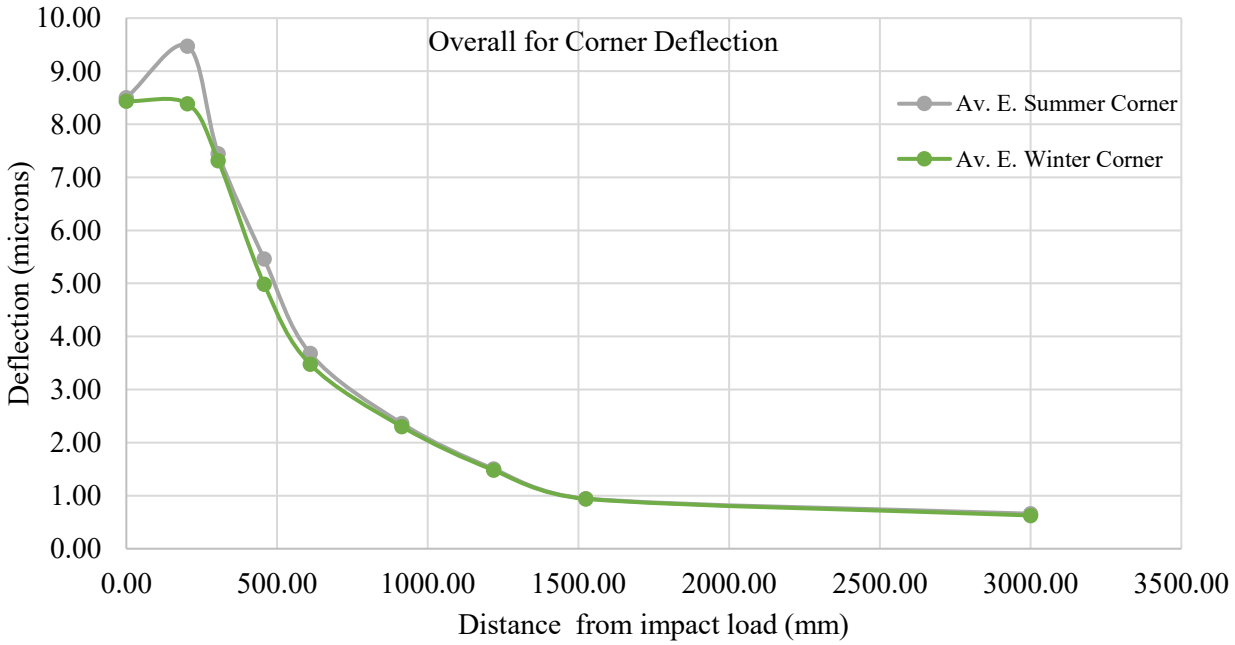

Figure C14: Overall average corner deflection for locations 11, 13, and 15 at the end of winter and summer seasons.

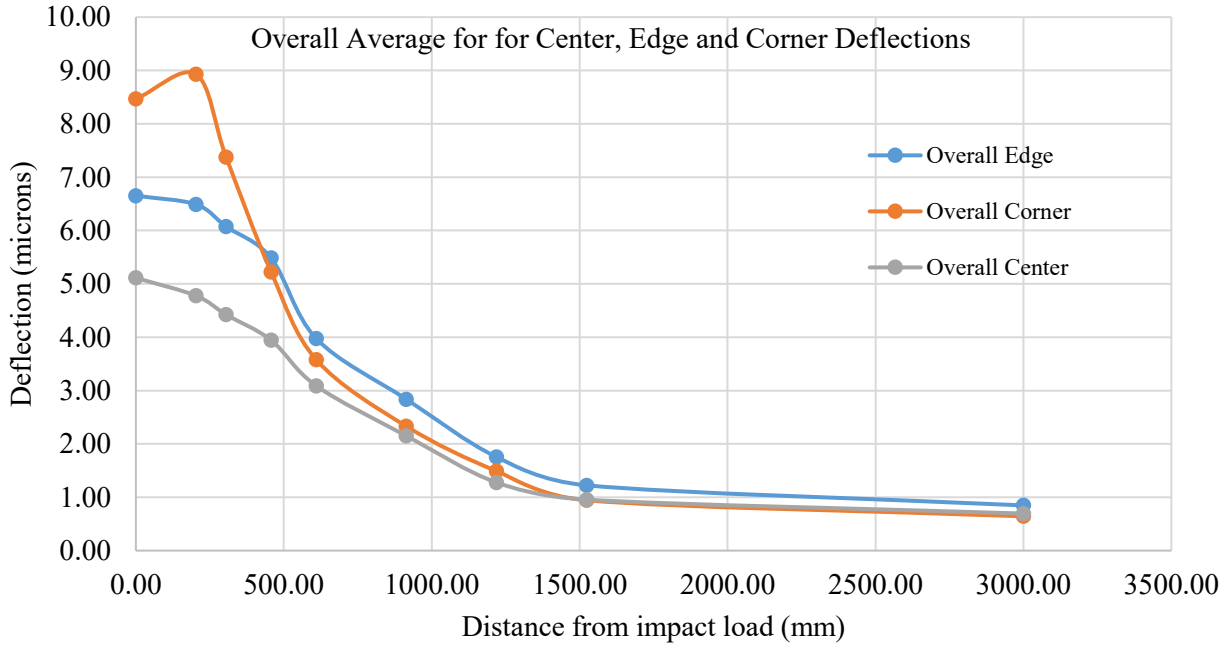

Figure C15: Overall average center, edge, and corner deflections.

Slab joint deflections

For the analysis of deflections at the joint of slab numbers two, eight, and thirteen or locations 4, 6, and 8, Figure C16 shows a summary of the readings. Generally, the two phenomena addressed in the center and edge deflection cases are apparent here, except during the site visit of 9/4/2018. There is no explanation for this except an error in the readings or calibration issues in the device. Figure C17 shows the overall average for each of the three locations at the joint of the slab at the end of winter and summer seasons, which relatively reflects the same trend except for the case of the 9/4/2018 visit.

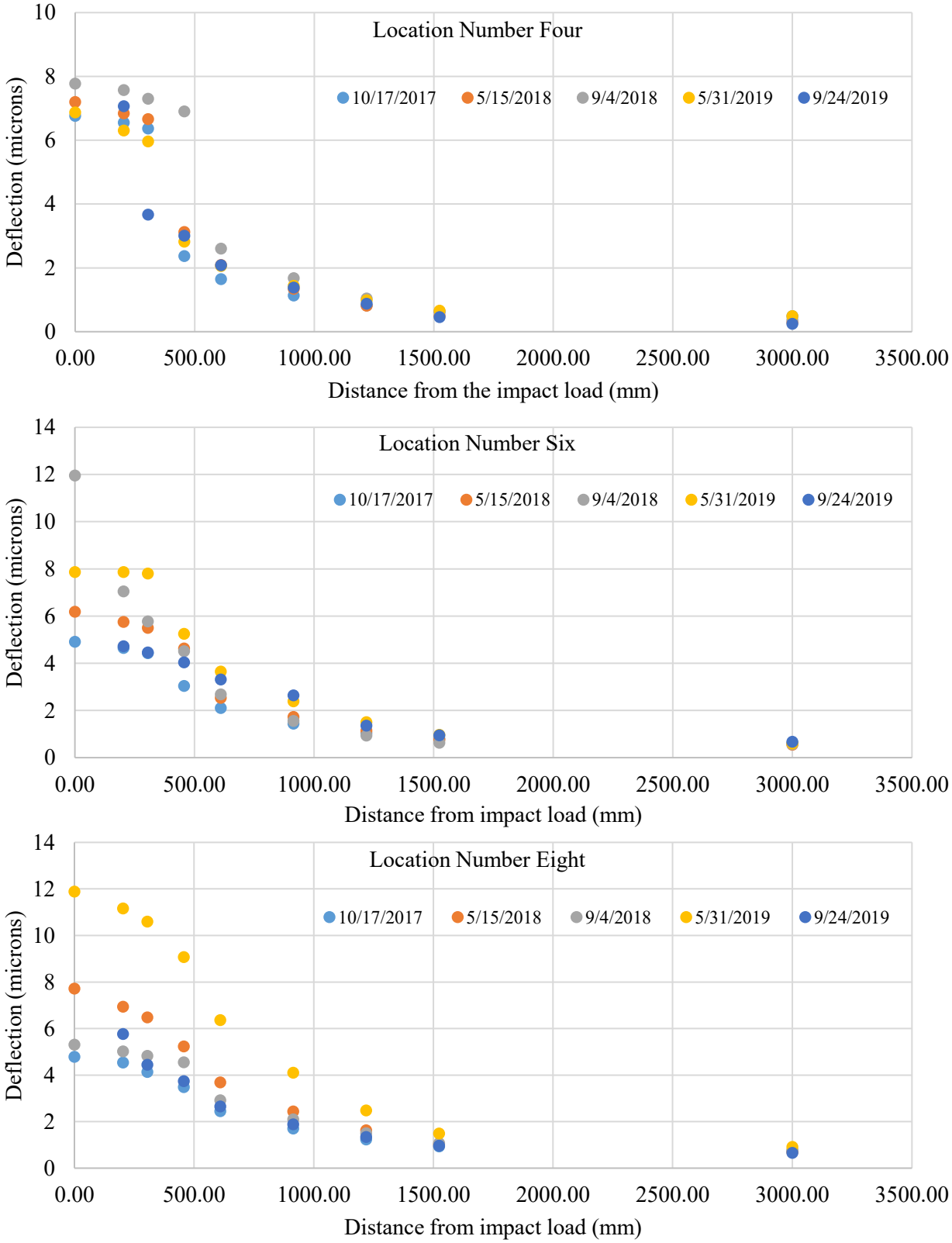

Figure C16: Deflections at the joint of slabs two, eight and thirteen, locations 4, 6, and 8.

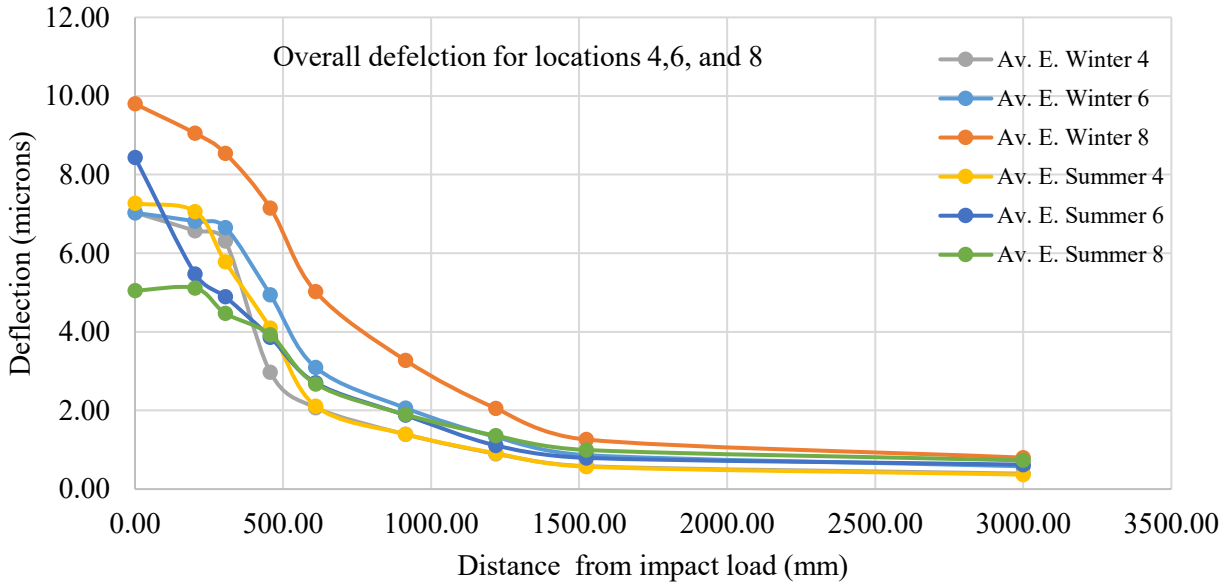

Figure C17: Graphical representation of joint deflections for locations 4, 6, and 8 at the end of winter and summer seasons.

In the analysis of deflections at the joint of slab numbers three, nine, and fourteen or locations 5, 7, and 9, which are opposite of locations 4, 6, and 8, Figure C18 shows a summary of the readings. Dowels provided at the joint have the function of transferring load from one side of the joint to the other; faulting can result if they do not. Analysis of deflections on both sides of the joints gives an idea of the LTE of the dowels, as defined in equation C1 (Pierce et al., 2003; Shoukry, 2005).

$$LTE = (D_{unloaded} / D_{loaded}) \times B \qquad (C1)$$

where

$D_{unloaded}$ = Deflection of the unloaded slab.
D_{loaded} = Deflection of the loaded slab.
B = Slab bending correction factor (Typical values for B are within the range 1.05 to 1.15 (AASHTO, 1993).

The slab deflections at the end of winter and summer seasons indicate the same behavior as addressed in the other loading locations. Figure C19 gives the overall average deflection for locations 5, 7, and 9. Generally, this overall average deflection follows the same trend as other deflection cases (center, edge, and corner).

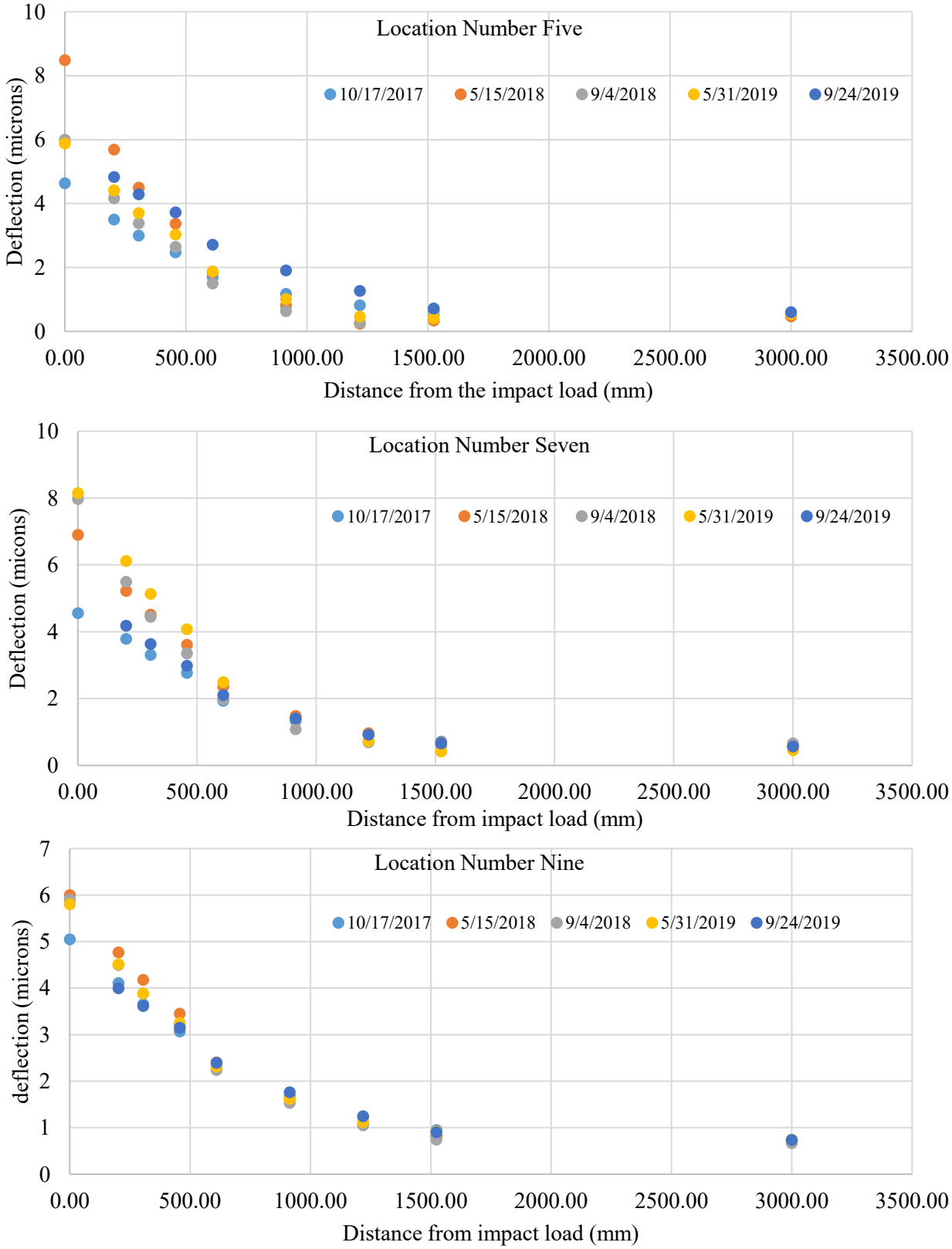

Figure C18: Deflections at the joint of slab numbers three, nine and fourteen, locations 5, 7, and 9.

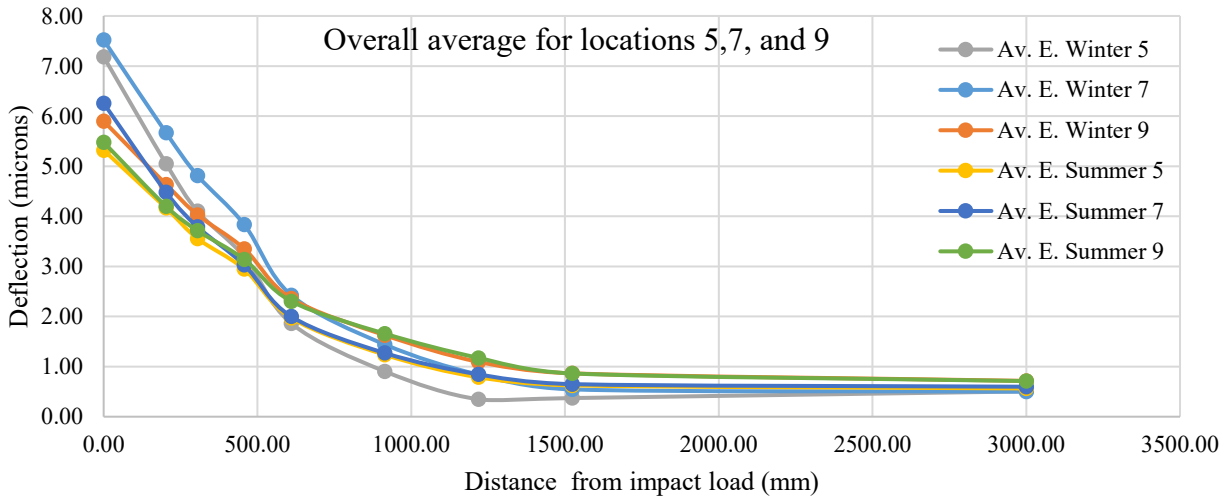

Figure C19: Graphical representation of joint deflections for locations 5, 7, and 9 at the end of winter and summer seasons.

Figure C20 gives a comparative analysis of deflections on both sides of the joints, where Joint A indicates locations 4, 6, and 8, and Joint B indicates 5, 7, and 9 at the end of winter and summer seasons, respectively. Though the theme of seasonal changes in deflection are the same as other cases, the deflections at Joint A locations are higher; this is due to the way the readings were taken during field testing. In other words, the FWD machine was moving forward across the SFRRC slabs, and the Joint B readings were taken across the joint. The estimation of LTE across the three joints is about 90% and 95% (overall average) at the end of the winter and summer seasons, respectively. The LTE depends on several factors, including temperature (which affects joint opening), joint spacing, number and magnitude of load applications, foundation support, aggregate particle angularity, and the presence of mechanical load transfer devices (dowel bars in this case). For comparson, AASHTO recommends that the value of LTE should be greater than 70% for sufficient load transfer of heavy loads (AASHTO, 1993) and the American Concrete Pavement Association (ACPA) requirement for joint effectiveness is LTE = 75% (ACPA, 1991).

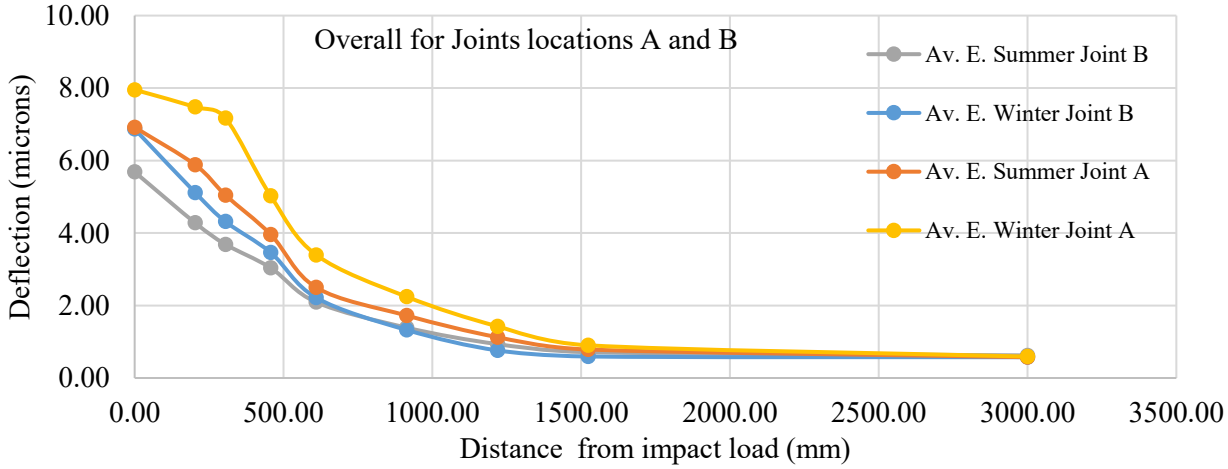

Figure C20: Overall deflections on both sides of the joints at the end of winter and summer seasons.

HMA deflections

In addition to measuring deflection of the SFRRC by running the FWD on the SFRRC test section, deflection was measured on the adjacent HMA section on Abbott Road with similar traffic and environmental factors. Figure C21 shows a summary of the readings of location 16 on the HMA section right after the end of the SFRRC test section. Trends of seasonal changes for the end of winter and summer reading on the SFRRC test section are seen here on the HMA section as well, reflecting the base/subgrade conditions. Figure C22 gives the overall deflection trends at the end of winter and summer. These results can be used to back-calculate the design for the HMA section on Abbott Road and as information for the restricted weight limits during the spring season. The best comparison of SFRRC and HMA deflection is the case of center 9 (interior) loading of SFRRC, as shown in Figure C23. The deflections in SFRRC are lower under the wheel load (impact load) compared with HMA, as SFRRC behaves similar to PCC pavement in distributing load over a larger area (less deflection), minimizing the local defects resulting from concentrated wheel loads as well as the action of frost heave from the basin. In addition, SFRRC allows for higher weight limits during the spring season if not eliminating weight limit restrictions. Values of 21% and 25% lower deflection were reported under the wheel load for spring and summer, respectively.

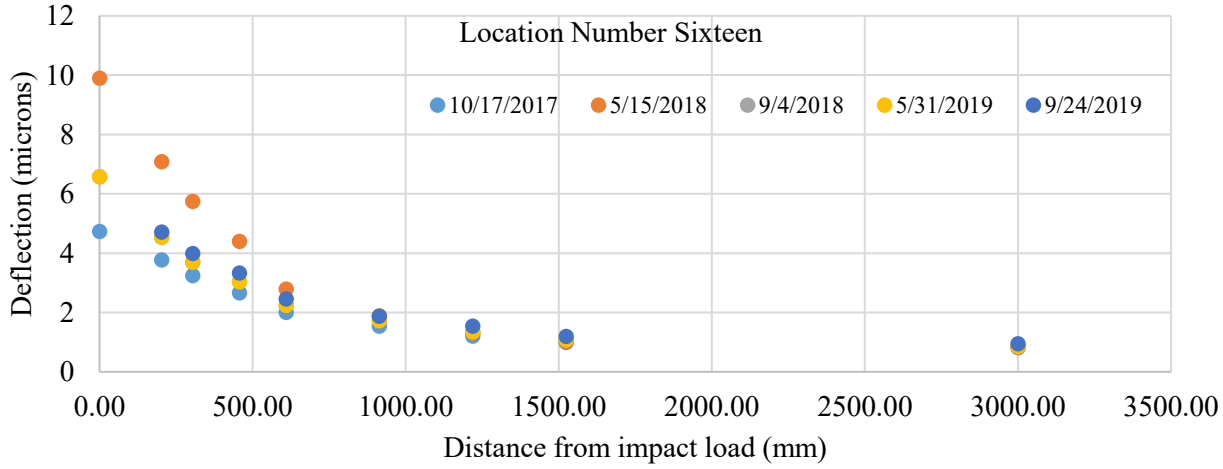

Figure C21: Deflections readings on the HMA for location 16.

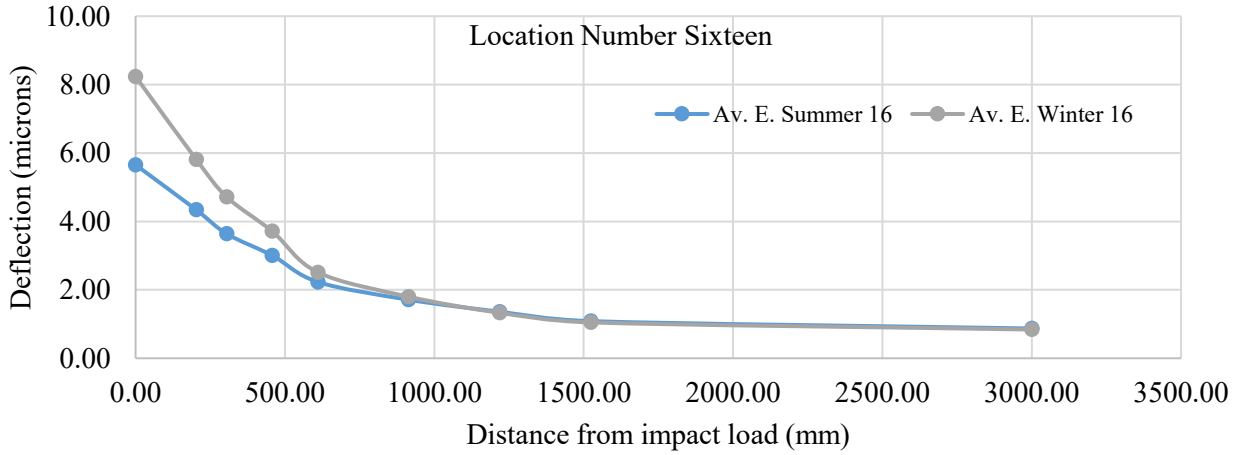

Figure C22: Overall deflections trends on the HMA for location 16.

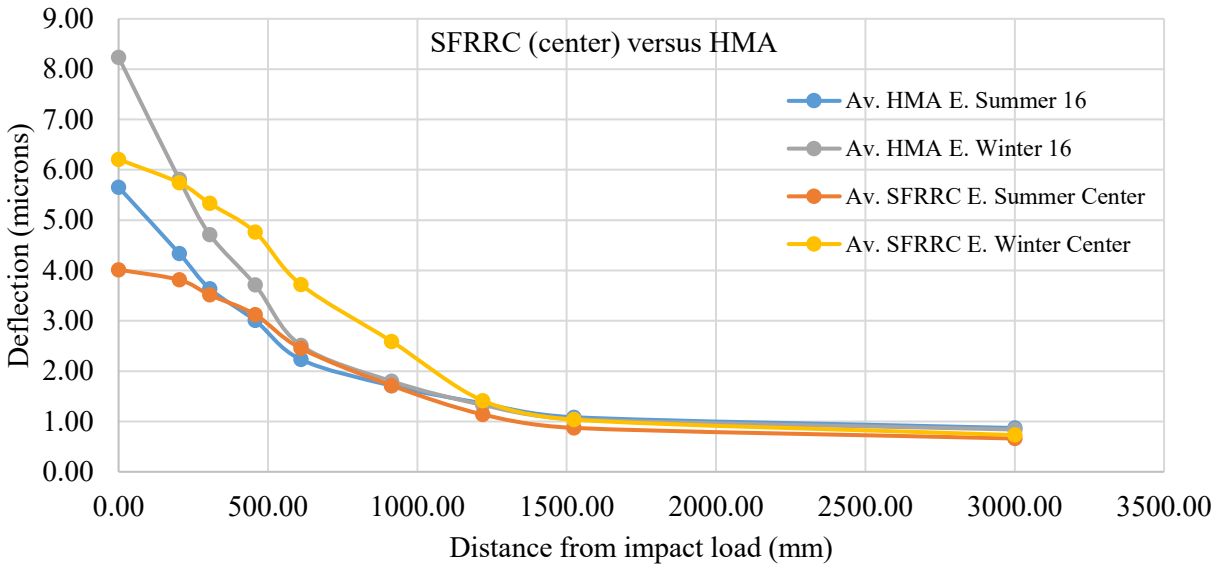

Figure C23: SFRRC versus HMA deflections.

Furthermore, back-calculation based on the field deflections of SFRRC compared with deflections from the ACI design method used in the thickness design in this project shows about 20% overdesign in overall thickness. Note that the ACI method is based on PCC, while SFRRC is a new material being introduced to the construction of highway pavements. This project is the first attempt to explore field responses to traffic load on this new material.

Summary of deflections analysis

Based on the analysis of the FWD testing, the following can be concluded:

- Cases of deflections in SFRRC follow the normal trends in rigid pavements, maximum deflections are reported at the corner of the slab, followed by the edge and center, respectively.
- FWD testing of the SFRRC test section showed seasonal deflection behaviors based on the conditions of the base/subgrade (basin). Higher deflection is reported for the three loading cases at the end of winter season than at the end of summer season.
- LTE recorded at the joints is 90% and 95% for end of winter and summer seasons, respectively. Dowel bars incorporated in the SFRRC joints are working efficiently to transfer loads across the joints.
- Deflection behavior in the SFRRC showed no signs of deficiency in the load-carrying capacity of the material or the dowel bars.
- Comparative analysis of deflection showed lower maximum deflections under the applied wheel load for SFRRC than for HMA, suggesting that SFRRC performs better at overcoming frost heave action in the pavement basin. This finding might affect truck weight limits and duration enforced during the spring season.
- Back-calculation based on the field deflection of SFRRC showed overdesign of about 20% in thickness compared with the ACI rigid pavement design method.

Appendix D – Rut Depth Analysis

Rut depth readings were collected over the project's duration to provide a comparative analysis of rut development in SFRRC and HMA paving materials on Abbott Road. Locations of rut measurements are shown in Figure 2. Table D1 and Figure D1 give the actual readings over the study period. Location 1 and 5 are on the HMA surface located before and after the SFRRC test section, and locations 2, 3, and 4 are on slab numbers four, seven, and eleven of the SFRRC surface test section. HMA rut development follows the normal trend in the area for arterial roads per the findings of the DOT&PF report titled "Survey and Economic Analysis of Pavement Impacts from Studded Tire Use in Alaska" (Abaza, 2019). SFRRC showed initial rutting of about 3.3 mm in the first year of construction, after which the rut depth stabilized below this value over the study period. The initial reading might reflect inconsistences in the leveling and finishing of the precast slabs. Furthermore, this initial rutting might be attributed to the soft paste on the surface that usually is accompanied by high water content during surface finish. This paste diminishes over the wheel path and surface. Concrete, however, does not rut under wheel loads (Halsted, 2009). The rut readings measured on SFRRC are due to studded tire use during wintertime and normal wear as a result of traction between wheel and surface.

Table D1: Rut depth reading from the Abbott Road test section.

Rut Depth Values (mm)					
Date	**5/9/2017**	**5/15/2018**	**9/1/2018**	**5/9/2019**	**9/24/2019**
Location 1	0	4.8	6.5	8.47	8.19
Location 2	0	3.5	2.5	3.18	2.89
Location 3	0	3.3	1.4	2.65	2.49
Location 4	0	3.0	3.4	3.05	3.34
Location 5	0	5.7	5	7.01	5.74

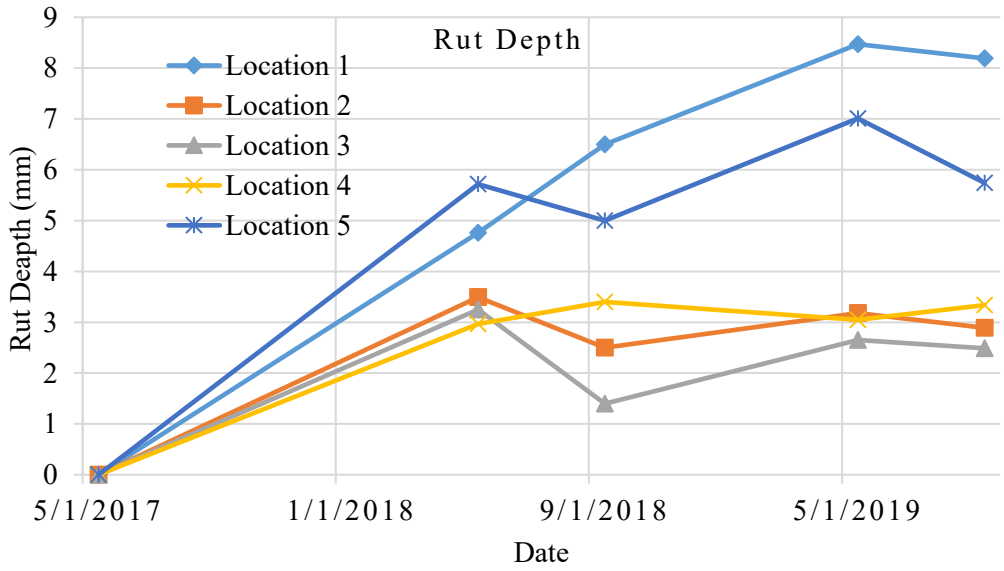

Figure D1: Actual rut readings on Abbott Road over the study period.

Average rutting for SFRRC and HMA based on the values measured are shown in Figure D2 as well as the historic rut data for Abbott Road (DOT&PF-PMS database) between Lake Otis Parkway and Elmore Road, where the test section is located. Figure D2 shows the general trend for rut development over the study period and the three historic maintenance cycles from 2000–2016. Based on the linear relationship for HMA documented for arterials in Alaska's South Central Region categorized as "Other Principal Arterials" (Trisch, 2019) and the historic trend for the same roadway section, trend lines were established as shown. The historic reduction in rutting over time for the three cycles reflects the improvement in mix designs using improved aggregates and polymer modifiers. In addition, the maintenance/reconstruction in 2017 showed further improvement in this regard. The rutting trend for the new SFRRC material indicates superior performance over the HMA.

Based on the FHWA threshold of 0.5 in. (12.7 mm) used by Alaska DOT&PF for maintenance of HMA, the projected new maintenance for the HMA on Abbott Road is about the year 2022, with an overall service life of about 5 years based on the best performance in the historic data. The actual average overall rut depth of the three historic cycles on the same road at the time of maintenance was 0.97 in., which projects the next maintenance for HMA based on this value to about the year 2030, with an overall service life of about 13 years. This agrees with the typical service life for similar arterials in the region (Abaza, 2019; Trisch, 2019). Comparative performance analysis shows that SFRRC can have a maintenance cycle that is about three times (3.28) longer than HMA. Note that understanding long-term rut development for SFRRC as new material is crucial for drawing long-term conclusions. Data collected in the last three visits showed very mild change and flattening of the curve, indicating much slower rut development for SFRRC than for HMA. Studies on PCC gave a comparable outcome. A study conducted in Oregon reported asphalt pavements experiencing average daily traffic (ADT) volumes of 35,000 and 20% studded-tire use will reach the threshold rut in 7 years. Portland cement concrete pavements experiencing 120,000 ADT and 20% studded-tire use will develop the threshold rut depth of 19 mm (0.75 in.) in 8 years (Brunette and Lundy, 1996). Note that studded tire use in Alaska was reported at 36% (Abaza, 2019).

Rut rates were calculated on the test section of Abbott Road using the AADT over the period of the project. The repetition of studded tires over the test section was calculated per the methodology reported by Abaza (2019). Traffic volume data were adjusted using factors for the relative level of traffic during the studded tire season, from September 15 until May 1. The percentage of traffic, made up of total passenger vehicles, was extracted, and the portion of vehicles in overall traffic volume using studded tires was applied to arrive at the overall number of passenger vehicles during the study period. Based on the reported traffic data from Alaska DOT&PF/Transportation Data Program and the rut data from Alaska DOT&PF/PMS for the period of the project for the section on Abbott Road between Lake Otis Parkway and Elmore Road, Figure D3 shows the rut development for HMA using the best regression fitting. The traffic component reflects the accumulated adjusted AADT as stated earlier versus each rut reading (total rut reported). This reflects an average overall HMA rut rate for this Abbott Road section of about 0.006335 in./100,000 studded-tire vehicles. Calculation of rut rate on Abbott Road for the same period using the actual field readings for HMA reflects a comparable rut rate using the same regression fitting approach. The values reported by Abaza (2019) for arterial roads as well as by Dahms (2020), reaching 0.0062 in./100,000 studded-tire vehicles, agree with the rut rate calculated on Abbott Road.

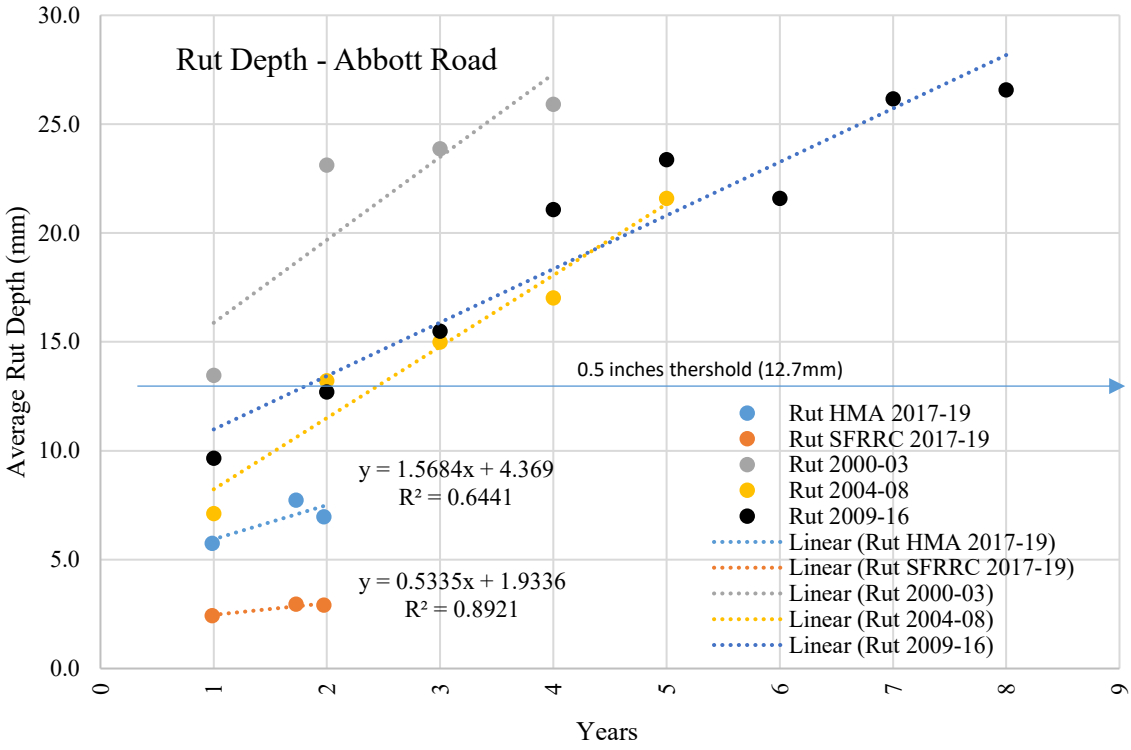

Figure D2: Average rut depth for HMA, SFRRC, and historic HMA rut on Abbott Road between Lake Otis and Elmore Road.

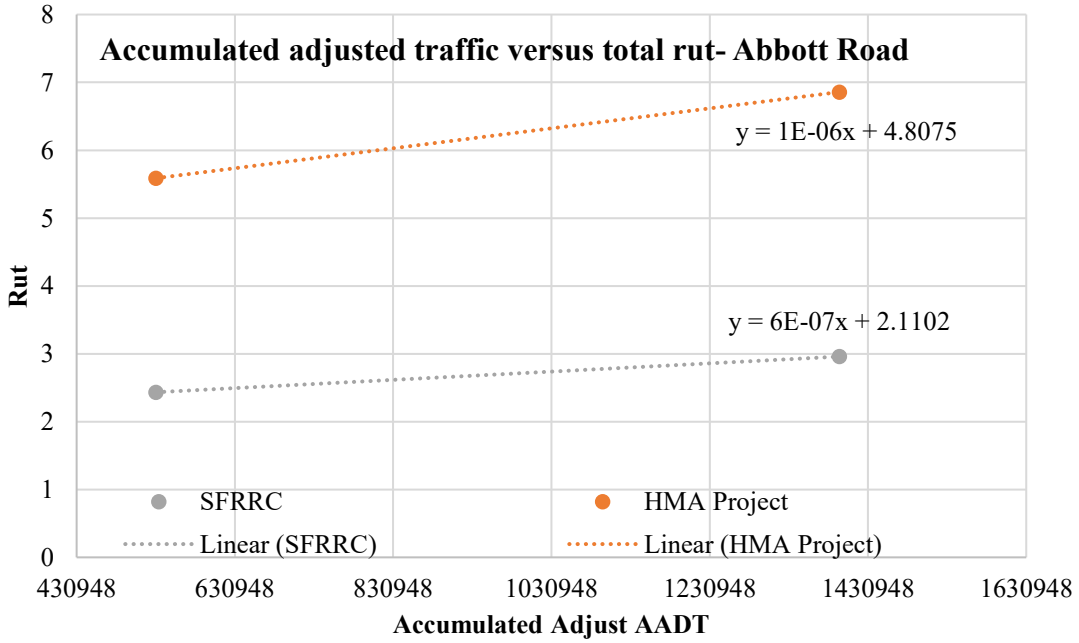

Figure D3: Relationship of average rut depth for HMA and SFRRC over the study period.

Using the same approach, the rut rate for SFRRC was calculated over the study period, reflecting 0.00283 in./100,000 studded-tire vehicles. Note that PCC does not rut due to wheel loads, unlike HMA, which might rut depending on the percent and weight of trucks. In addition, the average rut rate over the life of the pavement will be lower than the values reported in this project for both pavement materials. Data over the period of the project from both data sources showed a decreasing trend in rut rates, though total rut depth still increases with time.

Summary of the rut analysis

This rut analysis reflects the performance of both SFRRC and HMA during the project period as well as the historic rut performance of HMA on Abbott Road. Findings showed superior performance of SFRRC over the current HMA section and the historic performance of HMA. This finding validates the lab results conducted in Phase I of the project. Comparative analysis of HMA and SFRRC rut development shows that SFRRC can have a maintenance cycle that is about three times (3.28) longer than that for HMA under the same traffic conditions. In addition, historic data showed improvement in HMA mix design reflected in the rut performance over several cycles of maintenance. This comparative analysis of rutting over time is used in the LCC analysis for SFRRC (Appendix G).

It is highly recommended that rut performance of SFRRC as a new material continues to be measured and analyzed, as the latest readings show mild change and flattening of the curve, indicating much slower rut development in SFRRC than in HMA.

Appendix E – Visual Inspection

Several parameters were used to evaluate the integrity of SFRRC using visual inspection including freeze-thaw deterioration, abrasion/erosion, plastic shrinkage cracking, drying shrinkage cracking, thermal cracking, overload damage, loss of support, corrosion of embedded steel fiber, frost heave, surface defects, joint openings, grout condition and finished surfaces. Table E1 gives the most common concrete pavement performance indicators (Qi et al., 2012). Some of these parameters are addressed in Chapter 3. The following subsections cover the remaining parameters.

Table E1: Concrete pavement performance indicators.

Performance Indicator	State Highway Agency												Count
	CO	IL	IN	LA	ME	MI	MN	MS	NM	OH	TX	WI	
Concrete Pavements													
Longitudinal cracking	✓	✓	—	✓	—	✓	—	✓	—	✓	—	—	6
Transverse cracking	✓	✓	—	✓	—	✓	—	✓	—	✓	—	—	6
Corner breaks	✓	✓	—	✓	—	✓	—	✓	—	—	—	—	5
Scaling	✓	✓	—	—	—	✓	—	✓	—	✓	—	—	5
Faulting	✓	—	—	✓	—	—	—	✓	—	✓	—	—	4
Joint seal damage	✓	—	—	✓	—	✓	—	✓	—	—	—	—	4
Spalling	—	✓	—	✓	—	✓	—	✓	—	—	—	—	4
Popouts or blowups	✓	—	—	✓	—	—	—	—	—	✓	—	—	3
Map cracking	—	—	—	—	—	✓	—	✓	—	—	—	—	2
Diagonal cracking	—	—	—	—	—	—	—	—	—	✓	—	—	1
Lane-shoulder separation	—	—	—	✓	—	—	—	—	—	—	—	—	1
Patching/patch deterioration	—	✓	—	—	—	—	—	—	—	—	—	—	1
Punchouts[a]	—	✓	—	—	—	—	—	—	—	—	—	—	1
Ride quality or IRI	—	—	—	—	—	✓	—	—	—	—	—	—	1
Shoulder or lane drop off	✓	—	—	—	—	—	—	—	—	—	—	—	1

Plastic shrinkage

Cracking occurs due to plastic shrinkage when water evaporates from the surface of freshly placed concrete faster than it is replaced by bleed water; the surface concrete shrinks. Due to the restraint provided by concrete below the drying surface layer, tensile stresses develop in the weak, stiffening plastic concrete, resulting in shallow cracks of varying depth (Figure E1a). These cracks are often fairly wide at the surface. SFRRC slabs were cured under a controlled environment in the plant. No signs of any plastic shrinkage were seen on the test section in the short-term or long-term (Figure E1b).

a. PCA (1311)

b. Abaza (2017)

Figure E1: (a) Typical plastic shrinkage cracks, (b) SFRRC test section.

Drying shrinkage

Cracking also occurs because of drying shrinkage when concrete is mixed with more water than is needed to hydrate the cement. Much of the remaining water evaporates, causing the concrete to shrink. Restraint of shrinkage, provided by the subgrade, reinforcement, or another part of the structure, causes tensile stresses to develop in the hardened concrete. Restraint of drying shrinkage is the most common cause of concrete cracking (Figure E2a). In the case of SFRRC, steel fibers act as the ultimate restraint of the drying shrinkage. No signs of drying shrinkage cracks are visible on the SFRRC test section in place or in the plant (Figure E2b, c).

b. Abaza (2017) c. Abaza (2016)

Figure E2: (a) Typical drying shrinkage cracks in concrete slabs (PCA [A5271]), (b) SFRRC field, (c) SFRRC plant.

Overload damage

Properly designed and constructed concrete members are usually strong enough to support the loads for which they are intended. But overloading can occur for a variety of reasons: a change in use of a structure without proper structural upgrades, unintentional overloading, and other unusual circumstances. Earthquake damage is a classic example of the overloading of concrete structures. No signs of overload damage on the SFRRC test section were noticed or reported after a magnitude 7.0 earthquake occurred north of Anchorage, Alaska, on November 30, 2018. In addition, in the case of SFRRC precast slabs, a common error occurs when precast members are not properly supported during transport and erection. No signs of damage resulted from transporting or erecting the SFRRC precast slabs. Damage caused by impact is another form of overload. A common form of impact overload occurs at slab edges of joints on vehicular traffic surfaces (Figure E3). No such signs are visible on the SFRRC test section.

Figure E3: Typical overload crack (PCA 70151).

Loss of support

Loss of support beneath concrete structures, usually caused by settling or washout of soils and subbase materials, can cause a variety of problems in concrete structures, from cracking and performance problems to structural failure (Figure E4). A common problem related to loss of support is slab curling. Curling is the rise of a slab's edges and corners caused by differences in moisture content or temperature between the top and bottom of a slab. No signs of any loss of support were detected in the SFRRC precast slabs. Minor corner bumps in some of the slabs were noticed, caused by leveling during construction with no crack or structural damage. This problem was treated by shaving and grinding these areas of concern. No recurrence of this issue was noted during the monitoring period.

(PCA 56521)

(Abaza, 2017)

(Abaza, 2017)

Figure E4 (a) Cracking and structural failure resulted from loss of support, (b) corner grinding, (c) edge grinding.

Surface defects

Most of the inconsistences in the surface during finishing of the SFRRC were treated and covered in Phase I of the project. No further development of surface defects was apparent during the monitoring phase. This includes bugholes, honeycomb, and sand streaking. The issues related to finished surfaces covered in this phase of the project are limited to delamination, dusting, pop-out, subsidence cracks, and crazing. Delamination occurs when air and bleed water become trapped under a prematurely closed (densified) mortar surface. The trapped air and bleed water separate the

upper 3 to 6 mm (1⁄8 to 1⁄4 in.) layer of mortar from the underlying concrete (PCA). Delamination is very difficult to detect during finishing and only becomes apparent after the concrete surface has dried and the delaminated area is crushed under traffic. No apparent sign of delamination on the SFRRC surface was noticed.

Dusting is the development of a fine, powdery material that easily rubs off the surface of hardened concrete (Figure E5a). Dusting is the result of a thin, weak surface layer, called laitance, which is composed of water, cement, and fine particles. Though no signs of dusting were apparent on the surface, the thin cover over some mixed crumbed rubber was removed by traffic (Figure E5b). Dusting does not pose any surface or structural issues.

a. (PCA 1297) b. Abaza, July 2020

Figure E5: Surface finish, (a) typical dusting occurs on concrete surface (PCA 1297), (b) exposed crumbed rubber on SFRRC.

A pop-out is a fragment that breaks out of the surface of concrete, leaving a hole that is usually 6 to 50 mm (1⁄4 to 2 in.) in diameter (Figure E6) (PCA). No such holes were visible on the SFRRC test section.

Figure E6: Example of a pop-out on concrete surface (PCA 0113).

Subsidence cracks may develop over embedded items, such as reinforcing steel, or adjacent to hardened concrete as the concrete settles or subsides (Figure E7). Subsidence cracking results from insufficient consolidation (vibration), high slumps (overly wet concrete), or a lack of adequate

cover over embedded items (PCA). No signs of subsidence cracks were noted on SFRRC during the monitoring period.

Figure E7: Typical example of subsidence crack on concrete surface.

Finally, the last possible surface finish damage for typical concrete is crazing, which is a pattern of fine cracks that do not penetrate much below the surface and are usually a cosmetic problem only (Figure E8). Crazing is barely visible, except when the concrete is drying after the surface has been wet. Preventing excessive evaporation during placement and proper curing can prevent crazing. No sign of crazing was noticed on the SFRRC in wet or dry conditions. Steel fiber embedded in the concrete mix controls all types of cracks throughout the concrete volume.

Figure E8: Typical crazing cracks on a concrete surface.

Joint openings and grout condition

Joint sealant damage is any condition that enables soil or rocks to accumulate in the joints or allows significant infiltration of water. Accumulation of incompressible materials prevents the slabs from expanding and may result in buckling, shattering, or spalling. A pliable joint filler bonded to the edges of the slabs protects joints from accumulation of materials, and prevents water from seeping down and softening the foundation that supports the slab (Iowa DOT). No signs of damage were noticed in the sealant between the sides of the slabs or in any opening in the joints that might allow

foreign debris to enter the joint or allow ejection of base material through the joint. Furthermore, no signs of joint spalling (breakdown of the slab edges within 2 ft of the side of the joint) were detected. Minor crystallization of the joint material was noticed with no damage to the joint. Figure E9 shows typical damage to the joints and the conditions of the sealant and material on Abbott Road.

a. (Iowa DOT, 2020) b.(Iowa DOT, 2020) c. (Abaza, 2020) d. (Abaza, 2020)

Figure E9: Joint conditions (a) typical joint damage, (b) joint spalling, (c) SFRRC joint condition, (d) joint material on Abbott Road.

Summary of visual inspection

All possible defects that might occur in normal PCC were monitored on the SFRRC test section, and no defects were noticed on the SFRRC surface based on visual inspection. Exposed crumbed rubber on the surface resulted from wearing of the thin surface layer of paste and poses no structural or functional issues. In addition, no pop-out steel fibers were noticed on the SFRRC surface during the monitoring period, nor were loose fibers noticed on the side of the road, which further confirmed a steel fiber concrete (SFC) description reported by WSHDRP (Phase I, 1973). Some exposed lateral/flat steel fiber was noticed on spots due to wearing of the thin surface layer of paste, which poses no structural or functional issues. Figure E10 shows different snapshots of the SFRRC surface taken in July 2020.

Figure E10: Snapshots of the SFRRC test section and HMA after about 3 years of service.

SFRRC surface

HMA surface

HMA-SFRRC joint

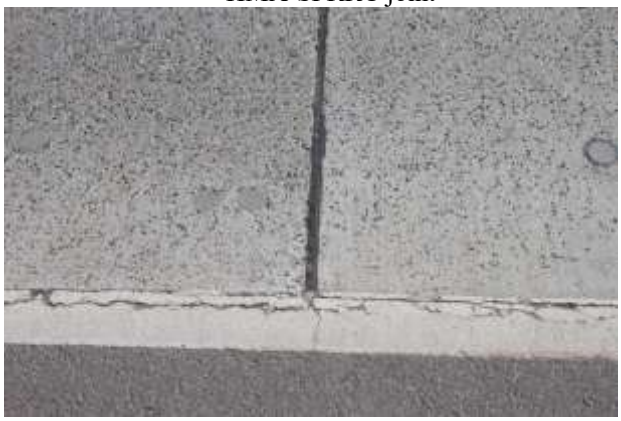

Slab corners

Figure E10 (continued).

Appendix F – Skid Resistance

Skid resistance testing was done to investigate surface microtexture differences between the two paving materials, SFRRC and HMA. Skid resistance readings were collected over the project duration to provide this comparative analysis. Locations of skid resistance measurements are addressed in Figure 2. Table F1 and Figure F1 show the actual readings over the project period. Readings one, two, and three were taken on the SFRRC test section, and reading four on the HMA surface after the test section. Skid resistance units are expressed in terms of the device used to measure surface skid resistance, in this case, as British pendulum numbers (BPNs). Typical BPN values for HMA differ mainly on type of mix and type/size of aggregate. Masad et al. (2008) reported comparable laboratory readings for HMA, with those of Abbott Road being on the higher side. On the other hand, the BPNs for PCC are usually higher depending on the kind of concrete and aggregate used. Ahammed and Tighe (1997) reported a corrected reading of skid resistance of PCC rigid pavement of about the same as that of SFRRC on Abbott Road. The general trend of skid resistance readings using the British pendulum are consistent with the trend in the two studies cited. SFRRC showed higher skid resistance than HMA. In general, skid resistance changes over time. Typically skid resistance increases in the first 2 years following construction as the roadway is worn away by traffic and as rough aggregate surfaces become exposed; it then decreases over the remaining pavement life as aggregates become more polished (Jayawickrama and Thomas, 1998). Figure F2 shows the average readings of skid resistance over the study period. The overall average difference between the two materials indicates that SFRRC skid resistance is higher by about 5%. Further monitoring of the skid resistance of SFRRC over time is highly recommended. Studies show that PCC pavements experience very little change in skid resistance over the life of the pavement (Ahammed and Tighe, 1997) compared with HMA (Masad et al., 2008). Analysis of the LTPP program data has shown that surface friction reduces at 0.7 skid number and 1.2 skid number (SN) per year for PCC and AC pavements, respectively (Ahammed, 2009).

Table F1: Skid resistance readings on Abbott Road.

Skid Resistance Readings (British Pendulum Numbers [BPNs])				
Date	**5/9/2017**	**5/15/2018**	**9/1/2018**	**5/1/2019**
Location 1 (SFRRC)	50.9	62.8	57	64
Location 2 (SFRRC)	49.6	62.7	56	69.33
Location 3 (SFRRC)	54.9	58.8	56	64
Location 4 (HMA)		57.8	51	58.33

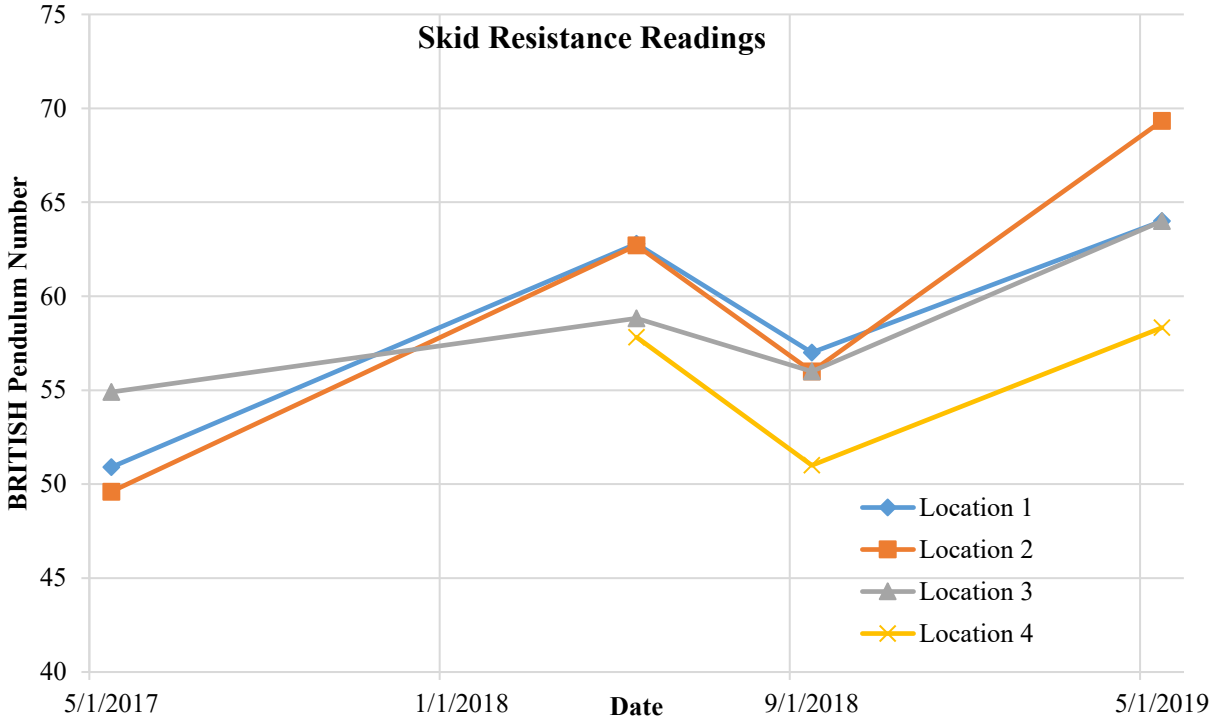

Figure F1: Skid resistance reading on Abbott Road.

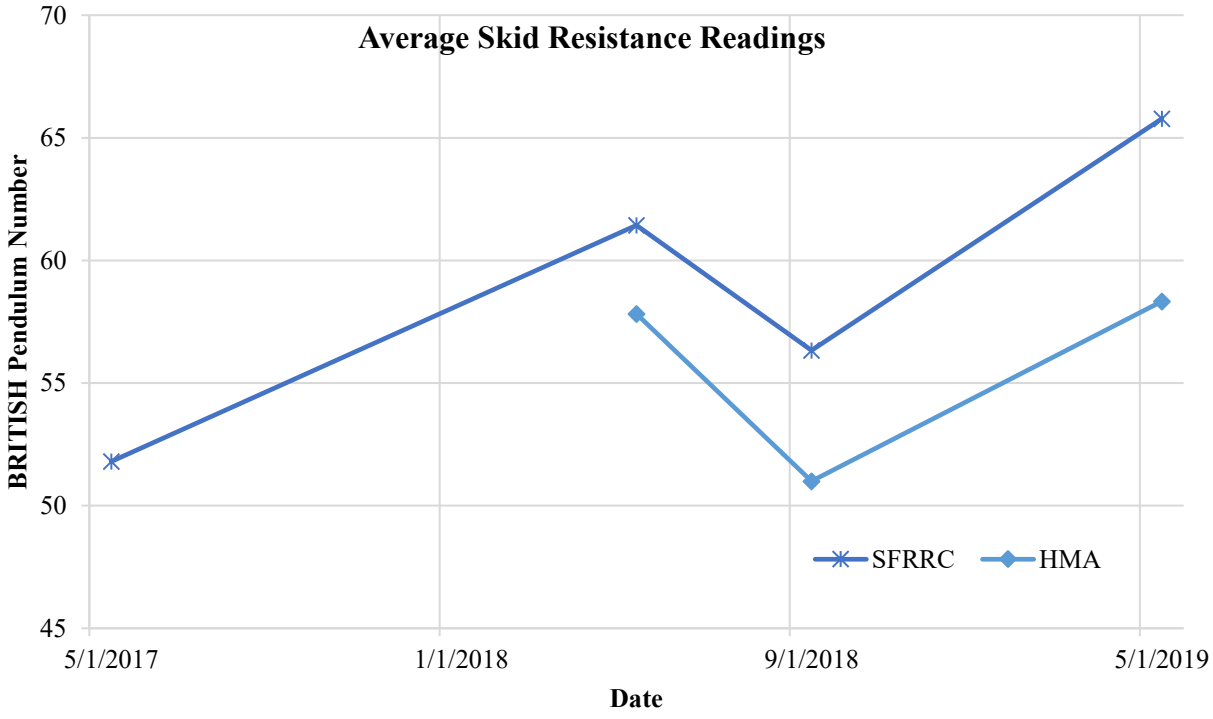

Figure F2: Average skid resistance readings on Abbott Road.

Summary of skid resistance analysis

The following are the key takeaways from the skid resistance analysis:

- BPNs reported for HMA are typical for this material, though on the higher side compared with those reported in the literature (Masad et al., 2008).
- BPNs for PCC are usually higher than HMA depending on the kind of concrete and aggregate. The general trend of SFRRC skid resistance readings is consistent with the trend in rigid pavement studies (Ahammed and Tighe, 1997).
- The overall average difference between HMA and SFRRC BPNs is 5%, with SFRRC being higher.
- LTPP program data have shown that surface friction reduces at 0.7 SN and 1.2 SN per year for PCC and AC pavements, respectively (Ahammed, 2009).
- Measurement of the skid resistance of HMA and SFRRC on the Abbott Road test section over time is highly recommended for validation of skid resistance performance.

Appendix G – Life-Cycle Cost Analysis

The life-cycle cost (LCC) analysis of SFRRC for use in pavement structures in Alaska is based on critical and common pavement deterioration in the South Central Region of the state that triggers rehabilitation and maintenance of the pavement structure. Rutting caused by studded tires has been identified as the main pavement distress that calls for rehabilitation and maintenance (Abaza, 2019). The typical life cycle of HMA in the South Central Region can reach half that in the Lower 48, which has an overall life cycle of 16.9–17.9 years depending on the type of base (Robbins and Tran, 2018). Alaska DOT&PF identified a threshold for rutting of 0.5 in. (1.27 mm) calling for corrective action. Actual average overall rut depth at the time of maintenance exceeds this threshold depending on the class of road and available budgets (Abaza, 2019; Trisch, 2019). Comparative analysis of HMA and SFRRC performance shows that SFRRC can have a maintenance cycle that is about three times longer than that of HMA based on the assessment done in this project. For the purpose of LCC in this study, a conservative value was used that depends on the rut development calculated on the test section of Abbott Road. Note that understanding long-term rut development in SFRRC as a new material is crucial for drawing long-term conclusions about LCC. Data collected in the last three visits showed very mild change and flattening of the curve, indicating much slower rut development in SFRRC than in HMA. In addition, historic data showed that rut development in PCC pavements is much lower than in HMA over the life of the pavement structure. A study conducted in Oregon (Brunette and Lundy, 1996) is a good example of the future trends of the two paving materials.

The methodology used for LCC analysis of HMA and SFRRC is presented in Chapter 2. The first step in the process was to determine the parameters needed to conduct the LCC analysis. A thorough literature review was conducted to better understand the needs of public and local agencies in using LCC as well as the tools used. The literature review is provided in Appendix B. The following parameters were determined and collected: AADT, roadway structural design, type of construction implemented (rehabilitation, maintenance), etc. Details on type of routine maintenance were collected, as well as HMA mix designs, other construction-related items, prices per item, etc. Additional details of the actual data are presented here.

The second step was to select a sample of roads in the network to set the basis for the cost of paving per square foot. Several resources were used to collect the data, for example, as-builts, bid taps, ArcGIS, etc. It was determined that twenty projects contain the necessary information to provide a realistic cost estimate for paving. Historical projects were identified, as well as the years of resurfacing/rehabilitation of each project. Details of the selected projects are shown in Table G1. Several asphalt mix designs with different structural sections were considered to calculate the unit cost per square foot of each project. Data for these structural sections and total price per ton are shown in Table G2. The repair costs were limited to a rehabilitation strategy of the structural section thickness (mill/fill). First, a realistic cost estimate was determined per pavement square foot of construction, which includes all direct overall resurfacing costs (milling, striping, traffic maintenance and control) and excludes indirect costs, which are insignificant compared with the main project costs. Then cost of total pavement repair was estimated for rutting damage on the highways, including rutting that reaches the rut threshold limit. Based on feedback from Alaska DOT&PF, a 0.5 in. rut threshold limit was taken into consideration to determine the cost of pavement resurfacing and rehabilitation. However, the exact weighted average for the rut threshold was estimated from the highway samples, including freeways and arterial and collector roads, to capture a range of costs and to provide future prediction cost estimates for Alaska DOT&PF. Tables G3 and G4 show the rut depth of the selected freeway

samples and the collector roads just before the scheduled year of maintenance, which reflects the actual threshold used for rehabilitation.

Table G1: List of as-built projects.

ID Num.	Title	HMA Type	Year	Length (ft)
51135	Minnesota Dr. Resurfacing, Intl. Airport Rd. to 13th Ave.	2” HMA Type V	2009	18849
51340	Minnesota Dr. Resurfacing, C St. to Intl. Airport Rd.	2” HMA Type V	2009	20250
52491	Seward Highway MP 115–124 Resurfacing	2” HMA Type R	2010	17280
51945	Glenn Hwy., Airport Heights to Highland Resurfacing	1.75”-2” HMA Type R	2009	55860
52015	Glenn Hwy. MP 34–42, Parks to Palmer Resurfacing	1.75” HMA Type V	2009	30650
55335	Glenn Highway, Gambell to McCarey Resurfacing	2” Stone Mastic Asphalt	2003	19846
56314	Glenn Highway King River to MP 100 Resurfacing	2” HMA Type IIA	2005	13200
52493	Sterling Highway MP 90–82 Resurfacing	2.5”-3” HMA Type IIA	2010	33800
51046	Sterling Hwy. Resurfacing MP 93.9–89.9	2” HMA Type IIA	2008	21460
53801	Dimond Blvd. Resurf. Jewel Lake Rd. to Seward Hwy.	2” – 3” HMA Type V	2013	18500
55657	Dimond Resurfacing, Jewel Lake to Seward Hwy.	2” Stone Mastic Asphalt	2003	16225
51987	Jewel Lake Rd. Resurf, Dimond Blvd. to West 63rd Ave.	3” HMA Type V	2010	8730
52512	C St. – Intl. Airport Rd. to Tudor Rd.	2” Stone Mastic Asphalt	1998	7720
52881	Resurfacing Glenn Hwy. to Eagle River Rd.	1.75” HMA Type V	2011	13393
53975	Northern Lights and Benson Resurfacing, Lois Dr. to Lake Otis	2” Stone Mastic Asphalt	2001	27000
56333	Anchorage Area Arterial Resurfacing, 2003 (3 Projects)	2” Stone Mastic Asphalt	2003	22440
50810	Muldoon Rd. Resurfacing 36th to Glenn Hwy.	2” HMA Type V	2008	14217

Table G2: Types of structural sections and unit price.

Number	Structural Section	Unit price ($/ton)
1	2" Stone Mastic Asphalt	65.00
2	2" & 4" Asphalt Concrete Type IA	135.00
3	2" HMA Type R	120.02
4	2" HMA Type V	95.00
5	1 .75" & 2" HMA Type R	105.54
6	2" HMA Type IIA*	84.45
7	2" HMA Type IIA*	65.85

Department of Transportation. (2017, November 20). Bid Tabulation Summaries. Anchorage, Alaska, USA.
* Unit price per ton for HMA Type IIA were different in some projects

Table G3: Rut threshold of the freeway samples.

Glenn Highway		Weighted Average	Seward Highway		Weighted Average	Minnesota Drive		Weighted Average
Length Miles	Rut 2008		Length Miles	Rut 2008		Length Miles	Rut 2008	
1.44	0.95	1.36	1.01	0.62	0.62	0.97	0.85	0.82
2.55	0.55	1.40	0.80	0.53	0.42	1.19	0.79	0.94
1.62	0.64	1.04	1.02	0.53	0.54	0.76	0.3	0.23
1.00	0.87	0.87	1.06	0.57	0.61	1.07	0.72	0.77
0.51	0.83	0.42	0.98	0.86	0.84	1.03	0.58	0.60
1.78	0.95	1.69	0.81	0.79	0.64	0.72	0.82	0.59
0.51	0.59	0.30	1.14	0.57	0.65	0.68	1.09	0.74
1.15	0.66	0.76	1.00	0.94	0.94	0.57	0.98	0.56
1.40	0.79	1.11	0.45	0.52	0.24	0.76	0.94	0.72
1.22	0.72	0.88	1.33	0.62	0.83	0.73	0.74	0.54
1.00	0.65	0.65	1.06	0.67	0.71	0.60	0.82	0.49
1.09	0.93	1.01	1.00	0.83	0.83	0.48	0.72	0.35
0.45	1.02	0.45	0.61	0.41	0.25	0.57	1.23	0.70
1.01	1.34	1.36	0.28	0.75	0.21	0.66	0.64	0.42
1.01	1.35	1.36	0.28	1.23	0.34	0.71	0.71	0.50
0.45	0.81	0.36				0.35	0.78	0.28
1.54	0.92	1.42				0.42	0.68	0.29
0.81			0.68			0.76		

Table G4: Rut threshold of the arterial samples.

Dimond		Weighted Average	Northern		Weighted Average	Tudor Road		Weighted Average	International		Weighted Average
Length Miles	Rut 2013		Length Miles	Rut 2001		Length Miles	Rut 2003		Length Miles	Rut 2014	
0.58	0.76	0.44	1.00	0.27	0.27	0.86	0.69	0.59	0.61	0.5	0.31
0.28	0.48	0.13	1.11	0.17	0.19	0.50	0.49	0.25	0.53	1.12	0.60
0.61	0.67	0.41	1.10	0.2	0.22	0.38	0.68	0.26	0.68	0.52	0.35
0.53	0.43	0.23	0.99	0.6	0.60	0.61	1.07	0.66	0.32	0.1	0.03
0.25	0.34	0.09	0.61	0.53	0.33	0.27	0.67	0.18	0.39	0.27	0.10
0.77	0.59	0.45	0.89	0.69	0.61	0.73	1.15	0.84	0.31	0.24	0.07
0.25	0.32	0.08	0.50	0.6	0.30	1.01	0.78	0.79			
0.75	0.21	0.16	0.50	0.53	0.27	1.00	0.92	0.92			
0.06	1.05	0.06	0.92	0.76	0.70	0.39	0.88	0.34			
0.14	0.69	0.10				1.01	0.78	0.79			
0.25	0.34	0.09				0.27	0.67	0.18			
0.77	0.61	0.47				0.84	0.69	0.58			
0.25	0.54	0.14				0.73	1.15	0.84			
0.53	0.48	0.26				1.00	0.92	0.92			
0.75	0.23	0.17				0.61	1.07	0.66			
0.28	0.52	0.14				0.51	0.49	0.25			
0.14	0.5	0.07									
0.51			0.46			0.84			0.52		

Many factors influence the price of an asphalt resurfacing job. Direct and indirect costs should be included in the pavement unit price for small projects, such as repaving a driveway or parking lot. However, for the purpose of this study, larger-scale projects that have at least 6 to 10 miles of mill and fill were selected for estimating the cost of pavement resurfacing. Indirect costs were excluded from the analysis, as stated earlier, as they are insignificant in the total price. Direct costs included in the unit price per square foot are as follows:

- Pavement planning/design
- Milling price, range from (1.92–2.5) $/square yard
- Marking and striping
- Traffic maintenance and control
- Construction signing
- Flagging

The third step, based on collected data, was to calculate the pavement resurfacing cost from the as-builts of 20 projects to establish a realistic estimated cost of construction/rehabilitation with consideration of pavement thickness in the estimate. Table G5 shows the cost per square foot for each project with an overall average of $3.32 per square foot for resurfacing and about $6.51 for full depth (reconstruction). In addition, the cost per square foot was calculated for SFRRC based on

realistic estimates for typical PCC pavement with consideration for the deviation of additives used to produce SFRRC. The cost per square foot for SFRRC on Abbott Road may not reflect the actual cost for a full stretch of road, considering quantities and the bidding process. To have a better comparative LCC analysis, the actual cost of SFRRC per the cost from the producer (AS&G) and that of PCC adjusted are incorporated. A sample of projects paved with PCC was collected on the national level and adjusted for SFRRC production and price deviations in Alaska based on feedback from local industry. Table G6 gives the cost data for SFRRC for the project and the adjusted PCC cost.

Table G5: Pavement resurfacing cost per square foot.

Project Name	Total Cost ($)	Cost/SF ($)	Cost per Year ($)
Northern Lights & Benson Resurfacing	2,392,208	1.70	341,744
Tudor Road Pavement Rehabilitation	5,928,633	3.08	846,948
Seward Highway MP 115–124 Resurfacing	6,516,993	2.86	930,999
C Street (52512)	1,068,535	15.83	152,648
Minnesota Drive Resurfacing	3,978,760	2.92	568,394
Glenn Highway	10,274,557	2.08	1,467,794
Muldoon Road Resurfacing	3,058,863	3.55	436,980
Sterling Highway Resurfacing	1,645,616	1.27	235,088
Minnesota Drive Resurfacing	3,679,828	4.17	525,690
Jewel Lake Road Resurfacing	1,635,944	3.64	233,706
Glenn Highway MP 34–42	1,617,275	1.93	231,039
Sterling Highway Resurfacing	2,779,942	3.11	397,135
Eagle River Loop Road Resurfacing	2,063,762	2.46	294,823
Dimond Boulevard Resurfacing	5,918,240	3.41	845,463
Glenn Highway Intersection Resurfacing	2,425,790	3.37	346,541
Dimond Resurfacing	3,856,123	2.85	550,875
Glenn Highway Resurfacing	7,728,503	2.04	1,104,072
Anchorage Resurfacing, Boniface Parkway	1,197,920	1.73	171,131
Anchorage Resurfacing, C Street	759,774	2.26	108,539
Anchorage Resurfacing, Lake Otis Parkway	853,825	2.07	121,975

Table G6: SFRRC pavement cost per square foot.

Item	Cost($)/cubic yard	Cost ($) per square foot
PCC (Anchorage, Alaska (2019 dollar value for 4000 Pounds per square inch (psi))	185	NA
PCC Anchorage adjusted for SFRRC for material cost (2019 dollar value)	303**	6.54
SFRRC project on Abbott Road (2019 dollar value) (AS&G)	470	10.15
PCC (Ohio, based LCC of 6 projects (2019 dollar value))*	137	NA
PCC adjusted for SFRRC for material and labor cost (Ohio, 2019 dollar value)	255**	5.51

*(Villacres, J, Pavement Life-Cycle Cost Studies Using Actual Cost Data)
** Two alternatives used in the LCC for SFRRC based on local and national level actual cost

The fourth step in the LCC analysis process was to develop the LCC using the present worth method per rut developed from the test section for SFRRC and HMA on Abbott Road. The LCC was analyzed on a project level basis, as the State of Alaska implements LCC on the network and project levels but not on maintenance levels (NCHRP synthesis 494, 2016). In addition, LCC is based on removal and replacement of pavement at the end of pavement life, which is based on the pavement analysis period with consideration of resurfacing for HMA during the period. A comparative analysis of rut development for HMA from other arterials in the Central Region of similar road characteristics was used to further validate the rut development of HMA on-site to take into consideration the full surface life rather than 2½ years of data. An analysis period of about 43 years was used with no salvage value at the end of the period. This analysis period represents one cycle of SFRRC pavement at the beginning of the period and 3.28 cycles of HMA paving, one of which is full rehabilitation/maintenance. In addition, typical discount rates in civil engineering projects are between 2.5% and 5% (Villacres, 2005); a lower percentage was used to reflect a conservative approach in the LCC outcome. Furthermore, the FHWA states that good practice suggests using an inflation rate of 3% to 5% (Villacres, 2005); 3.5% was used in this project. Table G7 gives the details of the LCC for HMA and SFRRC cost scenarios. The actual cost of SFRRC for Abbott Road was adopted to reflect the worst-case scenario for comparative analysis.

Note that routine maintenance costs during the period of resurfacing/rehabilitation of HMA were not included, and the same applies for SFRRC during the analysis period. Studies showed that routine maintenance costs for PCC pavements are less frequent and less expensive over the life of the pavement structure. In addition, thickness design for SFRRC was based on the PCA method for PCC. Back-calculations based on field deflections using FWD showed SFRRC thickness can be reduced by up to 20% to provide the same structural capacity for the condition of loading given, but this thickness reduction was not taken into consideration. Furthermore, a 0.97 in. rut was used in the LCC analysis to prompt resurfacing instead of the DOT&PF threshold of 0.5 in. Higher rut depth is associated with higher crash rates and is eventually a cost for the community. Finally, highway user costs resulting from construction delays during maintenance/rehabilitation were not accounted for in the LCC.

Note that the local cost of SFRRC should be reviewed, as the current cost per cubic yard for Abbott Road showed a value of about 2.5 times that of PCC with the same compressive strength, while material and labor in place showed about 1.6 times as much.

Table G7: Life cycle cost for HMA and SFRRC.

Item	Type	Alternative one, HMA	Alternative two, SFRRC Abbott Road	Alternative three, SFRRC material cost	Alternative four, Ohio cost basis adjusted for SFRRC
Cost per square foot ($)	Reconstruction	6.51	10.15	6.54	5.51
	Resurfacing/ rehabilitation	3.32	NA	NA	NA
Analysis period	NA	43	43	43	43
Number of reconstruction cycles during analysis period		2	1	1	1
Number of resurfacing/ rehabilitation cycles during analysis period		1	0	0	0
LCC per square foot ($)/analysis period		21.53	10.15	6.54	5.51
Cost per linear lane mile ($) million		1.36	0.64	0.41	0.35

Summary of life-cycle cost analysis

The following are the key takeaways from the LCC analysis:

- Evaluation of the LCC of HMA was based on real HMA resurfacing/rehabilitation projects implemented by ADOT&PF in the state.
- LCC for SFRRC was based on the cost of the precast slabs installed on Abbott Road as well as real-life projects implemented in the Lower 48 for PCC, adjusted for cost of additives of steel fiber and rubber contents to account for the limited scale of the job on Abbott Road as well as the lack of a bidding process for a full-scale application of this material.
- A SFRRC LCC worst-case scenario was adopted for comparative analysis for potential trial use of this material at highway intersections.
- An analysis period of 43 years was considered for comparative analysis between HMA and SFRRC.
- LCC for SFRRC over the analysis period showed $0.64 million per linear lane mile compared to $1.36 million for HMA over the same period.
- The cost ratio of HMA to SFRRC is about 2.1 to 1.0.
- Several cost items were not considered in the LCC analysis, such as routine maintenance during the analysis period, the thickness adjustment for SFRRC based on back-calculation of field deflections, FHWY-DOT&PF adopted rut threshold, crash costs as a result of ruts, and highway user costs due to traffic interruptions during resurfacings/rehabilitations.

- Based on the comparative LCC analysis of the materials considered for future paving, SFRRC can be explored further for use on an experimental basis at highway intersections as well as for test sections on major arterials.